Ion solvation in water

femtosecond spectroscopy of hydrogen-bond dynamics

Ion solvation in water

femtosecond spectroscopy of hydrogen-bond dynamics

ACADEMISCH PROEFSCHRIFT

ter verkrijging van de graad van doctor
aan de Universiteit van Amsterdam
op gezag van de Rector Magnificus
prof. mr. P. F. van der Heijden
ten overstaan van een door het college voor promoties ingestelde
commissie, in het openbaar te verdedigen in de Aula der Universiteit
op donderdag 19 februari 2004, te 14.00 uur

door

Michel François Kropman

geboren te Eindhoven

Promotor: Prof. Dr. H. J. Bakker

Faculteit der Natuurwetenschappen, Wiskunde en Informatica

The work described in this thesis was performed at the FOM-*Institute for Atomic and Molecular Physics* (AMOLF), Kruislaan 407, 1098 SJ Amsterdam, The Netherlands. The work is part of the research programme of the *Stichting Fundamenteel Onderzoek der Materie* (FOM), which is financially supported by the *Nederlandse Organisatie voor Wetenschappelijk Onderzoek* (NWO). The work is also partially supported by the *Netherlands Research Council for Chemical Sciences* (NWO-CW).

Contents

Publications covered in this thesis

M. F. Kropman and H. J. Bakker. Dynamics of water molecules in aqueous solvation shells. *Science* **291**, 2118 (2001).

M. F. Kropman and H. J. Bakker. Femtosecond mid-infrared spectroscopy of aqueous solvation shells. *J. Chem. Phys.* **115**, 8942 (2001).

M. F. Kropman, H.-K. Nienhuys and H. J. Bakker. Real-time measurement of the orientational dynamics of aqueous solvation shells in bulk liquid water. *Phys. Rev. Lett.* **88**, 77601 (2002).

M. F. Kropman and H. J. Bakker. Comment on: Water in the vicinity of solvated ions: modified dynamical and structural water properties resolved by sub-picosecond IR-spectroscopy by R. Laenen and A. Thaller. *Chem. Phys. Lett.* **362**, 349 (2002).

M. F. Kropman and H. J. Bakker. Vibrational relaxation of liquid water in ionic solvation shells. *Chem. Phys. Lett.* **370**, 741 (2003).

A. W. Omta, M. F. Kropman, S. Woutersen and H. J. Bakker. Negligible effect of ions on the hydrogen-bond structure in liquid water. *Science* **273**, 347 (2003).

A. W. Omta, M. F. Kropman, S. Woutersen and H. J. Bakker. Influence of ions on the hydrogen-bond structure in liquid water. *J. Chem. Phys.* **119**, 12457 (2003).

M. F. Kropman and H. J. Bakker. Vibrational relaxation of liquid water in ionic solvation shells. *submitted.*

Other publications

I. M. A. E. Giebels, M. A. F. H. van den Broek, M. F. Kropman and H. J. Bakker. Vibrational dynamics of hydrogen-bonded HCl–diethyl ether complexes. *J. Chem. Phys. 112*, 5127 (2000).

M. F. Kropman, H.-K. Nienhuys, S. Woutersen and H. J. Bakker. Vibrational relaxation and hydrogen-bond dynamics of HDO:H_2O. *J. Phys. Chem. A 105*, 4622 (2001).

M. A. F. H. van den Broek, M. F. Kropman, and H. J. Bakker. Ultrafast pump-probe spectroscopy of strongly hydrogen-bonded hydrogen fluoride-pyridine complexes. *Chem. Phys. Lett. 357*, 8 (2002).

1 Introduction

The importance of salt solutions may be best illustrated by the fact that two thirds of the earth's surface is covered by a salt solution of approximately 10^{21} litres. The salt content is an important parameter for the oceanic flow patterns, since it affects the density of water and its melting temperature. On a smaller scale, the fysiological fluids that constitute a principal part of the human body consist mainly of water, and contain significant amounts of ionized solutes. Human blood can be (partly) replaced by 'fysiological salt', which is nothing but a solution of salts and minerals in water, with a salt content similar to that of blood. The chemical reactions that take place in the human body are closely related to the behaviour of water molecules. The hydrolysis of adenosine triphosphate (ATP), forming adenosine diphosphate (ADP), a solvated phosphate group, and a solvated proton, is only one example of a chemical reaction in which solvation plays a crucial role.

A salt molecule consists of a cation and an anion, ions of positive and negative charges, respectively. The ions are held together by an ionic bond; the separate charges give rise to strong electrostatic attraction. When dissolved, the molecule falls apart in its constituent ions, that are separately solvated by the solvent molecules. These solvation interactions must overcome the rather strong ionic bond, in addition to the solvent–solvent interactions that may be distorted to accomodate the ions. It is surprising how well soluble many salts are in water. Potassium Fluoride, for example, is soluble up to 18 M: three water molecules for each pair of solvated K^+ and F^- ions.

In this thesis, solutions of salt in water are studied. Water is the common solvent in nature, and may be considered the most important for that reason. However, solvation is in itself by no means limited to water. There are several practical applications for non-aqueous or mixed solvents. Since the reactivity of dissolved ions will depend on the solvation interactions, the solvent can be chosen so as to optimize the ions' reactivity, e.g. in batteries.

Connected to solvation, two notions are important in this thesis, that of hydrogen bonding and of solvation shells.

1.1 Solvation shells

The first theories that deal with electrolyte solutions, e.g. the Debye-Hückel theory at the beginning of the 20^{th} century, did not take any molecular structure into account, but simply treated the solvent as a homogeneous medium with a dielectrical constant. The development of X-ray diffraction (1920s) and infrared spectroscopy (1930s) techniques revealed that liquid water does have a structure on the molecular scale, that is altered by the presence of solute molecules.[3,40,38] Around many solutes, among which ions, the solvent molecules were found to reside preferrably at specific distances from the solute molecule. These layers of solvent molecules around the solute are called solvation shells,

or hydration shells when the solvent is water. Because the solvation structure and its dynamical behaviour are of great importance to the reactivity of the solute, there has been an ever-growing interest in the study of these solvation shells.[3,132,81]

A salt is said to be dissolved if its constituent ions reside separately within the solvent. The solvent structure around the ion is characterized by the pair correlation function $g(r)$, that gives the (time- and ensemble-averaged) probability of finding a water molecule (usually either an oxygen or a hydrogen atom is measured) at a distance r from the ion. For small r, $g(r)$ will be zero because the Van der Waals repulsion prevents the molecules to come too close to the ion. For greater r, $g(r)$ will go through a series of maxima and minima, corresponding to subsequent solvation shells. In liquid water, only one or two such maxima are pronounced.[96] The number of molecules in the first solvation shell can be calculated from $g(r)$, by integrating $g(r)$ from 0 to the first minimum, or by fitting the first peak. Note that the existence of these shells does not provide much information on the ion–solvent interaction: even a non-interacting hard sphere in a condensed-phase solvent will give rise to their formation, since otherwise a cavity would exist within the solvent. The distance between the shells, and the orientation of the solvent molecules within the shells will be more strongly dependent on the interactions.

Experimentally, the pair correlation functions $g(r)$ can be obtained by X-ray, neutron or electron diffraction, or with EXAFS (extended X-ray absorption fine structure). In the latter technique, the modulation of monochromatic X-ray radiation is measured, resulting from the interference of low-energy electrons that scatter from different atoms in the sample. The modulation depends on the distance between the atoms.[96]

The solvent structure, and so the radial distribution function, are the result of four structuring forces that act on the conformation of water molecules around ions.[81] First, in the case of anions, a hydrogen-bond interaction can exist between the ion and first-layer solvent molecules that is directional. Second, both for anions and cations, the electric field of the ion tends to align the dipole moment of the solvent molecules; this latter effect may extend beyond the first shell, although decreasing outward due to the Coulomb potential. Resulting from the hydrogen-bond interactions between water molecules, two other forces can be identified. From the ion on outward, the first solvation shell tends to align the water molecules in the second shell, and so on. Reversely, the bulk liquid will try to impose its structure on the molecules closer to the ion.

Traditionally, the net structuring effect has been considered in terms of structure-making and structure-breaking ions. Some ions are considered to promote a more rigid hydrogen-bond structure around the ion, others would not change it or even weaken it over relatively large distances. Of the four above-mentioned structurizing interactions, the interactions that alter the hydrogen-bond structure are the ion–dipole interaction and the anionic hydrogen bonds. In this thesis, experiments are presented that challenge this view of structure-making and structure-breaking ions, by showing that there is no marked change in structural rigidity even around the strongest structure-making ions.

Several new experimental and computational methods have been developed since the first investigations of the solvation structure. One of the greatest obstacles in these studies is that one has to separate the response from water molecules in the bulk solvent from those that participate in the solvation structure.

Nuclear magnetic resonance (NMR) has been used since 1948.[11,48] With NMR, the 'chemical shift', the change in magnetic resonance frequency of a nuclear spin, is measured.

The chemical shift depends very sensitively on the direct environment of the nucleus, and can be measured with great accuracy. Although NMR has been very valuable, e.g. in obtaining hydration numbers,[48] with respect to hydration there are two disadvantages to this technique.[96] First, the interpretation of the spectra is not straightforward: several effects contribute to the chemical shift, the separation of which is complicated, especially for protons. The second disadvantage is that the frequency of the magnetic field is at most 100 MHz, so that the time scale of the phenomena that can be measured with full accuracy is restricted to nanoseconds. A very precise measurement of the linewidth can partly compensate for the loss of accuracy, and extend the range to picoseconds. However, this linewidth must correspond to one specific type of nucleus; the molecules in the solvation shells that we study do exchange with the bulk solvent hundreds of times within the measurement of the linewidth, rendering NMR unsuitable for separating the responses from bulk and shell molecules.

The problem of distinguishing the solvating molecules can be solved by studying clusters existing of one ion and a fixed number of water molecules. In vibrational predissociation experiments,[4,6,5,7,20,16,110,128] such clusters are prepared and selected using a mass spectrometer. The spectrum of frequencies at which one molecule is 'shattered' off the cluster is measured by shining laser light on the clusters and detecting the mass-selected fragments. Clusters have also been studied in molecular dynamics simulations.[140,102,80,52] It must be realized that they are not real solutions. The hydrogen bonds and the vibrational spectra are different and furthermore, in real liquids, many more interactions are present due to the greater number of molecules.

Another experimental method that circumvents the problem of the strong inhomogeneity of an aqueous system, comprises the use of a probe molecule dissolved in water.[32,55,103] In this type of experiment, information on the dynamics of the solvating water molecules is inferred from the time-dependent response of the molecule after excitation. For instance, it was observed that the fluorescence of a dye molecule dissolved in water shows a very rapid redshift with a time constant smaller than 100 femtoseconds, which indicates that solvating water molecules can show a very rapid reaction.[32,55] A disadvantage of this technique is that it probes the dynamics and structure of the solvating water molecules rather indirectly.

In the past decade, computer power has increased enormously, and better modeling potentials for water molecules have been developed, resulting in a large number of molecular dynamics (MD) simulations of aqueous solutions.[2,17,22,28,27,26,25,46,54,62,64,102,101,104,114,143] These simulations produce the position variables of all molecules at a discrete series of time steps, from which easily all relevant structural and dynamical parameters can be calculated. For example, statistics of configurational parameters in solvation structures were studied;[22,28,27,26,25,143] ion-pairing was found to take place, even the pairing of ions with charges of equal sign.[26,54,101,108] Also dynamics is easily accessed: the exchange of water molecules between the shell and the bulk solvent can be followed in detail;[22,47,108,114] for monovalent ions these exchanges are found to take place on the order of one to a few hundreds of picoseconds. However, results from MD simulations should be regarded with some reservation, since they strongly depend on the potentials chosen: without experimental verification, their value is limited.

1.2 HYDROGEN BONDING

Hydrogen bonds play an important role in the solvation interactions. A hydrogen bond is an attractive directional interaction between a proton-donating D–H group and an acceptor A, denoted D–H···A. With directional it is meant that the bond has a preferred DHA angle, namely 180°. D and A are usually one of the following electronegative elements: F, O, Cl, N, Br or I.

The first reportings of interactions that are now called hydrogen bonds, date shortly after 1900. Weak interactions were identified, e.g. in ammonia salts, and given names like 'secondary valence'[129,29] or 'weak union'.[87,29] The term 'hydrogen bond' was first used by Pauling,[99] who later gave it widespread attention by devoting a chapter to it in his book 'The nature of the chemical bond'.[100]

Today, the role of the hydrogen bond in chemistry is widely acknowledged. Its importance lies in the association of molecules. Since the interaction is directional, it favors certain configurations and thus brings some order in liquids, and promotes the formation of certain crystal structures over others. The interaction energy is in the range of 0.1 to 20 kJ/mole.[29] The thermal energy available for each vibrational coordinate at room temperature is 1.2 kJ/mole, so that most hydrogen bonds are easily formed or broken. Recent research identifies electrostatic and covalent interactions as the main physical interactions that constitute the hydrogen bond.[23]

Hydrogen bonds are particularly important in liquid water, which would be a gas at room temperature when hydrogen bonds would not hold the molecules together. Each water molecule can participate in up to four hydrogen bonds, with an average of 3.4 at room temperature.[122] The hydrogen bonds form an extensive network throughout the liquid, that is responsible for many remarkable macroscopic properties of water. For example, water reaches its maximal density at 4 °C, instead of at its melting point.

Dissolution of salt in water may lead to several changes with respect to the hydrogen-bond interactions. First, the hydrogen-bond structure that exists in liquid water may be 'mechanically' changed by the fact that the ions occupy a certain space in the solvent. The structure may either be enhanced, by promoting the local formation of ice-like structures, or weakened when the hydrogen bonds are bended or even broken if the size of the solute does not match the undisturbed hydrogen-bond structure. Second, the interaction of the ion's charge with the dipole moment of the water molecules can lead to a restructuring of the network; the electric field may polarize the hydrogen bonds, especially around cations. Finally, new hydrogen bonds can be formed between water molecules and anions.

1.3 THE O–H STRETCH VIBRATION

We have already remarked that in the study of aqueous solvation, hydrogen bonds are extremely important. The ideal probe of hydrogen-bond interactions is the O–H stretch vibration, since its frequency is directly correlated with the hydrogen-bond length, i.e. the intermolecular distance.

In figure 1.1, the absorption spectrum of the O–H stretch vibration in liquid water is shown. The symmetric and antisymmetric stretching vibrations in liquid H_2O are spectroscopically nearly indistinguishable. To avoid this latter effect, experimental work has mainly been devoted to dilute solutions of HDO in D_2O,[91,90,137,139] where the O–H

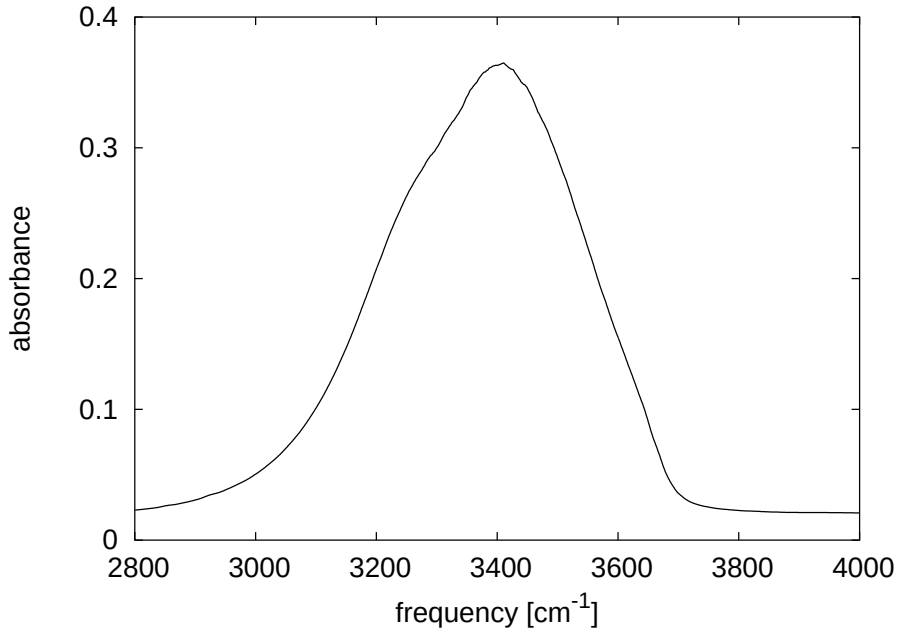

FIGURE 1.1. Spectrum of the O–H stretch vibration in liquid water.

and O–D stretching bands are well separated, being centered at 3400 and 2505 cm^{-1}, respectively, while the chemical (hydrogen-bonded) structure remains nearly unchanged.

Experimentally[83,84] and theoretically,[74] it has been shown that the frequency of the O–H stretch vibration and the hydrogen-bond length are linearly correlated within a large regime for water–water and ion–water hydrogen bonds. It appears that a stronger hydrogen bond weakens the covalent O–H bond, and reduces its vibrational frequency.

Due to the variation of hydrogen-bond lengths in liquid water, the spectrum is strongly inhomogeneously broadened (the term 'inhomogeneous' refers to the fact that the broadening results from the different environments that the molecules have in the liquid). The spectrum can be thought of as the sum of individual absorption bands. The width of one individual band is called the homogeneous linewidth. Experimentally, inhomogeneous broadening with an exchange between subbands that is faster than the time resolution of the experiment, cannot be distinguished from homogeneous broadening. Recent photon-echo experiments estimate the homogeneous linewidth between 60 and 120 cm^{-1}.*[121,120,119,142] Lifetime-broadening alone leads to a homogeneous linewidth of 7 cm^{-1}.[3]

Infrared[126,125,58,10,118] and Raman[57,124,126,127] spectroscopic studies show that the most significant change of the O–H stretch spectrum is due to the anions. For most halogenic anions, notably Cl^-, Br^- and I^-, a new component appears on the blue side of the spec-

*In this thesis, we will often use the wavenumber unit for frequency

trum, depending on the nature of the anion and its concentration. Only for the strongest electronegative ion, F^-, an increased absorption at the red side of the spectrum is observed. It was concluded that in aqueous salt solutions, a new hydrogen bond is formed between the anion and the water molecule, which we will denote O–H$\cdots$X$^-$, where X represents the anion, the solid line connecting O and H a covalent interaction, and the dotted line denotes the hydrogen bond. For X^- = Cl^-, Br^- or I^-, this hydrogen bond is weaker than the O–H$\cdots$O hydrogen bond between two water molecules, and its strength decreases within the halogenic series. The decreasing redshift can be understood from the increasing diameter (decreasing field strength) in the series F^-, Cl^-, Br^-, I^-. For the even bigger perchlorate ion (ClO_4^-), the redshift is so small that the anion-bonded O–H absorption is well separated from the bulk absorption. The spectrum of a solution containing ClO_4^- is shown in figure 8.1.

The spectral changes are too small to allow for an accurate study of the individual components. ClO_4^- forms one of the few exceptions. Still, an approximate spectrum of the individual components can be extracted by subtracting known components from the full spectrum.[10] To isolate the anion contribution, e.g. I^- of a solution of NaI in water (HDO:D_2O), one can subtract the other components in two steps: first, the background absorption of pure D_2O with NaI must be subtracted. Second, a similarly prepared difference spectrum of a Na^+-containing salt with a large anion, that does not change the spectrum, must be subtracted. The absorption component thus obtained contains the absorption by the O–H stretch vibration in O–H$\cdots$$I^-$ hydrogen-bonds, but may not be free from (inseparable) disturbances of the bulk-water structure by the I^- ion. In addition, the absorption likely is still inhomogeneously broadened, as in pure water, as a result of which no information on the dynamical behaviour of these hydrogen bonds can be obtained from the spectrum.

The effect of cations on the absorption spectrum is smaller than that of anions. For the single-charged, moderately large cations Na^+ and K^+, almost no effect is observed. In a solution containing Li^+ or small double-charged ions such as Be^{2+} or Mg^{2+}, the absorption at the red side of the spectrum increases. In contrast to the anion, cations cannot participate in hydrogen bond formation; their influence is limited to polarizing existing hydrogen bonds. The presence of anions and cations makes the absorption band of the O–H stretch vibration even more inhomogeneous than it already was for pure liquid water, which makes it even more difficult to obtain sensible information out of the absorption spectra.

It will be shown in this thesis that non-linear spectroscopy on the O–H stretch vibration of O–H$\cdots$X$^-$ groups is an ideal tool to study the dynamical behaviour of the molecules in the solvation shells of anions. In real solutions, the dynamics of the solvating molecules is probed directly and exclusively.

1.4 OUTLINE

In this thesis, the dynamical behaviour of solvation shells is studied using femtosecond mid-infrared pump–probe spectroscopy. In chapter 2, this experiment is described that has significant advantages over linear spectroscopy, as well as over the techniques discussed in 1.1. In chapter 3 and chapter 4, the vibrational relaxation of the O–H stretch mode

is described, focusing on its dependence on temperature, and on the nature and concentration of the ions, respectively. A critical discussion of recently published related work of Laenen and Thaller is presented in chapter 5. Experiments on the dynamics of the anionic hydrogen bond are discussed in chapter 6. The reorientational motions of solvation shells are studied in chapter 7. The final chapter is devoted to the study of the changes induced by ions in the bulk-water structure, i.e. the hydrogen-bond structure of water outside the first solvation shell.

2 Experimental method and setup

In this chapter, the experiment is explained. First, in section 2.2, some basic principles of (non-linear) spectroscopy are summarized. In section 2.3, we describe the way in which the femtosecond mid-infrared pulses are generated from a commercial 800 nm laser source, and finally we describe the pump–probe setup in section 2.4.

2.1 Introduction

In the past, a lot of information on the hydrogen-bond structure of liquid water has been obtained with spectroscopy of the O–H stretch vibration. However, due to the considerable inhomogeneous broadening, which is even larger in salt solutions, no information on the hydrogen-bond dynamics can be extracted. To this end, new techniques have been developed that make use of short laser pulses. In the mid-infrared, pulse durations of 200,[34] 150[41] or even 100 fs[141] have become available in the past decade. This opened a whole new field of research, since on the molecular scale, most dynamical processes in liquids like water take place within picoseconds.

In most ultrafast spectroscopy experiments, the pump–probe technique is used. In this technique, the (strong) pump pulse prepares the system in a certain state, e.g. exciting molecules or inducing some chemical reaction. The probe beam monitors the change of the system, by being attenuated, amplified, or refracted as a result of the changes in the sample. Dynamical information can be obtained by delaying the pump and probe beams with respect to each other. The time resolution is characterized by the cross-correlation time of the two pulses. If the excitation pulse has a narrow spectrum and the absorption that is studied is inhomogeneously broadened, only a subset of the molecules is excited, characterized by their absorption frequency. A 'hole' will then appear in the absorption spectrum, for which reason this technique is referred to as 'hole-burning' spectroscopy. In the context of this thesis, pump–probe spectroscopy is used to study the vibrational excitation of water molecules. The vibrational lifetime T_1, and, by performing polarization-resolved measurements, the orientational-correlation time τ_{or} of the water molecules are measured. In the next section, we will explain these techniques in more detail.

Another spectroscopic technique that can be used to study liquids is photon-echo spectroscopy. With this technique, in various forms and degrees of complexity, the homogeneous-dephasing time, vibrational lifetime, rotational-correlation time and spectral-diffusion time can be measured. The latter time can also be determined with hole-burning spectroscopy.

In this thesis, we are primarily interested in the intermolecular (hydrogen-bond) dynamics of water molecules in aqueous salt solutions, for which the O–H stretch vibration is an excellent probe. It is studied using femtosecond mid-infrared pump-probe spectroscopy. Unlike electronic excitations, the energy of this vibration is sufficiently small

that the spontaneous dynamics of the system is not significantly changed.

2.2 PRINCIPLES OF PUMP–PROBE SATURATION SPECTROSCOPY

2.2.1 LAMBERT–BEER LAW

If I denotes the intensity of a light beam directed along the x-axis, the absorption during its passage through a layer of absorbing material is given by the following relation:

$$dI = -\sigma\rho_3 I dx, \tag{2.1}$$

where σ is the absorption cross section, ρ_3 the concentration (in moles/m^3) of the absorbing species. Integrating over the layer of thickness d, and dividing by the initial light intensity I_0, the transmittance T is obtained:

$$T = I/I_0 = e^{-\sigma\rho_3 d}. \tag{2.2}$$

For convenience, in the remainder of this section we will use a concentration per unit of surface perpendicular to the incoming light: $\rho = \rho_3 d$. The product $\sigma\rho$ is called the absorbance α of the absorbing layer. The absorbance is proportional to the concentration of the absorbing molecule.

In the experiments described in this thesis, the absorbing species is the O–H group of a water molecule, more specifically an HDO molecule (see section 1.3). Central in the experiments is the excitation of water molecules using a powerful pump beam, while monitoring the population of excited molecules by a weak probe beam. The probe beam measures the absorption of either the $0\rightarrow1$ or the $1\rightarrow2$ vibrational transition, that can be distinguished by their frequencies (see the Appendix at the end of this chapter). By varying the time delay between the two laser pulses, the evolution of this population can be monitored.

When both pump and probe pulses are tuned to the $0\rightarrow1$ transition, the population of absorbing species, i.e. the water molecules in the vibrational ground state, will decrease as a result of the interaction with the pump beam. At the same time, the excited molecules will show stimulated emission. According to the Einstein theory of absorption, stimulated emission occurs from the excited state, with the same probability as absorption.[79] Both decrease of ground-state population and excited-state stimulated emission lead to a decrease of the absorbance of the sample for the probe beam. This is called 'bleaching' of the sample.

Excitation of a fraction f of the molecules will lead to a change in the absorbance at the $0\rightarrow1$ transition:

$$\ln(I/I_0)^* = -(1-f)\sigma\rho + f\sigma\rho, \tag{2.3}$$

where the first term is due to absorption of non-excited molecules, and the second due to stimulated emission from the excited state. Defining $T_0 = I/I_0$ and $T = (I/I_0)^*$, equation (2.3) becomes

$$\ln(T/T_0) = 2f\sigma\rho. \tag{2.4}$$

Alternatively, the probe beam may be tuned to the frequency of the 1→2 transition. For anharmonic vibrations, the excited molecule absorbs at a different frequency. In the case of the O–H stretch vibration of a water molecule, the 1→2 transition is redshifted with respect to the 0→1 transition. At room temperature, the number of water molecules in excited states is negligible; the only excited molecules are the ones that were excited by the pump pulse to the $v = 1$ state. The absorbance at the 1→2 transition becomes different from zero only after an excited-state population has been created by the pump pulse. There is no stimulated emission due to the absence of population in $v = 2$. For the excited-state absorption we find, equivalent to equation (2.4),

$$\ln(T/T_0) = -f\sigma^*\rho. \tag{2.5}$$

σ^* is the absorption cross section for excited-state absorption. It is approximately twice as large[*] as the ground state absorption σ, so that the pump–probe signals are comparable in size for both situations.

The quantity $\ln T/T_0$ is the principal quantity studied in this thesis. It is linearly proportional to the ground-state population change $f\rho$ induced by the pump pulse.

2.2.2 VIBRATIONAL LIFETIME

The population of excited molecules, $n_x \propto f\rho$, will decay exponentially in time. The exponential decay is simply the result of equal transition probability per unit of time: the number of molecules that relax between t and $t + dt$, dn_x, is proportional to the number of excited molecules, n_x, which leads to

$$n_x(t) = n_x(0)\, e^{-t/T_1}\, \Theta(t), \tag{2.6}$$

where $\Theta(t)$ is the Heavyside function, that ensures that the excitation takes place at $t = 0$. T_1 is the lifetime of the excitation.[†]

If there are n absorbing species, their individual absorption (changes) can be simply added. For example, equation (2.5), combined with equation (2.6), becomes

$$\ln(T/T_0)(t) = \sum_{i=1}^{n} f_i\sigma_i^*\rho_i\, e^{-t/T_{1,i}}\, \Theta(t). \tag{2.7}$$

Sofar, the excitations considered were created instantaneously at $t = 0$. To take the finite pump-pulse duration into account, we should convolve the excited population with the pump pulse intensity. However, we also need to take into account the finite probe-pulse duration, since this is what measures the transmission change in equation (2.7). Therefore, we must also convolve with the probe-pulse intensity profile. Since the operation of convolution is distributive, $F * (f + g) = F * f + F * g$, and associative, $F * (G * f) = (F * G) * f$, we should convolve each term in equation (2.7) with the cross correlation of pump and probe pulses, which can be easily determined experimentally (see section 2.3.5). The cross correlation function is approximately gaussian:

[*] It can be shown that for harmonic potentials, the transition dipole moment for the 1→2 transition is exactly twice as large as for the 0→1 transition

[†] The symbols T_1 and T_2 are used for the vibrational lifetime and the dephasing time, respectively. The homogeneous linewidth $\Delta\nu$ is given by $\pi\Delta\nu = \frac{1}{2T_1} + \frac{1}{T_2}$.

$cc(t) \propto \exp(-t^2/2d^2)$. We may now perform the convolution to obtain the following function:

$$\ln(T/T_0)(t) = \sum_{i=1}^{n} A_i e^{-t/T_{1,i}+(d/T_{1,i})^2/2} \left[1 + erf\left(\frac{t}{\sqrt{2}d + d/(\sqrt{2}T_{1,i})}\right)\right]. \qquad (2.8)$$

The amplitudes A_i depend on the concentration and absorption cross section of the species. The $1 + erf(-t/T_1)$ ensures that there is no absorption change before the pump pulse has arrived. There are $2n + 1$ free variables, the amplitude and lifetime of each component, and the cross correlation time. Equation 2.8 will be used in the main part of this thesis to describe the pump–probe signals. It is nothing more than a sum of exponentials, convolved with the gaussian cross correlation.

2.2.3 Background absorption

It should be noted that, by taking the absorption difference in equations (2.4) and (2.5), any constant background absorption is cancelled. For the samples used in the experiments covered in this thesis, the high-frequency wing of the O–D stretch vibration forms the main contribution to the background. In principle, it is not exactly constant since this vibration can be excited as well, and contribute to the pump–probe signal. The non-linearity of the measurement strongly reduces this contribution. If the O–D stretch band is modeled by a gaussian function, with a central frequency of 2500 cm^{-1} and a width of 170 cm^{-1}, its absorption should have decreased with a factor of 10^6 at 3400 cm^{-1}, the center of the O–H stretch frequency. Therefore, rather than being a pure O–D stretch mode, this background absorption probably results from a combination tone of the O–D stretch mode and some other mode, e.g. a libration. Such a combination mode has a very low cross section, that can be roughly estimated as follows. In the samples used, the background absorption is typically an order of magnitude weaker than the O–H stretch absorption, depending on the proton concentration. However, since the density of O–D groups is about two orders of magnitude higher than of the O–H groups, the absorption per molecule (i.e. the cross section) at the excitation frequency is three orders of magnitude smaller. Since the excited fraction is proportional to σ, the background contribution to the pump–probe signal will be three orders of magnitude smaller than the real signal, which is outside the dynamic range of our experiments.

2.2.4 Polarization

Equations (2.1–2.8) were formulated for unpolarized light. The laser pulses that are used in the experiments however have a well-defined polarization. The probability to excite an O–H stretch vibration depends on the angle θ between the O–H vector and the polarization of the light. Vibrational excitations are dipole transitions, for which the excitation probability is proportional to $\cos^2(\theta)$. Therefore, if the pump is directed along the z axis ($\theta = 0$), the normalized initial distribution of the orientation of an ensemble of excited O–H groups is given by $g(\theta) = 3\cos^2(\theta)/4\pi$. The absorption of a probe beam with polarization vector (ϕ_p,θ_p) can then be calculated by performing the integration

$$\alpha = \alpha_o \int g(\theta) \cos^2 \chi \, d\Omega, \tag{2.9}$$

where $\int d\Omega = \int d\phi \int \sin\theta \, d\theta$, and χ is the angle between the probe polarization and the integration variables θ and ϕ. α_o is the absorption if the polarization would not matter. For a probe polarization along (0,0), i.e. parallel to the excitation axis, $\cos^2 \chi$ simplifies to $\cos^2 \theta$. The integral then gives $\alpha = 3\alpha_o/5$. When the probe polarization is perpendicular to the excitation axis, say $(\phi_p,\theta_p) = (\pi/2,\pi/2)$, $\cos\chi = \sin\theta \ \sin\phi$. In this case, $\alpha = \alpha_o/5$.

ROTATION-FREE MEASUREMENTS It now seems logical to do the experiments with equal pump and probe polarizations, to obtain as large as possible signals. However, it has not yet been taken into account that the molecules may reorient. The initial $\cos^2\theta$ distribution will evolve to being completely isotropic. This reorientation leads to a faster decay of T/T_o at parallel polarizations, and a slower decay at perpendicular polarizations.

It is clear that a rotating molecule will disappear out of the 'angular window' of the parallel probe, and appear in the perpendicular probe window. If we define $\alpha_{rf} = \alpha_{||} + 2\alpha_{\perp}$ (the factor 2 is there because of both perpendicular directions, we measure only one), we are sure that each molecule always contributes equally to α_{rf}, independent of its orientation. The same is obtained by rotating the polarization of the probe beam such that the projection on the parallel and perpendicular axes have the same ratio, i.e. at an angle of $\arctan\sqrt{2} \sim 54.7$ deg. This angle is sometimes called the 'magic angle', for mysterious reasons.

ANISOTROPY MEASUREMENTS Instead of eliminating the rotational effects on the signals and retain the vibrational relaxation, one can also do the reverse, and construct a parameter that only reflects the reorientational motion, being independent of vibrational relaxation. A possible definition for such a parameter, that we will call the anisotropy parameter R, is

$$R = \frac{\alpha_{||} - \alpha_{\perp}}{\alpha_{||} + 2\alpha_{\perp}}. \tag{2.10}$$

The denominator in the definition of R is just the rotation-free signal α_{rf}. It can be shown that R is proportional to the ensemble average of the second Legendre polynomial.

2.3 PULSE GENERATION

2.3.1 INTRODUCTION

The vibrational modes in a water molecule are optically active in the mid-infrared.[49] The O–H stretch vibration in liquid water absorbs around 3400 cm^{-1} (3 μm) (figure 1.1). At these wavelengths, however, there are no laser sources available that deliver short and powerful pulses. Therefore, frequency-conversion processes in nonlinear crystals such as $LiNbO_3$ must be used to convert the wavelengths of the available short laser pulses (e.g. 1064 nm for Nd:YAG lasers or 800 nm for Ti:sapphire lasers) into mid-infrared light. Because this conversion requires a high-intensity source laser, the experiments that could be performed have been limited by the progress in pulse duration and energy of these lasers.

In the 1970's, Nd:glass lasers were developed,[73] producing 6 ps pulses with an energy of 1 mJ, at a rather low repetition rate (less than 1 Hz). They were followed up by Nd:YAG lasers, that produced longer pulses, typically 20 ps, at a higher repetition rate, 10 Hz, with an energy of 40 mJ.[63] With the advent of Ti:Sapphire lasers, and after the discovery of self-modelocking in this material in 1991,[116] powerful sub-picosecond laser pulses could be produced.

The techniques to compress the laser pulses have developed in the past decade. Passage of the laser puls through optical materials, inevitable in any laser system, induces chirp: temporal separation of different frequency components. A pair of gratings or prisms can be used to compensate for linear chirp by letting the different frequency components follow paths of different length. Alternatively, specially made double-chirped mirrors can be used to induce a specific chirp on the reflected beam. A modern way to compress laser pulses comprises the use of a pulse-shaper, that consists of an array of liquid crystal cells, placed between two gratings. The gratings spectrally disperse the beam, so that different part of the spectrum pass through different cells. The cells can alter the phase and/or amplitude of each frequency component by applying a voltage over the cell. In this way, the pulse can be shaped to any desired form, including the shortest possible pulse. It is usually operated such that a computer determines the required values of the applied voltages by optimizing the outcome of some event that depends on the pulse duration, such as second-harmonic generation.

With these pulse-compression techniques, pulse durations of 4.5 fs can be achieved.[92,142] Recently, for the first time attosecond laser pulses have been detected.[98]

2.3.2 PARAMETRIC GENERATION

In this section, we will describe in short the process of parametric generation and amplification of light. For more details, we refer to textbooks such as Refs. 13, 113.

In nonlinear media, the relation between an electric field $\vec{E}$, and the polarization $\vec{P}$ it induces in a medium , is given by

$$\vec{P} = \chi^{(1)}\vec{E} + \chi^{(2)}\vec{E}^2 + \chi^{(3)}\vec{E}^3 + \cdots \tag{2.11}$$

$\chi^{(2)}$ is the second-order susceptibility, and $\vec{P}^{(2)}(t) = \chi^{(2)}\vec{E}^2(t)$ the second-order polarization. When two optical fields with frequencies ω_p and ω_s are present in the medium, the induced polarization will have a component that oscillates with a new frequency $\omega_i = \omega_p - \omega_s$ ($\omega_p > \omega_i > \omega_s$). This component of the polarization will generate an electric field with frequency ω_i. Thus, energy is transferred from the fields at ω_p and ω_s to the field at ω_i. The field with frequency ω_p is called the pump field, those at ω_s and ω_i are called signal and idler fields, respectively. In principle, new fields can be generated at all combinations of the input fields, but usually at most one combination will be amplified effectively, determined by the phase-matching condition explained below. In the rest of this section, when speaking of polarization, the polarization of the light waves is meant, in contrast to the above induced crystal polarization.

For the conversion to be efficient, the phase-matching condition, $\vec{k}_p = \vec{k}_s + \vec{k}_i$, or, equivalently, $\omega_p n_p = \omega_s n_s + \omega_i n_i$, where n is the refractive index, has to be satisfied. In media with normal dispersion, the refractive index increases with frequency. In that

case, $n_p > n_i > n_s$, so that the phase-matching condition cannot be fulfilled. In a birefringent crystal, however, the index of refraction, experienced by a light beam, depends on its polarization with respect to the optical axis of the crystal: light polarized parallel (extra-ordinary) to the optical axis will experience a different index of refraction than light polarized perpendicular (ordinary) to it. If the three interacting waves do not all have the same polarization, it is possible to satisfy the phase-matching condition by changing the orientation of the optical axis, i.e. by rotating the crystal, which affects the index of refraction differently for different polarizations. Instead of rotating the crystal, one can also change pressure or temperature to change the index of refraction.

The second-order susceptibility in equation (2.11) is actually a tensor, relating all components of the input fields to the induced polarization in the medium. To assure effective conversion, the configuration of the three polarizations are chosen such that the appropriate component of this tensor is as large as possible.

In our setup, parametric generation and amplification is used, first in the TOPAS (section 2.3.4), generating signal and idler beams from an 800 nm pump beam (amplified quantum noise), and secondly in generating an idler wavelength of 3 μm out of a pump beam of 800 nm and signal beam of 1100 nm (parametric amplification, section 2.3.5). The following coupled equations hold for the amplitudes A of the signal, idler and pump waves:

$$\frac{dA_s}{dz} \propto \frac{\omega_s}{n_s} A_p A_i, \tag{2.12}$$

$$\frac{dA_i}{dz} \propto \frac{\omega_i}{n_i} A_p A_s, \tag{2.13}$$

$$\frac{dA_p}{dz} \propto \frac{\omega_p}{n_p} A_s A_i, \tag{2.14}$$

where n_s, n_i, n_p denote the indices of refraction for the polarization of the signal, idler and pump beams, respectively, and z denotes the distance that has been travelled through the medium. As the conversion efficiency for these processes is usually less than 10 % (in our case, typically 2 %), we can neglect the change in A_p due to energy transfer to the signal and idler waves. From equations (2.13) and (2.12) it can be seen that, in order to generate a signal (idler) field, no signal (idler) input field is needed: it is generated from the idler (signal) and pump fields. It is even possible to generate the two fields by one pump field alone: in this case, quantum fluctuations in the medium act as input signal or idler field. This is called superfluorescence.

2.3.3 800 NM

The laser setup used for the experiments in this thesis consists of a Millennia pump laser, a Tsunami Ti:sapphire oscillator, and a Quantronix Titan regenerative amplifier (RGA) / multipass laser system.

The oscillator is pumped by 5 W continuous light at 532 nm. Self-modelocking in the Ti:sapphire crystal ensures that a short pulse of 800 nm light, rather than a continuous beam, oscillates in the laser cavity. At each roundtrip, at a frequency of 80 MHz, part of

the pulse leaves the cavity. The pulse duration is below 100 fs, and the energy per pulse is about 10 nJ. Unfortunately, this energy does not suffice for the subsequent conversion steps into mid-infrared frequencies.

To amplify the pulses, they are first stretched to approximately 100 ns, by passing the pulses over a grating, inducing a linear chirp. The stretched pulses are coupled into the RGA, in which a Ti:sapphire crystal is pumped by approximately 3 W of 527 nm light from a Nd:YLF laser. This laser delivers pulses of a few hundred nanoseconds at 1 kHz, synchronized with the oscillator output. One in 80.000 pulses from the oscillator is selected to be amplified in the RGA. Without having been stretched, the pulse intensity would be too high and would damage the Ti:sapphire crystal. The amplified pulse, with an energy of approximately 500 μJ, is further amplified during two passes through another Ti:sapphire crystal, that is pumped with 13 W from the same Nd:YLF laser that pumps the RGA. The pulse energy is now 4 mJ. Finally, the pulses are compressed to some 100 fs. The compressor has a transmittance of approximately 70%, so that a pulse energy of almost 3 mJ is left for conversion into mid-infrared light.

2.3.4 TOPAS

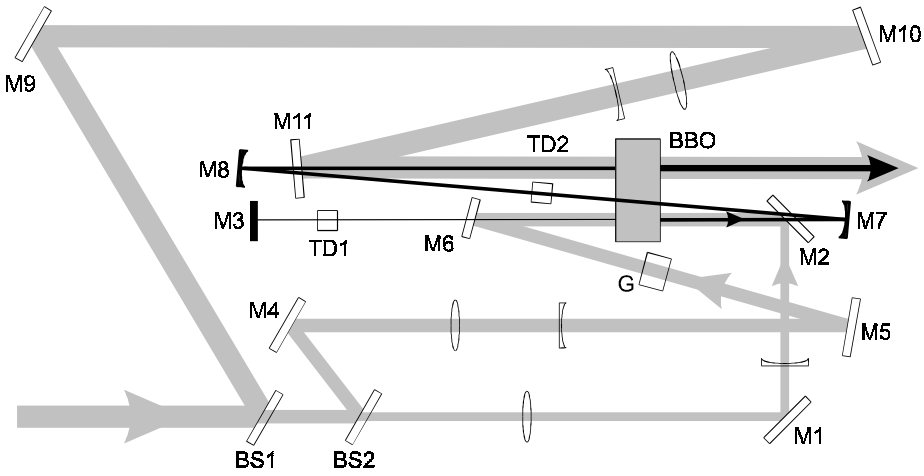

FIGURE 2.1. Schematic picture of the TOPAS. The broad grey lines denote 800 nm pump light, thinner black lines are used for the signal and idler beams. The broader the line, the more intense is the light. Abbreviations: M1-M11: dielectric mirrors, except M3,M7,M8: broadband metallic mirrors; BS1,BS2: beam splitters; G: glass plate; TD1,TD2: birefringent plates, used to induce a time delay between signal and idler beams; BBO: β-barium borate, nonlinear crystal.

The first conversion step takes place in the TOPAS (Travelling wave Optical Parametric Amplifier of Superfluorescence), an optical parametric generation and amplification device (OPG/OPA). It is capable of generating mid-infrared light from a 800 nm pump beam. It is based on β-barium borate (BBO). BBO is used because of its high damage threshold, which is necessary because the 800 nm light has to be focused in the crystal

quite strongly. BBO absorbs at wavelengths $> 2.6\ \mu$m, which limits the tunability range from ~ 1.1 to $\sim 2.6\ \mu$m. Conversion is most efficient at degeneracy, when signal and idler have the same wavelength (1600 nm).

In our setup, we make use of two TOPASes of different generations. The older one is used for the probe branch, and is described below. The newer one operates more stably and is used for generation of the pump beam. The differences between the two versions will be pointed out.

A schematic picture of the probe-TOPAS is shown in figure 2.1. Inside the TOPAS, the pump beam is split in three parts, each part passing the crystal at a different moment. In the first pass (M1–M3), broadband mid-infrared signal and idler beams are created from amplification of quantum noise (superfluorescence). In order to be efficient, the first pass 800 nm beam has to be very intense, and is therefore down-telescoped fairly strongly. The signal is redirected toward the crystal, to arrive simultaneously with the second-pass pump beam. Signal and idler have different polarizations, so the idler can be separated in time from the signal by passing them through a birefringent plate. This is done to prevent both the loss of conversion efficiency due to re-conversion into 800 nm, and the start of an additional amplification processes from the idler pulse, resulting in double-pulse structures. In the third and final pass, the main part (95 %) of the pump intensity is used for amplification of the pre-amplified signal pulse. The frequencies of signal and idler are tuned by rotating the BBO crystal.

The newer pump TOPAS differs from the probe TOPAS in two aspects. First, the first pass is replaced by three passes. Second, the mirror M3 is replaced by a movable grating, that is rotated so that a higher order reflection of the signal generated in the first three passes is redirected toward the crystal. In this way the separation between signal and idler pulses is accomplished without the use of an extra dispersive element, that results in elongation of the pulses.

In our setup, 0.8 and 0.3 W of the 800 nm light is used to pump the pump and the probe TOPAS, respectively. To generate 3000 nm from 800 nm light, 1100 nm light from the TOPAS is needed as a seed pulse. Since 1100 nm is on the edge of the range, we tuned the TOPAS to generate 2200 nm light instead, that is efficiently converted into 1100 nm light, by second harmonic generation in another BBO crystal. The total energy of signal and idler pulses (1270 nm and 2200 nm) produced by the probe TOPAS was approximately 120 μJ. The 1100 nm light had an energy of 10 μJ per pulse.

The TOPASes are based on the generation of superfluorescence. Today, newly built devices usually start from white-light generation. In this way, the generated mid-infrared pulses can be more stable and possibly shorter.[141] It may improve the setup to replace the TOPASes by seed-generating setups that use white-light generation.

2.3.5 MID-INFRARED PULSE GENERATION

To generate mid-infrared light around 3 μm, the 1100 nm seed and 800 nm pump pulses are collinearly directed through a KTP crystal. The conversion is most efficient for high pump intensity. Therefore, a telescope is used to make a collimated pump beam, as narrow as possible without damaging the crystal. To improve the beam profile of the seed pulse, sometimes a spatial filter is used, that consists of a 50 or 100 μm pinhole in the focus of a +50/+100 mm telescope.

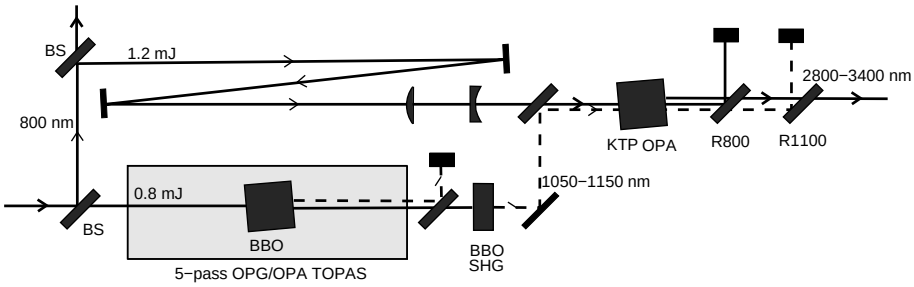

FIGURE 2.2. Schematic picture of the pulse generation scheme. The pump and probe pulses are independently produced following this scheme to enable the independent tuning of their frequencies. Each branch has a TOPAS, an optical parametric generation and amplification stage based on a BBO crystal, that is used to generate 1250 nm (signal) and 2200 nm (idler) light. The idler is frequency-doubled in BBO, obtaining an 1100 nm pulse that is used as a seed pulse in the final conversion step, where a fresh part of the 800 nm light is converted into 1100 nm and 3000 nm light using a 5 mm KTP crystal. The indicated intensities of 800 nm light are for the pump pulse; for the probe pulse, less intensity is used: 0.3 μJ for the TOPAS, and 0.15 μJ for pumping the KTP crystal.

By tuning the seed pulses and adjusting the phase-match angle of the KTP crystal, the pulses can be tuned from 2600 to 3500 nm ($\sim$2900–3800 cm^{-1}). The pump (probe) pulses have a typical energy of 20 (1) μJ and a bandwidth of 80 (60) cm^{-1}. The broader pump spectrum is probably due to saturation at the center frequency in generating the pump pulse. The cross-correlation trace typically has a width of 300 fs, which is measured either by second harmonic generation in a $LiIO_3$ crystal, or two-photon absorption in a semi-conductor such as germanium, as a function of delay between pump and probe pulses. Mathematically, the crosscorrelation of two light beams is the convolution over the time coordinate of their intensities. Measuring the crosscorrelation can easily be done using the pump-probe setup, described in section 2.4.1.

The spectral widths of the pump and probe pulses can be reduced to $\sim$40 cm^{-1} by using two KTP crystals to generate the mid-infrared light instead of one; this was done in chapter 4 to gain pulse-to-pulse stability, and in chapter 5 to narrow the bandwidth. By doing so, the pulses are elongated to 450 fs.

2.4 PUMP–PROBE MEASUREMENTS

2.4.1 PUMP–PROBE SETUP

The principles of pump–probe saturation spectroscopy have been explained in section 2.2. To perform this type of measurement, one needs a powerful pump beam to excite molecules to an excited state, and a weaker probe beam to measure the induced transmission change. It is required that the probe beam can be delayed with respect to the pump beam, and that its polarization can be changed. The measured quantity is T/T_0, where

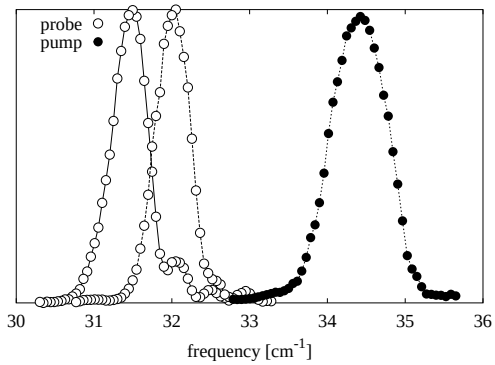

FIGURE 2.3. Typical spectra of the pump and probe pulses used in the experiments. The probe spectra are narrower because 2 KTP crystals are used instead of one.

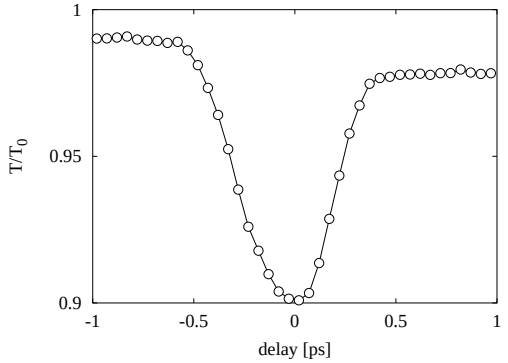

FIGURE 2.4. Typical cross-correlation trace of the pump and probe pulses used in the experiments (1 KTP crystal). The traces are obtained by two-photon absorption in the semiconductor Ge.

$T = I^*/I_{ref}$ is the normalized intensity of transmitted probe light in the presence of the pump; $T_0 = I/I_{ref}$ is the same quantity in absence of the pump. To perform polarization-resolved measurements, the transmitted probe light is detected at different polarizations using polarizers.

The pump–probe setup is depicted in figure 2.5. In the pump beam, a chopper chops at 500 Hz, blocking every other pump pulse. The beam is focused in the sample using a +150 mm CaF_2 lens. The probe beam is delayed with respect to the pump beam using a delay stage, that can be set with an accuracy of 1 μm, i.e. with a temporal resolution of 1.5 fs. The reflection of a CaF_2 wedged window is used to measure the reference intensity. Since the pulse-to-pulse stability, in particular of the probe pulses, is not always satisfactory, it is necessary to compensate for these intensity fluctuations. For the pump pulses this is not so easily done. The best option would be to measure the pump intensity,

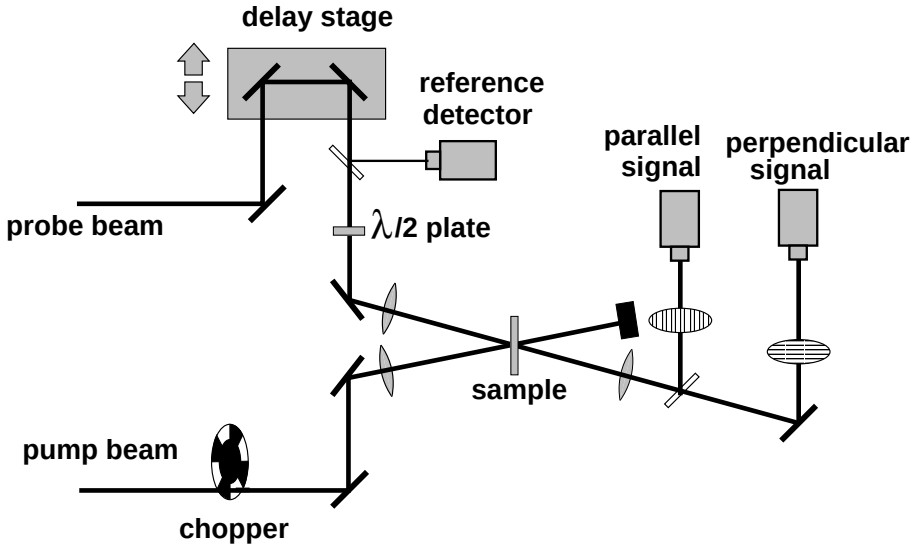

FIGURE 2.5. Schematic picture of the pump–probe setup. Here, the probe beam is detected parallel as well as perpendicular to the pump pulse. When only rotation-free measurements are required, one signal detector without a polarizer is used.

and only count the data point if the pump intensity falls within some specified range; this is not done in our measurements. Fortunately, the stability of the pump pulses is quite good, owing to the more stable pump-TOPAS (section 2.3.4). The intensity fluctuations of the pump pulses are typically within a few percent. A zero-order half-wave plate is used to rotate the polarization of the probe beam over 54.7 degrees (the 'magic angle'), in case the rotation-free signal is detected, or over 45 degrees if the anisotropy is measured (section 2.2.4).

The probe beam is focused in the sample using a +100 mm CaF_2 lens. The focal length of the lens used to focus the probe is shorter than that of the pump, to make sure the probe has a smaller focus; in this way, the pump intensity is (almost) constant over the probe focus. This is necessary for the following reason: the desired quantity is $\ln(T/T_o)$ averaged over the focal region, i.e. $\sum \ln(T_i/T_{o,i})$, while the actual quantity we determine is $\ln(\sum T_i/T_{o,i})$. These two quantities are the same only if the T_i and $T_{o,i}$ do not depend on i, i.e. on variations within the focus.

The measurements take place in a fully automated way, thanks to the computer program Irismeet[†]. It records the transmission changes T and T_o at a rate of 500 Hz, and provides averages of $\ln(T/T_o)$ over a specified time interval. A detailed description of the data acquisition can be found in Refs. 89, 90.

CROSS-PHASE MODULATION ARTEFACT Care must be taken that no 'artefacts' in the measurements are mistakenly interpreted as 'signals'. One such artefact is due to cross-phase

[†]The program was written by Han-Kwang Nienhuys, and was later further developed by Frederik van den Broek to incorporate new detection techniques, not covered in this thesis

modulation: the index of refraction can change due to the powerful pump field. This results in a change of the spectrum of the probe pulse, and consequently a changed transmission during the time the pump pulse is present, if the absorption is not constant with frequency. Typically, a 'swing' is seen around delay zero. In the experiments covered in this thesis, such signals are sometimes observed, but with a much lower amplitude than the real saturation signals. Furthermore, in the interpretation, we only consider the data at delays much larger than the cross correlation time of the pulses, so that the effect is not of great importance here.

COHERENT ARTEFACT Another measurement artefact that should be taken care of, is the 'coherent artefact', that shows up in pump–probe delay scans as a sharp peak around delay zero if the pump and probe frequencies are the same. Physically, interference of the pump and probe pulses in the sample leads to the formation of a grating that can scatter pump light in the direction of the probe. It can be shown[33,133] that at delay zero this coherent-coupling peak should have the same amplitude as the pump–probe signal. In this thesis, most measurements have been performed with different frequencies for the pump and probe beams, in which case no coherent coupling occurs. Moreover, because of the large bandwidths of the transitions studied, this effect will only be important when the pump and probe pulses overlap in time.

2.5 APPENDIX: POTENTIALS AND ENERGY LEVELS

2.5.1 THE HARMONIC OSCILLATOR

The harmonic oscillator provides the simplest approximation of any system that is in a state near its potential minimum, and in many cases suffices to describe the main characteristics. The existence of equilibrium implies that the derivative of the potential to any coordinate R is zero, so that the first non-zero term in a Taylor expansion will be the quadratic term. The harmonic potential can thus be written as

$$V_{harm}(r) = \frac{k}{2}(r - r_0)^2, \tag{2.15}$$

where r_0 is the equilibrium value of the (generalized) position coordinate.

With this potential, the eigenvalues of the Schrödinger equation become the well-known

$$E_n = \hbar\omega\ (n + \frac{1}{2}). \tag{2.16}$$

Transitions between two levels involve a change in energy of $\hbar\omega$. This energy can also be expressed as $\hbar\sqrt{k/m_r}$, where m_r is the reduced mass of the oscillator. Thus, similar to the classical harmonic oscillator, the oscillation frequency, and the transition frequency, are proportional to the inverse of the square root of the reduced mass.

The discrete energy levels are a quantum mechanical effect, and so are the selection rules. For a dipole transition, the probability (per unit of time) to go from one state ψ_1 to another ψ_2 is given by

$$P \propto |\langle\psi_2|x|\psi_1\rangle|^2. \tag{2.17}$$

'Forbidden' transitions are those for which the above integral is equal to zero. For the harmonic oscillator, it turns out that only transitions for which $n_2 = n_1 \pm 1$ are 'allowed'.

It is readily understood that the harmonic oscillator cannot provide a complete description of intermolecular motion. For example, it cannot be symmetric: the two molecules will experience a strong repulsion when they approach each other; on the other side, since dissociation is possible, the potential energy must go to zero at large distances. Several other potentials are used to more accurately describe intermolecular dynamics. One of these is the Lennard-Jones potential, $V_{\mathrm{LJ}}(r) = C\left[\frac{1}{2}(\frac{r_0}{r})^{12} - (\frac{r_0}{r})^6\right]$, that we will not discuss here; another is the Morse potential.

2.5.2 THE MORSE POTENTIAL

The Morse potential is an empirical anharmonic potential that in many cases quite accurately describes reality. It is given by

$$V_M(r) = D_e\left[1 - e^{-a(r-r_0)}\right]^2. \tag{2.18}$$

where D_e is the dissociation energy, not present in the harmonic potential. The constant $a = (m_r/2D_e)^{1/2}$; it is specific to the system. The Morse potential is plotted in figure 2.6. The energy levels can be approximated by

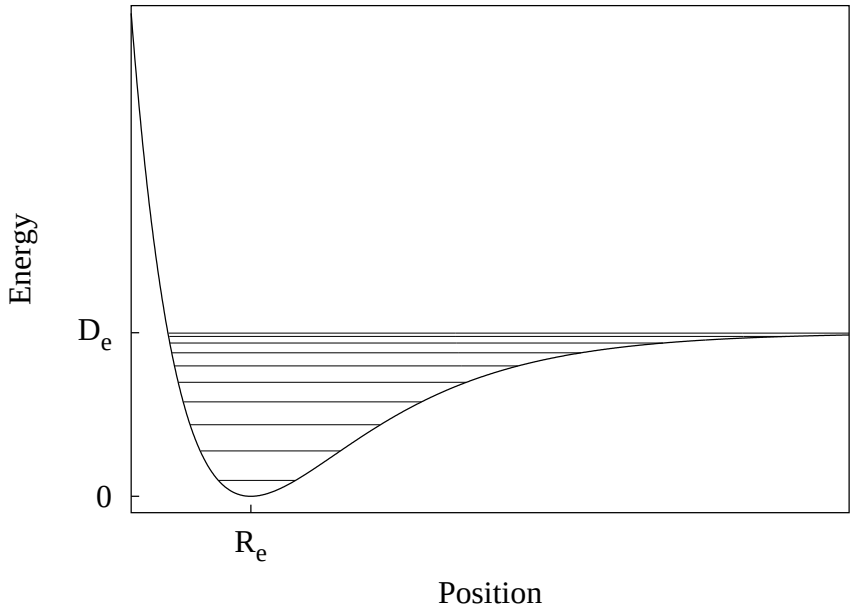

FIGURE 2.6. The Morse potential function and its energy levels.

$$E_n = \hbar\omega\,(n+\frac{1}{2}) - \; x_e\hbar\omega\,(n+\frac{1}{2})^2. \tag{2.19}$$

x_e is called the anharmonicity constant, and is usually of order 0.01. The spacing between energy levels can be calculated from equation 2.19:

$$E_{n+1} - E_n = \hbar\omega\;\left[1 - 2x_e(n+1)\right]. \tag{2.20}$$

Thus, the anharmonicity leads to a decrease of the spacing between subsequent energy levels, which enables one to distinguish spectroscopically between the different transitions. Without anharmonicity, non-linear spectroscopy would be impossible, since excitation would not lead to a different transmission of the sample. The anharmonicity also enables transitions other than between adjacent levels, though still with small probabilities ($P(\Delta n) \propto x_e^{\Delta n}$).

3 Vibrational energy relaxation in aqueous solvation shells

Femtosecond two-color pump–probe spectroscopic measurements are described, in which the vibrational lifetime of the O–H stretch vibration in solutions of KF, NaCl, NaBr and NaI in HDO:D_2O is measured. The pump–probe signal decays in a bi-exponential manner. The fast-decaying component is similar to the decay of pure HDO:D_2O, which has a lifetime of 740 fs. The slow component (roughly 2 to 5 times as slow as the fast component) is due to O–H groups that are hydrogen bonded to the dissolved anions. The time constant of this slow component depends on the nature of the anions and decreases with temperature, in contrast with the temperature dependence of the O–H stretch lifetime in pure HDO:D_2O.

3.1 Introduction

Chemical reactions can be catalyzed by vibrational energy. For example, the potential energy barrier for the dissociation of water was found to decrease strongly when the O–H stretch mode is in an excited state.[8] The lowering of the energy barrier is such that the most efficient pathway for autodissociation probably involves the excitation (by thermal energy) of the water molecule to the second excited state, instead of directly breaking the O–H bond.

Vibrational relaxation is the result of anharmonic coupling between the excited vibration and the accepting modes. If a vibrationally excited molecule relaxes, the energy must go somewhere. In macroscopic situations, the energy then 'converts into heat', but since the vibration is on the molecular scale, both in space and time, this 'heat' must be considered explicitly as the occupation of excited states of a specific collection of lower-energy modes. For molecules in the gas phase, the accepting modes are in many cases exactly known, as well as the potentials that describe the coupling to these modes. For solid-state materials, in particular for crystals, often a discrete set of accepting modes (phonons) can be identified, so that these are also reasonably accessible for theory.[93,15] For liquids the situation is different. Vibrational energy relaxation of molecules in liquids is one of the fields in which theory is behind experiment. It is not yet possible to obtain vibrational lifetimes within 1 or 2 orders of magnitude from first principles.

Theories of vibrational relaxation often start from Fermi's 'Golden Rule'. To calculate transition rates, it is necessary to use (anharmonic) potentials that sufficiently well describe the system. These potentials must include the coupling to all bath modes, and one must integrate over all the modes that match the energy of the original excitation. Except for a few simple systems, neither the correct potentials are available, nor can all possible accepting modes be taken into account. The usual way to proceed is to select a few accepting modes that are treated quantum mechanically, and to deal with the remaining 'bath' modes in a more indirect way, for example by assuming a continuous density of

states of low-frequency bath modes.[59,86,117] The bath modes are required to match the initial and final energies of the system.

An interesting way to obtain information on the local environment is to change it and observe the effect on the vibrational lifetime. For example, changing the pressure in the liquid reduces the freedom of translational motion. With temperature, the occupation of accepting modes and equilibrium bond lengths change. The direct environment can be changed by substituting one molecule for another. In many cases, the effect of such changes on the vibrational lifetime reveals the specific interactions that lead to the vibrational relaxation. Vibrational lifetimes in the liquid state have been measured for a variety of systems, including liquid water[137,41,42,43,91,24,70,77] and ethanol.[69,77,136]

In this and the next chapter, we will present measurements on the vibrational lifetime of the O–H stretch vibration of anion-bonded water molecules. First, we will focus on the temperature dependence of the vibrational lifetime. In chapter 4, the anion and cation content is varied. Although a full theoretical description is not yet possible, certain trends are observed and modeled. Hopefully, the work that is presented here will stimulate future theoretical developments.

3.2 EXPERIMENT

The experiments described in this chapter are two-color mid-infrared pump-probe experiments on the O–H stretch vibration in solutions consisting of 3 M or 6 M of salt (KF, NaCl, NaBr and NaI) and less than 1 M of HDO in D_2O. KF is used instead of NaF because the solubility of the latter salt is too low, approximately 1 M. The sample was a 200 μm thick layer of liquid kept between CaF_2 windows, which was continuously rotated to avoid accumulation of heat. The temperature of the body of the rotating device was kept constant (within 2 °C) at a certain specified temperature. The temperature in the sample was measured with a thermocouple placed between two windows that are identical to those used in the experiments. This should provide a realistic estimation of the temperature within the sample; the absence of water in this measurement hardly alters the measured temperature since the heat conduction takes place mainly through the windows.[89]

In the experiment, the pump pulse excites the O–H stretch vibration of the molecules. The probe pulse measures the induced transmission change (T/T_0) at the $1\rightarrow2$ transition. The polarization of the probe pulse was set at the magic angle (54.7°) with respect to the pump polarization, so that the measured signals are not affected by the reorientational motion of the excited molecules. The spectral widths of the pump and probe pulses were approximately 80 and 60 cm^{-1}, respectively. Details about the experiment and the experimental setup can be found in chapter 2.

3.3 RESULTS

In figure 3.1, infrared spectra of the O–H stretching band of protonated heavy water (HDO:D_2O), and of different salt solutions (KF, NaCl, NaBr, NaI) in HDO:D_2O are shown. The O–H stretching band of the HDO:D_2O solution is centred at 3410 cm^{-1};

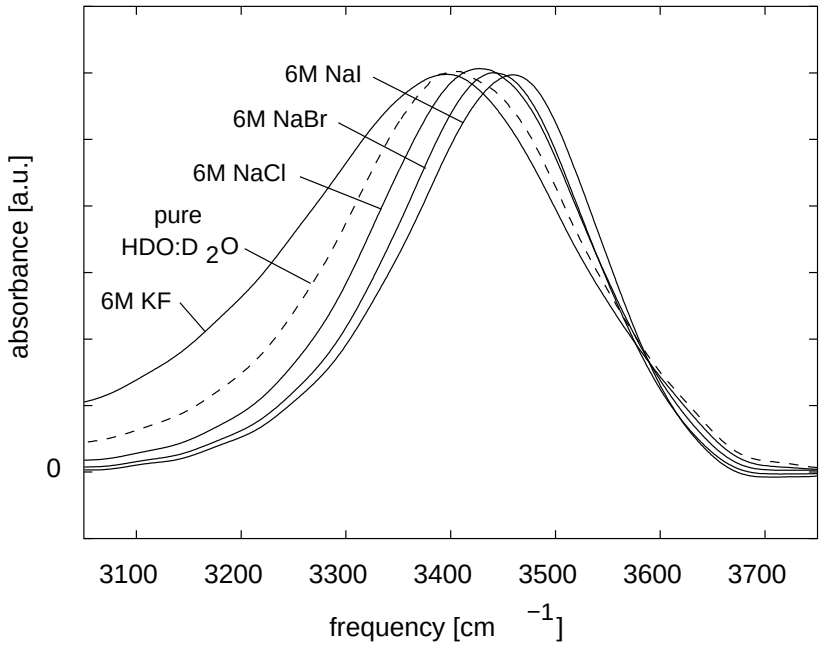

FIGURE 3.1. The O–H stretch absorption spectrum of solutions of 6 M of NaI, NaBr, NaCl and KF, respectively, and less than 1 M of HDO, dissolved in D_2O. Also shown is a solution containing no salt. The D_2O background is subtracted.

upon dissolution of salt this band shifts to the blue (NaCl, NaBr and NaI), or to the red (KF).

In the experiments on KF, NaCl, NaBr and NaI, the pump frequency was tuned to the approximate center of the $0\rightarrow1$ transition (3450 cm^{-1}), and the probe frequency to the $1\rightarrow2$ transition (3200 cm^{-1}). At these particular pump and probe frequencies, the measured signals are quite insensitive to spectral diffusion of the O–H stretch vibration.[134,24] In chapter 6, it will be seen that the spectral diffusion of the anion-bonded O–H groups is slow and only becomes observable when the pump frequency is in the wings of the absorption band and when the probe is tuned through the $0\rightarrow1$ absorption spectrum. If the probe is resonant with the $1\rightarrow2$ absorption, spectral diffusion effects are not observed, probably because the spectral diffusion is slow, and because each particular probed $1\rightarrow2$ frequency corresponds to a broad distribution of $0\rightarrow1$ frequencies. We observed that changing the pump and probe frequencies within a range of 100 cm^{-1} did not change the results. The measured dynamics thus directly represent the vibrational relaxation of the O–H stretch vibration.

In figure 3.2, pump-probe measurements of 6 M solutions of KF, NaCl, NaBr and NaI are shown. Clearly, for the solutions of NaCl, NaBr and NaI, the signals decay non-exponentially, showing a fast and a slow component. The pump-probe signal can be modeled well with a sum of two exponential functions, convolved with the crosscorrelation trace (equation 2.8, with $i = 2$); the fits using these functions are shown in the figure. The

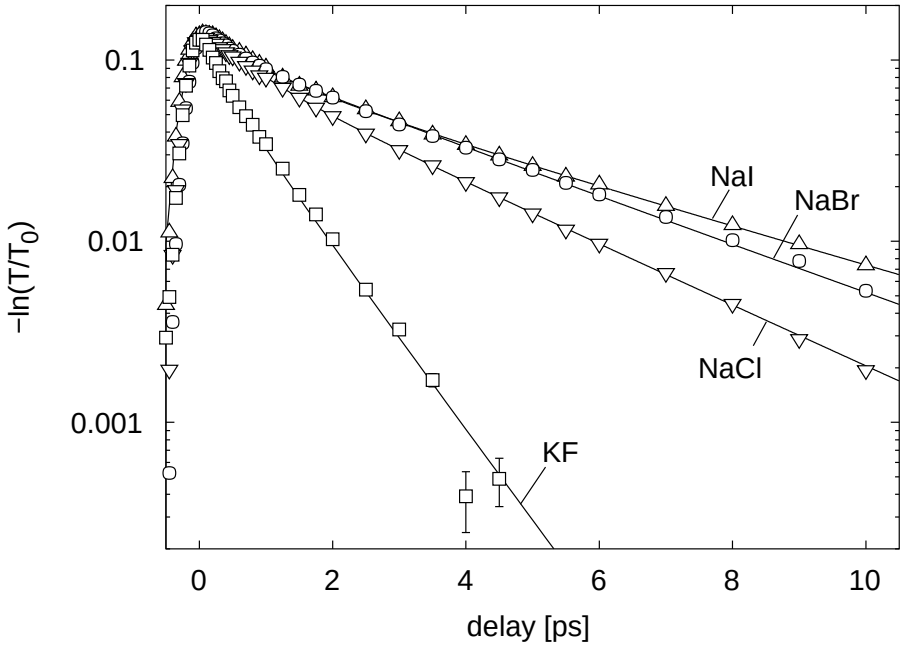

FIGURE 3.2. Room temperature isotropic pump-probe scans of 6 M solutions of KF, NaCl, NaBr, and NaI, and bi-exponential fits described in the text. The pump frequency was 3450 cm^{-1}, the probe frequency was 3200 cm^{-1}. For a solution of KF, the decay is almost identical to that of pure $HDO:D_2O$.

fast component decays with a time constant of approximately 740 fs that has been observed before for pure, i.e. containing no ions, $HDO:D_2O$ [138]; the slow component decays much slower (e.g. 2.6 ps for NaCl). The time constant of the fast component is the same for all solutions. The time constant of the slow component depends on the dissolved salt, and increases within the halogenic series. The relative amplitude of the slow component scales with the salt concentration. Interestingly, for the solution containing KF, no slow component is observed; the signal decays with a time constant similar to that in pure water.

In figure 3.3, the absorption change is plotted as a function of time delay for a 3 M solution of NaCl at several temperatures between room temperature and 106 °C. In figure 3.4, the anion-bound O–H stretch lifetimes of Cl^-, Br^- and I^- are shown as a function of temperature. We observe that the vibrational lifetime decreases with temperature.

3.4 DISCUSSION

A few conclusions can be drawn from the data presented in figures 3.2–3.4. First, the slow component in the vibrational relaxation depends on the anion species (figures 3.2 and 3.4). Second, the slow component becomes faster when the temperature is increased (figures 3.3 and 3.4).

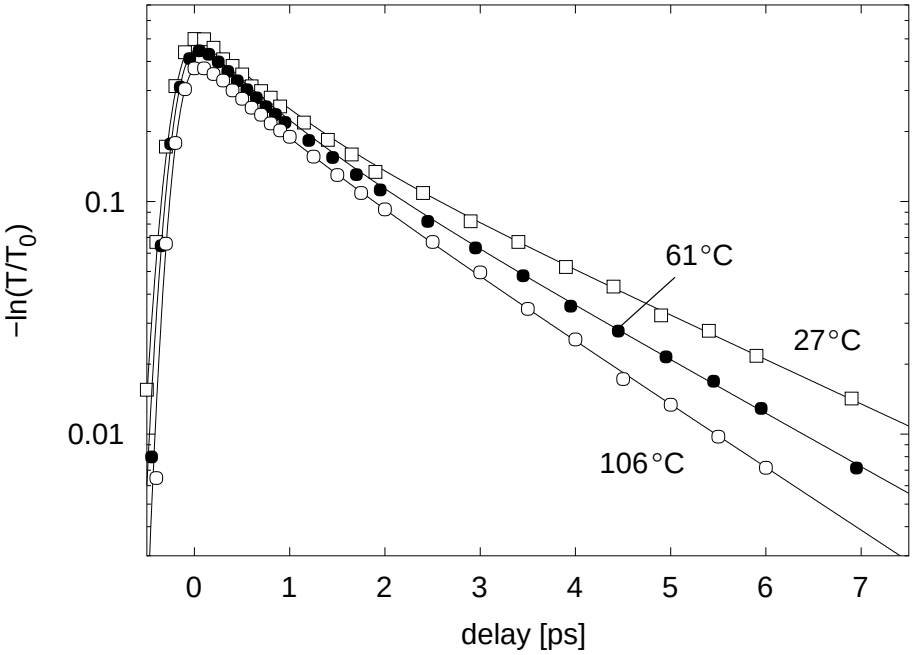

FIGURE 3.3. Isotropic pump-probe scans of a solution of 3 M NaCl in HDO:D_2O at different temperatures, and bi-exponential fits described in the text. The pump frequency was tuned to 3475 cm^{-1}, the probe to 3200 cm^{-1}. The decay time constant (obtained by fitting to a bi-exponential function) decreases from 2.2 ps at room temperature to 1.5 ps at 106 °C.

For a solution of pure HDO:D_2O, it was found that the hydrogen bond plays an important role in the relaxation of the O–H stretch vibration.[138,91] The excited O–H stretch relaxes via excitation of the hydrogen bond or by transferring its energy to a combination tone of the hydrogen-bond vibration and the bending vibration.[24] For the salt solutions studied here, the vibrational lifetime is found to depend on the nature of the anion, which indicates that again the hydrogen bond, in this case to the anion, plays a substantial role in the relaxation of the anion-bonded O–H groups.

There exists a strong correlation between the frequency of the O–H stretch vibration and the vibrational lifetime: the O–H stretch lifetime has been found experimentally to increase with frequency.[85] The relation between the frequency and lifetime of the O–H stretch vibration has also been studied theoretically.[93,117,108] The existing theories do not provide a quantitative description of the vibrational relaxation of aqueous systems, but they may be used in the present context to elucidate the trends we observe in our data.

In the analytical theory developed by Staib and Hynes,[117] vibrational relaxation in an isolated O–H$\cdots$O system is described with Fermi's 'golden rule', using Lippincott-Schroeder potentials (see 2.5) for the covalent bond and for the hydrogen bond. The coupling between the hydrogen bond and the O–H stretch vibration is described adiabatically, with a non-adiabatic coupling term giving rise to vibrational relaxation. This non-adiabatic coupling is smaller for longer and weaker hydrogen bonds, resulting in longer

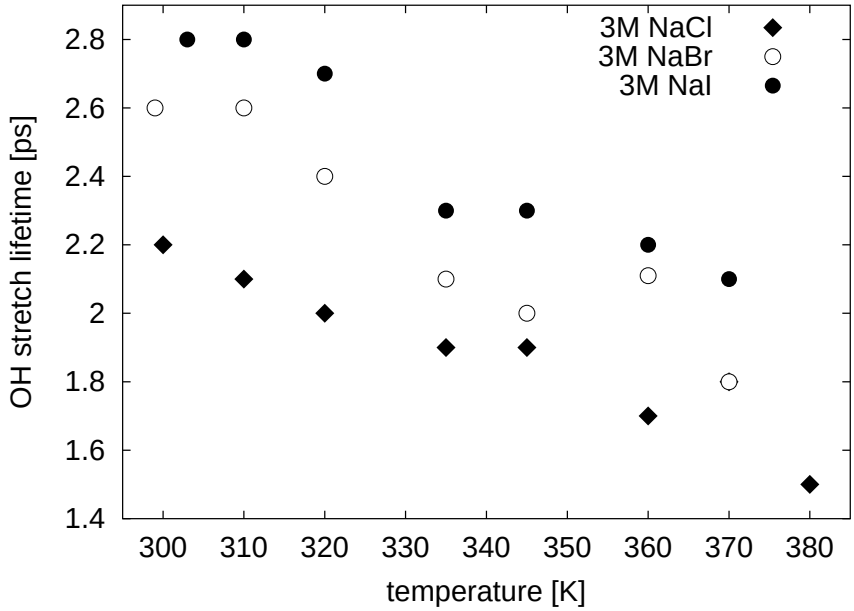

FIGURE 3.4. The O–H stretch vibrational lifetime of anion-bound water molecules as a function of temperature for 3 M solutions of Cl^-, Br^-, and I^- in liquid water. The lifetimes are obtained by fitting the data to a bi-exponential function. The uncertainty is approximately 0.1 ps.

O–H stretch lifetimes. The linear spectra in figure 3.1 show that the O–H stretch frequency increases going from a KF solution to pure water to solutions containing Na^+ and Cl^-, Br^- or I^-, which indicates that the hydrogen-bond interaction decreases in that order. Hence, the observed increase of T_1 in the series F^-, Cl^-, Br^-, I^- can be explained qualitatively from a decrease of the anharmonic interaction between the O–H stretch and the O–H$\cdots$X$^-$ hydrogen bond.

An additional effect is the increase in the reduced mass of the hydrogen bond in the series F^-, Cl^-, Br^-, I^-. In the theory of Staib and Hynes, the non-adiabatic coupling responsible for the energy transfer is inversely proportional to the reduced mass. Thus, the increase of T_1 in the series F^-, Cl^-, Br^-, I^- can be explained from a decreased anharmonic coupling due to a weakening of the hydrogen bond, and from the reduced mass of the hydrogen-bond oscillator. For O–H$\cdots F^-$, both the O–H stretch frequency and the reduced mass of the hydrogen bond are similar to that of the O–H$\cdots$O system, which explains why the T_1 of O–H$\cdots F^-$ is observed to be similar to that of HDO:D_2O.

For the temperature dependence of the relaxation rate of the O–H stretch vibration in hydrogen-bonded systems, two counteracting effects are important. First, the hydrogen bond becomes longer and weaker (as indicated by the blue shift of the O–H stretch frequency) when the temperature increases, which leads to an increase of the vibrational lifetime.[117] Second, increasing the temperature leads to a higher average occupation number of the accepting modes. The relaxation rate is, applying Fermi's 'golden rule', propor-

tional to $|\langle f|H_c|i\rangle|^2$, where i,f denote the initial and final states of the system, and H_c denotes the coupling terms in the Hamiltonian. For a single accepting harmonic oscillator with vibrational coordinate x that takes k quanta in the relaxation process, the matrix element $\langle n|x^k|n+k\rangle$ increases with n, because the wavefunctions for higher n are more spatially extended.[14] If the frequency of the accepting mode is smaller than, or on the order of kT, as is the case for the hydrogen-bond mode, n will show a significant temperature dependence. In this case, a temperature increase leads to a decrease of the vibrational lifetime.

Previous work on liquid water (i.e. HDO:D_2O)[138] showed that the O–H stretch lifetime in pure water increases with temperature. Apparently, for liquid water, the effect of the weakening of the hydrogen-bond interaction with temperature is dominant in the temperature dependence of the relaxation rate. In Ref. 138, the O–H stretch frequency (as a measure for the hydrogen-bond strength) as a function of temperature was used in combination with the theoretical dependence of the vibrational lifetime on the O–H stretch frequency by Staib and Hynes.[117] By using only the frequency shift of the O–H stretch with temperature, the data could be quite well described over the whole temperature range (30 to 363 K). However, a close observation of the data of Ref. 138 shows that the measured increase of the lifetime with temperature is somewhat less steep than the theory predicts based on the frequency shift alone. This difference may be attributed to the neglect of the change of accepting-mode occupation numbers with temperature.

For the O–H$\cdots$$X^-$ (X^- = Cl^-, Br^-, I^-) hydrogen-bonded systems, we observe that the lifetime *decreases* with temperature. In order to understand this opposite temperature dependence of the lifetime, we compared the temperature dependence of the O–H stretch absorption spectrum of the O–H$\cdots$O oscillators measured for HDO:D_2O (without the D_2O background) with that of the O–H$\cdots$$I^-$ oscillators measured for a solution containing 6 M NaI. The latter spectrum is a difference spectrum of a solution of 6 M NaI, 1 M HDO and D_2O, and D_2O containing 6 M of NaI and pure D_2O, from which the difference spectrum of HDO in D_2O and pure D_2O was subtracted. A small residual broadening due to bulk-water disturbance, or due to cation solvation may still be present. The spectra are shown in figure 3.5. For the O–H$\cdots$O oscillators of pure water, the O–H band shows a strong blueshift of about 50 cm^{-1} when the temperature is increased from room temperature to 93 °C. In contrast, the O–H stretch band of O–H$\cdots$$I^-$ oscillators shifts by only 10 cm^{-1} in this temperature range. Hence, the lifetime-increasing effect of the O–H stretch frequency shift is much weaker for the salt solution, so that the dominant effect in the temperature dependence of the O–H stretch lifetime is now formed by an increased occupation number of the accepting hydrogen-bond mode, which leads to a decrease of the lifetime.

3.5 Conclusions

In this chapter, we have presented femtosecond mid-infrared pump-probe spectroscopy on the O–H stretch vibration of water molecules in aqueous salt solutions. The transients decay in a bi-exponential manner, with a fast component that originates from O–H$\cdots$O groups (all O–H groups that are hydrogen bonded to another water molecule), and a slow component due to O–H$\cdots$$X^-$ groups (i.e. O–H groups that are hydrogen bonded to Cl^-,

Br^- or I^-). For F^-, no slow component was observed. The increase in vibrational lifetime of the O–H$\cdots$$X^-$ group (X^- = F^-, Cl^-, Br^- or I^-) results from the decreased hydrogen-bond interaction, and from the decreased frequency of the hydrogen-bond mode.

We observe that the O–H$\cdots$$X^-$ lifetime becomes shorter when the temperature is raised. This behaviour is expected on theoretical grounds, and is observed for most molecular vibrations, except for the O–H stretch in bulk water, for which the vibrational lifetime increases with temperature. This opposite behaviour can be explained from the much stronger temperature dependence of the hydrogen-bond interaction for bulk water than for water in an ionic solvation shell.

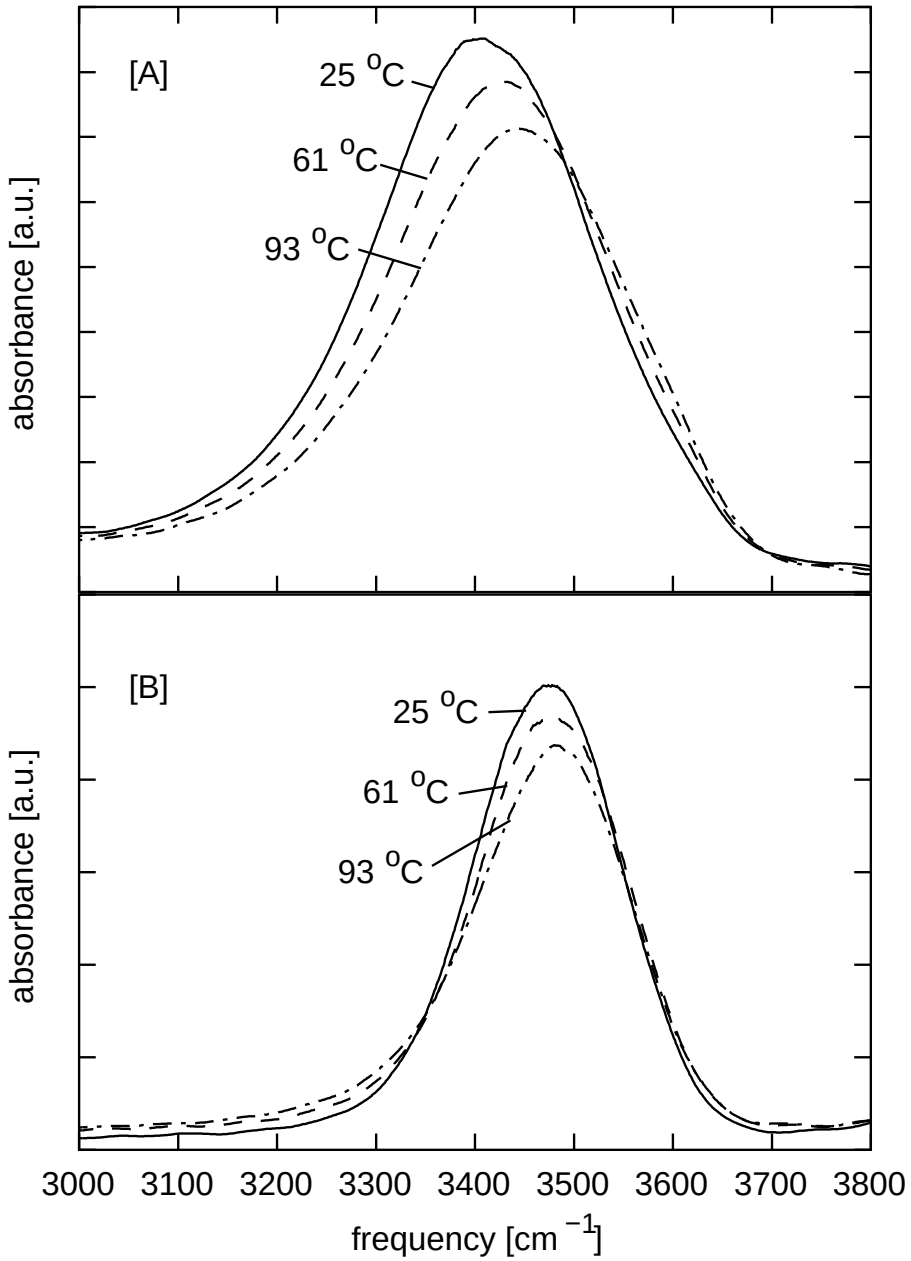

FIGURE 3.5. Spectra of the O–H stretch vibration of HDO:D_2O (The D_2O background was subtracted, panel A) and of a solution of 6 M NaI in HDO:D_2O (background D_2O and bulk O–H band were subtracted, panel B) at three temperatures. For HDO:D_2O the band shifts to the blue by about 50 cm^{-1}, the O–H$\cdots I^-$ band shifts only by approximately 10 cm^{-1}.

4 Concentration and cation dependence of the vibrational relaxation of anionic solvation shells

Femtosecond two-colour pump-probe spectroscopy is used to study the dependence of the vibrational relaxation on the nature of the anion and the cation, and their concentration. The vibrational lifetime of the anion-solvating molecules has been determined for a series of salts consisting of the anions Cl^-, Br^- and I^-, and the cations Li^+, Na^+ and Mg^{2+}, for a range of concentrations from 0.5 M up to 6 M (chloride salts), 9 M (bromide salts), and 10 M (iodide salts). A quantum mechanical model is presented that describes the observed dependencies. In addition to the previously found strong dependence on the nature of the anion, the lifetime is found to show a small but significant dependence on the nature of the cation and a strong concentration-dependence.

4.1 Introduction

In the previous chapter, the vibrational relaxation of water molecules in aqueous salt solutions was observed to differ drastically from that of pure liquid water. The O–H stretch lifetime was found to be much longer for the anion-bound molecules: after vibrational excitation, the bulk and cation-bonded water molecules relax in about 0.8 picoseconds, whereas the water molecules in the anion shell remain excited 3 to 6 times as long.

Notwithstanding the dominant influence of the anions, it can be expected that at high concentrations the cations should also affect the vibrational relaxation: at concentrations above approximately 6 M, almost all water molecules are involved in solvating ions, and ions are sharing water molecules in their first solvation shells.[27] Between 1 and 6 M, the salt concentration becomes an important parameter because in this regime, the local environment of the anion changes drastically.

In the present chapter, the effect of the cation on the vibrational relaxation of the anion-bonded O–H stretch vibration is studied. It is observed that the cations do change the vibrational lifetime of water molecules in the solvation shell of the anion, albeit to a lesser extent than do the anions. The experiments and modeling presented in this paper aim to understand the influence of anions and cations on the O–H stretch vibrational lifetime of water molecules in anionic solvation shells.

4.2 Experiment

We performed two-color mid-infrared pump-probe experiments on the O–H stretch vibration in several salt solutions. The salt solutions were LiCl, NaCl, $MgCl_2$, LiBr, NaBr, $MgBr_2$, LiI, NaI, or MgI_2, dissolved in D_2O and less than 1 M of HDO. The salts were

studied at the following anion concentrations: 0.5, 1, 2, 3, 4, 6 and 9 M (bromide salts), 10 M (iodide salts). Below 0.5 M, the concentration was too low to allow for an accurate determination of the vibrational lifetime. The maximum concentrations are limited by the solubilities in each series of three salts of the same anion. The samples were kept between two CaF_2 windows, separated by a 200 μm teflon spacer. The transmission of the samples at the approximate center of the O–H stretch absorption band (3450 cm^{-1}) is generally between 5 and 20 %, depending on the HDO concentration.

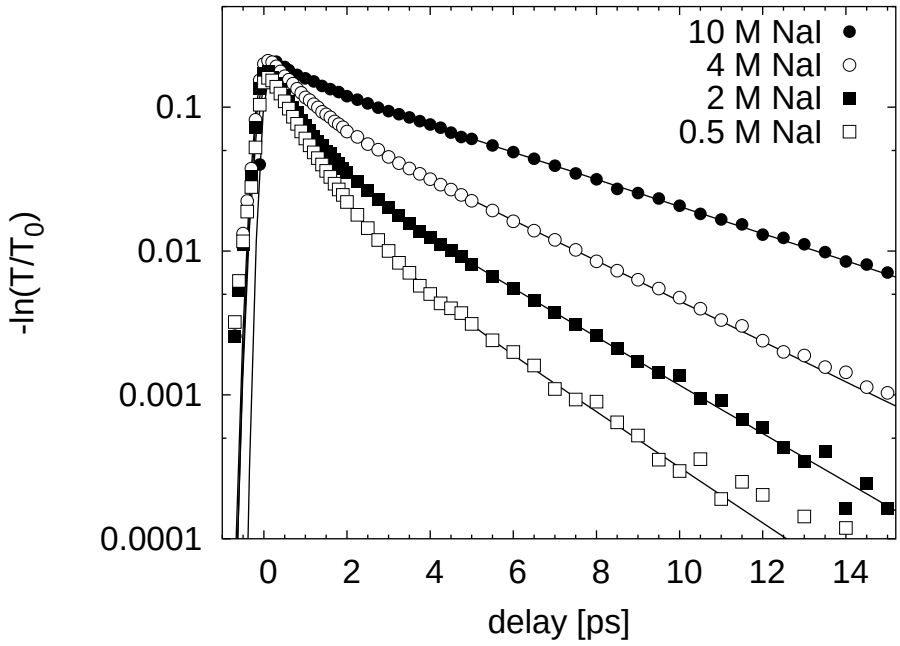

Figure 4.1. Pump-probe traces of solutions of several concentrations of NaI in HDO:D_2O. The measurement was performed at a pump frequency of 3450 cm^{-1}, and a probe frequency of 3200 cm^{-1}. The lines are fits to the data. The fit function is a bi-exponential function convolved with a gaussian crosscorrelation function.

The experimental methods applied in this chapter are similar to those of the previous chapter. The polarization of the probe pulse was again set at the magic angle (54.7°) with respect to the pump polarization, so that the measured signals are not affected by the reorientational motion of the excited molecules. The spectral widths of the pump and probe pulses were approximately 80 and 40 cm^{-1}, respectively. The probe now has a narrower spectral width, because two KTP crystals have been used instead of one for better pulse-to-pulse stability. The pump pulses have an energy of typically 20 μJ, the energy of the probe pulses is less than 1 μJ. The cross-correlation trace typically has a width of 400 fs. Variation of the pump energy leads only to a change in signal amplitude, and does not influence the dynamics.

4.3 RESULTS

In figure 4.1, pump-probe traces of solutions of NaI are shown. The decay is non-exponential, which is most clearly seen at low concentrations. The data can be well fitted with a bi-exponential function, convolved with a gaussian cross-correlation trace (equation 2.8 with $n = 2$). In this way, two time constants are obtained, the shorter of which, 0.8 ps, is approximately the same as obtained previously for pure HDO dissolved in D_2O.[138,91] It originates from O–H groups that are hydrogen bonded to another water molecule, which makes them similar to the O–H groups in HDO:D_2O. The longer time constant ranges from roughly 2 to almost 5 picoseconds, and was found to correlate mainly with the type of anion and its concentration. The slow component of the vibrational relaxation, denoted in this chapter by T_1, is the focus of the present study.

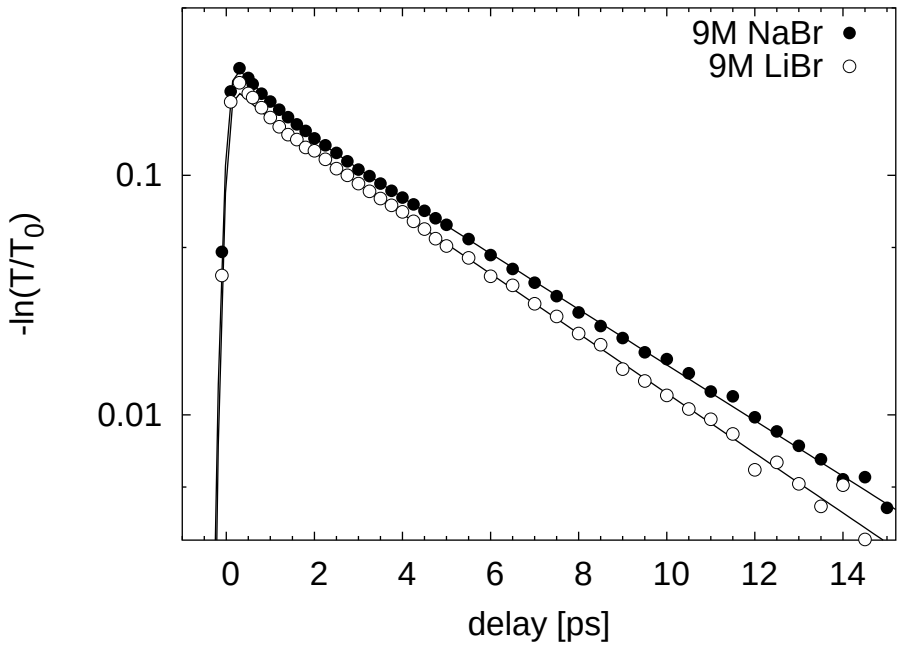

FIGURE 4.2. Pump-probe traces of 9 M solutions of LiBr and NaBr in HDO:D_2O. The measurement was performed at a pump frequency of 3450 cm^{-1}, and a probe frequency of 3200 cm^{-1}. The lines are fits to the data. The fit function is a bi-exponential function convolved with a gaussian crosscorrelation function.

T_1 shows a clear concentration dependence, that can already be seen from the raw data (figure 4.1). Less well pronounced are the differences in T_1 for different cations: in figure 4.2, raw data are shown for 9 M solutions of NaBr and LiBr.

In figure 4.3, T_1 is plotted as a function of anion concentration, for a series of lithium salts. For all anions, the lifetime increases with concentration, but different slopes are observed for different anions; the slope increases going from Cl^- to Br^- to I^-. Below 3 M

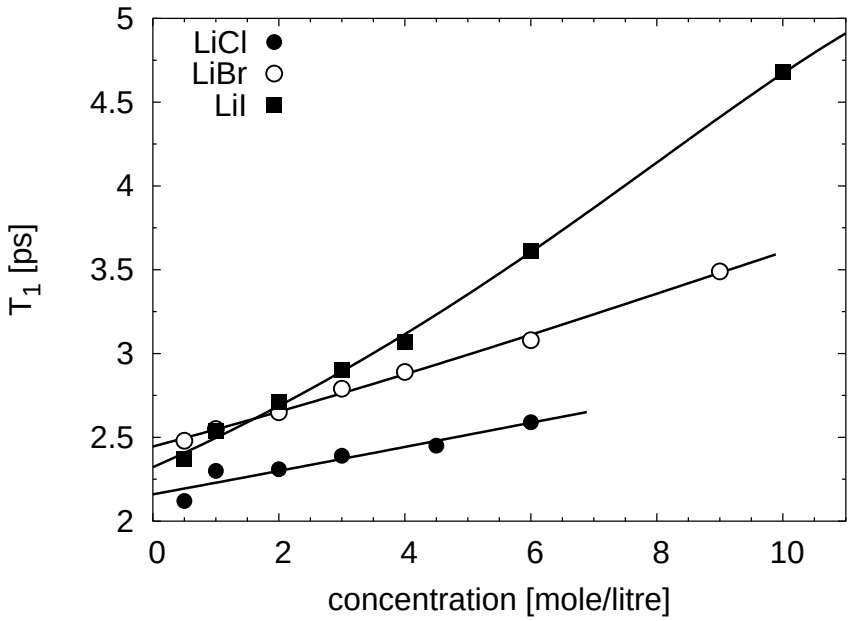

Figure 4.3. T_1 as a function of concentration for three salts containing the same cation: LiCl, LiBr and LiI. The lines are fits to the data.

of anion concentration, the lifetimes of Br^- and I^- are almost the same; Cl^- is faster at all measured concentrations. The sodium and magnesium salts show the same features.

In figures 4.4, 4.5 and 4.6, T_1 is plotted for solutions of salts containing chloride, bromide and iodide, respectively. Each anion is combined with lithium, sodium and magnesium. The difference between the data in these figures, in which the cation is varied, is much smaller than in figure 4.3, in which the anion was varied. For example, at a concentration of 6 M, T_1 of an iodide salt is 50 % longer than for a chloride salt, whereas the change of the cation from Mg^{2+} to Na^+ leads to an increase of T_1 of at most 10 %. The lithium salts have T_1's in between sodium and magnesium salts.

4.4 Model

In this section we will develop a model for the vibrational relaxation of HDO molecules in the solvation shells of Cl^-, $Br^-$and I^- that can explain the trends observed in the previous section. The relaxation rate of the initially excited state of the O–H stretch vibration with wave function $\varphi_{\mathrm{OH,v=1}}$ can be described by a Fermi 'golden rule' expression:

$$1/T_1 = \int dE_\mathrm{f} |\langle \varphi_{\mathrm{acc,E_f}} \varphi_{\mathrm{OH,v=0}} | V_\mathrm{anh} | \varphi_{\mathrm{acc,E_i}} \varphi_{\mathrm{OH,v=1}} \rangle|^2 \delta(E_f - E_i) \rho(E_f), \qquad (4.1)$$

with E_f the energy of the final combination state of accepting modes, represented by the wavefunction $\varphi_{\mathrm{acc,f}}\varphi_{\mathrm{OH,v=0}}$, E_i the energy of the initial state $\varphi_{\mathrm{acc,i}}\varphi_{\mathrm{OH,v=1}}$, and $\rho(E_\mathrm{f})$ the

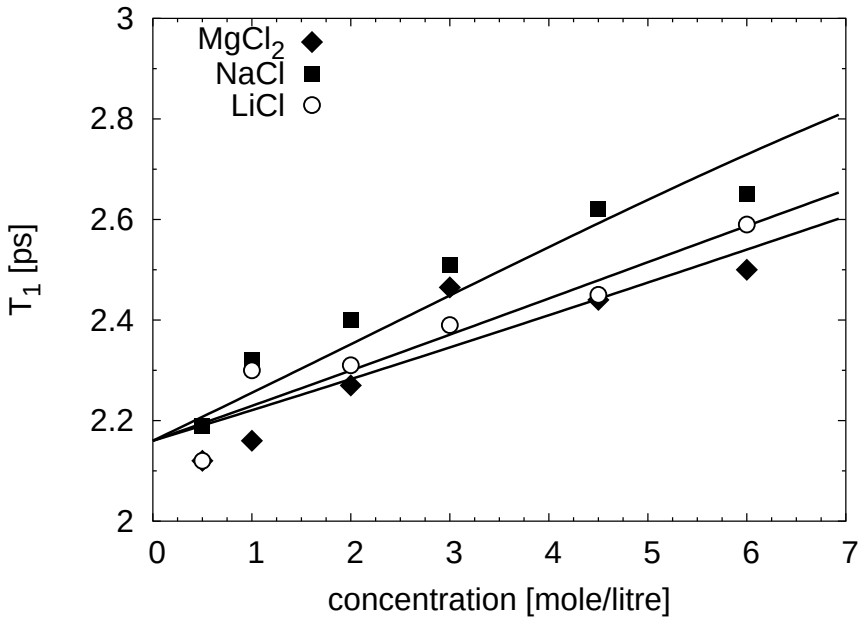

FIGURE 4.4. T_1 as a function of concentration for three salts containing Cl^-: LiCl, NaCl and $MgCl_2$. The lines are fits to the data.

density of states.

In the condensed phase, the combination of accepting modes will contain both high-frequency intramolecular modes and low-frequency intermolecular (bath) modes. The latter modes often play an important role in making the energy transfer resonant, i.e. making the $\delta(E_f - E_i)$ function different from zero. Two different cases can be distinguished. In the first, the anharmonic coupling only depends on high-frequency intramolecular coordinates. Then the energy transfer gets resonant because the energies of the initially excited mode and the combination of intramolecular accepting modes are both subject to fluctuations induced by the interactions with the bath modes.[9] In the second case, the anharmonic coupling depends explicitly on the bath coordinates. In this case, the anharmonic coupling V_{anh} is often assumed to be a product of an intramolecular system part $V_{\text{anh,S}}$ and a bath part $V_{\text{anh,B}}$. By representing the delta function in the time domain, the transition rate can be written in the form of a product of an intramolecular anharmonic coupling and a Fourier transform of a $\langle V_{anh,B}(t)V_{anh,B}(0)\rangle$ bath correlation function.[59] The latter is often evaluated with molecular dynamics simulations.

For polyatomic molecules in the condensed phase, it is not possible to evaluate the transition rate exactly. In most cases only the trends, e.g. the dependencies on certain parameters like pressure, temperature or solvent, can be described. These dependencies often result from changes in the character, energy and density of states of the low-frequency bath modes.

In the relaxation of the O–H stretch vibration of HDO:D_2O, at least part of the energy has to be accepted by the hydrogen bonds, because in contrast to H_2O, there is

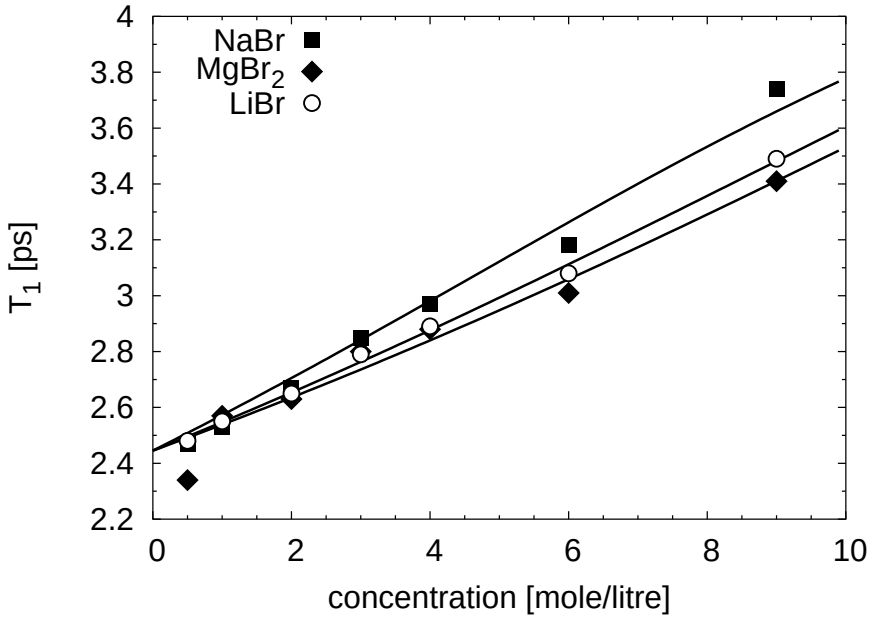

Figure 4.5. T_1 as a function of concentration for three salts containing Br^-: LiBr, NaBr and $MgBr_2$. The lines are fits to the data.

no combination of intramolecular modes that is resonant with the O–H stretch vibration. A special role is expected to be played by the hydrogen bond that involves the hydrogen atom of the excited O–H group. In the following we will denote this hydrogen bond as the donated hydrogen bond. The present experiments indeed demonstrate that this hydrogen bond plays an essential role, because the change of this hydrogen bond from O–H$\cdots$O to O–H$\cdots$$Cl^-$ to O–H$\cdots$$Br^-$ to O–H$\cdots$$I^-$ leads to a significant slowing down of the vibrational relaxation. However, it should be realized that the hydrogen bonds in liquid water form a strongly coupled network. This means that the energy of the excited O–H stretch vibration in the solvation shell of the anion is not only dependent on the local O–H$\cdots$$X^-$ coordinate, but also on the O–D$\cdots$$X^-$, O–D$\cdots$O and Y^+O-D$\cdots$O coordinates of the other hydrogen bonds in the liquid. Hence, the donated hydrogen bond is not a pure local O–H$\cdots$$X^-$ (X=Cl^-, Br^-, I^-) mode, but in fact will be a delocalized mode showing admixture of surrounding hydrogen bonds. We therefore anticipate that the small but significant influences of the cations and concentration on the relaxation rate result from changes in the wavefunction of this delocalized hydrogen bond.

We assume that the anharmonic coupling $V_{\rm anh}$ can be written as $V_{\rm OH}V_{\rm dhb}V_{\rm oth}$, with $V_{\rm OH}$ the dependence of the anharmonic coupling on the O–H stretch coordinate, $V_{\rm dhb}$ the dependence on the delocalized hydrogen-bond coordinate, and $V_{\rm oth}$ the dependence on all other coordinates including intramolecular coordinates (bending mode, O–D stretch vibration) and intermolecular modes (librational modes, other hydrogen bond stretch and bend vibrations). The wavefunction $\varphi_{\rm acc,f}$ can then be written as the product $\varphi_{\rm oth,f}\varphi_{\rm dhb,f}$. The wavefunction $\varphi_{\rm dhb,f}$ has contributions from four different hydrogen

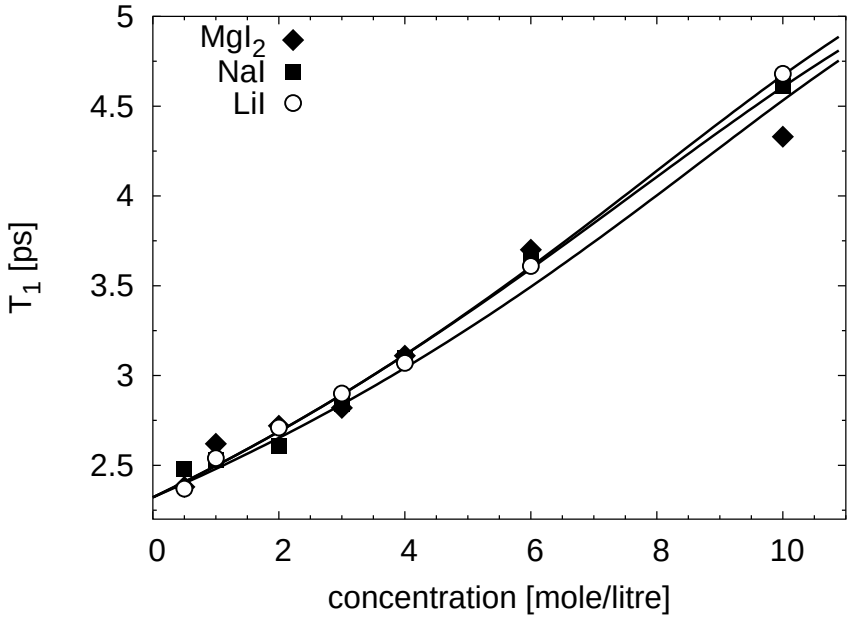

FIGURE 4.6. T_1 as a function of concentration for three salts containing I^-: LiI, NaI and MgI_2. The lines are fits to the data.

bonds: the local anionic (O–H$\cdots$X$^-$) mode, other anionic hydrogen bonds (O–D$\cdots$X$^-$), bulk (O–D$\cdots$O), and cationic (Y$^+$O-D$\cdots$O) hydrogen bonds. Since almost all solvent molecules are D_2O molecules, the latter hydrogen bonds are actually deuterium bonds. This does not hold of course for the donated hydrogen bond next to the excited O–H group. The stretching frequency of a deuterium bond is almost the same as for a hydrogen bond, because the reduced mass of the hydrogen-bond vibration does not change very much when hydrogen is substituted by deuterium. The delocalized hydrogen bond wavefunction $\varphi_{\mathrm{dhb,f}}$ can be written as:

$$\begin{aligned}\varphi_{\mathrm{dhb,f}} \;=\; & C_{a'}\,\varphi_{\mathrm{O-H\cdots X^-,f}} + \sum_{a''} C_{a''}\,\varphi_{a'',\mathrm{O-D\cdots X^-,f}} + \\ & \sum_{b} C_b\,\varphi_{b,\mathrm{O-D\cdots O,f}} + \sum_{c} C_c\,\varphi_{c,\mathrm{Y^+O-D\cdots O,f}}. \end{aligned} \tag{4.2}$$

The contribution of each hydrogen-bond mode is denoted by the coefficients $C_{a'}$, $C_{a''}$, C_b, and C_c, where the subscripts a, b, c denote anion (single prime for O–H$\cdots$X$^-$, double prime for admixing O–D$\cdots$X$^-$), bulk water and cation, respectively. The wavefunction likely will be dominated by the local anionic hydrogen bond. Hence, $C_{a'}$ will be greater than $C_{a''}$, C_b and C_c at all concentrations. The coefficients further depend on the components' abundance, which changes with concentration; they will be calculated below.

If we now substitute the expression for $\varphi_{\mathrm{dhb,f}}$ of equation (4.2) in $\varphi_{\mathrm{acc,f}}$ and $\varphi_{\mathrm{acc,i}}$ in equation (4.1), and use the product form of the anharmonic coupling, we get:

$$
\begin{aligned}
1/T_1 \;=\; & \Big\{ \big| C_{a'} \langle \varphi_{\mathrm{O-H\cdots X^-,f}} | V_{\mathrm{dhb}} | \varphi_{\mathrm{O-H\cdots X^-,i}} \rangle + \\
& \sum_{a''} C_{a''} \langle \varphi_{a'',\mathrm{O-D\cdots X^-,f}} | V_{\mathrm{dhb}} | \varphi_{a'',\mathrm{O-D\cdots X^-,i}} \rangle \big|^2 + \\
& \sum_{b} |C_b|^2 \big| \langle \varphi_{b,\mathrm{O-H\cdots O,f}} | V_{\mathrm{dhb}} | \varphi_{b,\mathrm{O-H\cdots O,i}} \rangle \big|^2 + \\
& \sum_{c} |C_c|^2 \big| \langle \varphi_{c,\mathrm{Y^+O-H\cdots O,f}} | V_{\mathrm{dhb}} | \varphi_{c,\mathrm{Y^+O-H\cdots O,i}} \rangle \big|^2 \Big\} \times \\
& \big| \langle \varphi_{\mathrm{oth,f}} | V_{\mathrm{oth}} | \varphi_{\mathrm{oth,i}} \rangle \big|^2 \big| \langle \varphi_{\mathrm{OH,v=0}} | V_{\mathrm{OH}} | \varphi_{\mathrm{OH,v=1}} \rangle \big|^2
\end{aligned} \tag{4.3}
$$

In this expression all cross terms have been neglected. The reasoning behind this is that the different $C_{a''}$, C_b, C_c will have different signs. Hence, the terms proportional to $C^*_{a'} \sum_b C_b$, $C^*_{a'} \sum_c C_c$, $\sum_{a''} C^*_{a''} \sum_b C_b$, $\sum_{a''} C^*_{a''} \sum_c C_c$, $\sum_b C^*_b \sum_c C_c$, $\sum_b C^*_b \sum_{b'} C_{b'}$ ($b \neq b'$), and $\sum_c C^*_c \sum_{c'} C_{c'}$ ($c \neq c'$), are all expected to be negligibly small.

We can write equation (4.3) as

$$
1/T_1 = \sum_a |C_a|^2 / T_{1a} + \sum_b |C_b|^2 / T_{1b} + \sum_c |C_c|^2 / T_{1c}, \tag{4.4}
$$

where the term $\sum_a |C_a|^2$ is equal to $|C_{a'} + \sum_{a''} C_{a''}|^2$ of equation (4.3). In this expression it is assumed that the coupling to the O–H$\cdots$X$^-$ hydrogen bond is the same as to the O–D$\cdots$X$^-$ hydrogen bond. The relaxation rate is now given by a sum of three contributions corresponding to the different characters of hydrogen bonds present in the solution. The T_{1i} (i = a,b,c) are the lifetimes of the O–H groups, in the case where $\varphi_{\mathrm{dhb,f}}$ would be purely anionic, bulk, or cationic in character. In the case of bulk, this corresponds to the situation of pure liquid HDO:D_2O with no ions added.

In the following we will determine the values of the $\sum_i |C_i|^2$ from the concentrations of the different types of hydrogen bonds present in a particular salt solution. We will calculate the concentration $N_{\mathrm{OD,i}}(\epsilon)$ of the three different types of hydrogen bonds as a function of the concentration ϵ of the anion. We assume that there is an equilibrium between unoccupied anion binding sites (the concentration of empty anion binding sites is denoted $[A\cdot]$), the actual concentration of anion-bonded O–D groups ($[A \cdot OD]$) and the concentration of O–D groups that are not bound to the anion solvation shell ($[\mathrm{O–D}\cdots\mathrm{O}]$). With the equilibrium an equilibrium constant K_a is associated defined by

$$
K_a = \frac{[A \cdot OD]}{[A\cdot][OD \cdots O]}. \tag{4.5}
$$

We now identify $[A\cdot\mathrm{OD}]$ with $N_{\mathrm{OD,a}}(\epsilon)$. It can be written in terms of K_a and ϵ using the following 'conservation laws':

$$
\begin{aligned}
[A\cdot] + [A \cdot OD] &= N_a \epsilon, \\
[A \cdot OD] + [OD \cdots O] &= N_{\mathrm{OD}}.
\end{aligned} \tag{4.6}
$$

N_a is the maximum number of water molecules in the anion's solvation shell, called the coordination number. N_{OD} is the concentration of O–D groups, equal to twice the molarity of water, 110 M.

An expression for the concentration of cation-affected O–D groups, $N_{OD,c}(\epsilon)$, can be obtained in a similar way. We describe these O–D groups in terms of water molecules, since in the solvation shell of the cation the water molecules are closest with their oxygen atom to the cation. The equilibrium is written as:

$$K_c = \frac{[C \cdot OD_2]}{[C\cdot][D_2O],} \tag{4.7}$$

and the conservation laws

$$\begin{aligned} [C\cdot] + [C \cdot OD_2] &= N_c\epsilon, \\ [C \cdot OD_2] + [D_2O] &= N_{OD}/2. \end{aligned} \tag{4.8}$$

N_c is the cation's coordination number, $[D_2O]$ is the concentration of water molecules that are not in the cation's solvation shell.

The concentration of O–D groups that are affected by the cation is equal to twice (two O–D groups per water molecule) the concentration of occupied cation bonding sites. However, a fraction of these O–D groups will bind to the anion (especially at high concentrations); these are considered to be anion-bound O–D groups, since the anion has a much stronger effect on the hydrogen bond than the cation. This is illustrated by the O–D stretch absorption spectra obtained from infrared spectroscopy [118,125,58,76] and Raman spectroscopy.[126] Hence, to arrive at $N_{OD,c}(\epsilon)$, the concentration of cation-affected O–D groups, 2 $[C \cdot OD_2]$, is multiplied with the fraction that binds to another water molecule and not to an anion. Hence,

$$N_{OD,c}(\epsilon) = 2[C \cdot OD_2]\left(1 - \frac{N_{OD,a}(\epsilon)}{N_{OD}}\right) \tag{4.9}$$

Neglecting changes in N_{OD} due to dissolution of salt, the concentration of bulk O–D groups, i.e. the ones that are neither affected by the anion nor by the cation, is given by

$$N_{OD,b}(\epsilon) = N_{OD} - N_{OD,a}(\epsilon) - N_{OD,c}(\epsilon) \tag{4.10}$$

The dominant character of φ_{acc} is that of O–H$\cdots$X$^-$. The admixture of bulk and cation behaviour is assumed to scale with $N_{OD,b}(\epsilon)$ and $N_{OD,c}(\epsilon)$, respectively. We assume that the coefficients $|C_b|^2$ and $|C_c|^2$ depend linearly on these concentrations. The coefficient $|C_a|^2$ then follows from the normalization of φ_{acc}. As a function of concentration, the coefficients are now defined as follows:

$$\begin{aligned}
\sum_b |C_b|^2(\epsilon) &= k_{\mathrm{b}} \frac{N_{OD,b}(\epsilon)}{N_{\mathrm{OD}}}, \\
\sum_c |C_c|^2(\epsilon) &= k_{\mathrm{c}} \frac{N_{OD,c}(\epsilon)}{N_{\mathrm{OD}}}, \\
\sum_a |C_a|^2(\epsilon) &= \left(1 - \sum_b |C_b|^2(\epsilon) - \sum_c |C_c|^2(\epsilon)\right),
\end{aligned} \tag{4.11}$$

with k_{b} and k_{c} proportionality constants that depend on the nature of the cation and the anion. Equations (4.4) to (4.11) fully describe the dependence of the vibrational lifetime on anion, cation and their concentration. Note that $N_{OD,b}(\epsilon)$ and $\sum_b |C_b|^2$ reach their maximum value at $\epsilon = 0$, while $N_{OD,c}(\epsilon)$ and $\sum_c |C_c|^2$ are equal to zero at $\epsilon = 0$.

4.5 Fit Results

In the previous section, we obtained an expression for the lifetime of the anion-bound O–H stretch vibration, as a function of concentration and composition of dissolved salt, in terms of the lifetimes of anionic (T_{1a}), bulk (T_{1b}) and cationic (T_{1c}) components. T_{1b} is known from previous studies on pure HDO:D_2O and equals 0.74 ps. For the T_{1c}, no data are available, and their contribution to the measured T_1 turned out to be too small to allow for an accurate determination of their values in the present work. Hence, we determine the value of T_{1c} using a phenomenological relation between the O–H stretch redshift (with respect to the gas-phase value of 3700 cm^{-1}) and the vibrational lifetime [85,117]:

$$T_1 = k(\Delta\omega_{\mathrm{OH}})^{-1.8}. \tag{4.12}$$

The form of this relation can be intuitively understood by appreciating that both quantities rely on the hydrogen-bond strength. The first spectral moment of the component of the O–D stretch absorption band due to several cations has been measured in Ref. 118. After multiplication by a factor of 1.36[131] to obtain the O–H stretch frequencies, the values are 3325 cm^{-1} (Li^+O–H$\cdots$O), 3456 cm^{-1} (Na^+O–H$\cdots$O) and 3340 cm^{-1} (Mg^{2+}O–H$\cdots$O). Compared to a frequency of 3410 cm^{-1} for HDO:D_2O without salt,[37] the Na^+ affected O–H stretch band is blueshifted with respect to pure water, whereas Mg^{2+} and Li^+, that have stronger electric fields, are redshifted. The constant k in equation (4.12) is determined using a lifetime of 0.74 ps for pure HDO:D_2O.[138,91] For T_{1c} the following values are obtained: 0.5 ps (Li^+), 1.0 ps (Na^+) and 0.5 ps (Mg^{2+}). For the determination of T_{1a} we cannot use equation (12) since it is only valid for O–H$\cdots$O hydrogen bonds. For O–H$\cdots X^-$ hydrogen bonds the frequency dependence will be different.

Values for the coordination numbers can be found in the literature.[96,81,10,31,107] We use coordination numbers of 4 for Li^+, 6 for Na^+, Mg^{2+}, $Cl^-$and Br^-, and 9 for I^-. The values of K_{a} and K_{c} appeared not to be very critical in the fit. We used a value of 0.25; a 1 M NaCl solution will then have 5 % of the available anion-binding sites unoccupied. At 6 M, this fraction is 7 %.

	T_{1a}	k_b	k_c
LiCl	3.5 ps	0.17	0.07
NaCl	3.5 ps	0.17	0.10
$MgCl_2$	3.5 ps	0.17	0.07
LiBr	5 ps	0.18	0.08
NaBr	5 ps	0.18	0.14
$MgBr_2$	5 ps	0.18	0.07
LiI	6 ps	0.22	0.08
NaI	6 ps	0.22	0.19
MgI_2	6 ps	0.22	0.06

TABLE 4.1. Fit values of T_{1a}, k_b and k_c. T_{1a} and k_b are considered to be characteristic of the anion, and therefore kept constant for each anion. The fits are shown in figures 4.3–4.6.

The remaining fit parameters are T_{1a}, k_b and k_c. Of these parameters T_{1a} and k_b should only depend on the nature of the anion. At zero concentration $N_{OD,b} = N_{OD}$ and $|C_a|^2 = 1 - k_b$. Therefore, for a given anion, k_b should be the same for all cations. Hence, for a particular combination of cation and anion only k_c is left as a fit parameter.

The fit values of T_{1a}, k_b and k_c are shown in table 4.1.

4.6 DISCUSSION

The model of section 4.4 provides a good description of the trends observed in section 4.3. From the comparison of the fit results with the experimental data we can now identify the origins of the trends observed. Within the framework of the model, the increase in T_1 going from Cl^- to Br^- to I^- finds its origin in an increase in T_{1a}. This increase implies that the coupling of the excited O–H stretch vibration to the local O–H$\cdots$X$^-$ mode decreases in the series Cl^- to Br^- to I^-. This can be understood in the following way. Within the halogenic series (F^-, Cl^-, Br^-, I^-), the absorption spectrum of the O–H stretch vibration shifts to higher frequencies, which indicates that the strength of the hydrogen-bond interaction decreases.[94,83] The weaker hydrogen-bond interaction in turn leads to a decrease of the anharmonic interaction between the O–H stretch vibration and the hydrogen-bond mode,[117] and thereby to a slow-down of the vibrational relaxation. In addition, the reduced mass of the O–H$\cdots$X$^-$ hydrogen-bond stretch vibration, which determines the energy spacing of the levels of this mode, increases within the halogenic series Cl^-, Br^-, I^-. The hydrogen-bond frequencies have been measured [6]: 210 cm^{-1} for O–H$\cdots Cl^-$, 158 cm^{-1} for O–H$\cdots Br^-$ and 135 cm^{-1} for O–H$\cdots I^-$. As a result, the dissipation of the excitation energy of the O–H stretch vibration will involve a higher level of excitation of the hydrogen-bond vibration for I^- than for Cl^-, which also decreases the anharmonic interaction.[93]

A second important effect is the increase of T_1 with concentration. According to the model, this increase mainly results from the decreased contribution of bulk O–D$\cdots$O bonds to the delocalized hydrogen bond wavefunctions $\varphi_{dhb,f}$ and $\varphi_{dhb,i}$. In figure 4.7, the fractions of the different types of hydrogen bonds are shown for NaCl and MgI. It is clearly

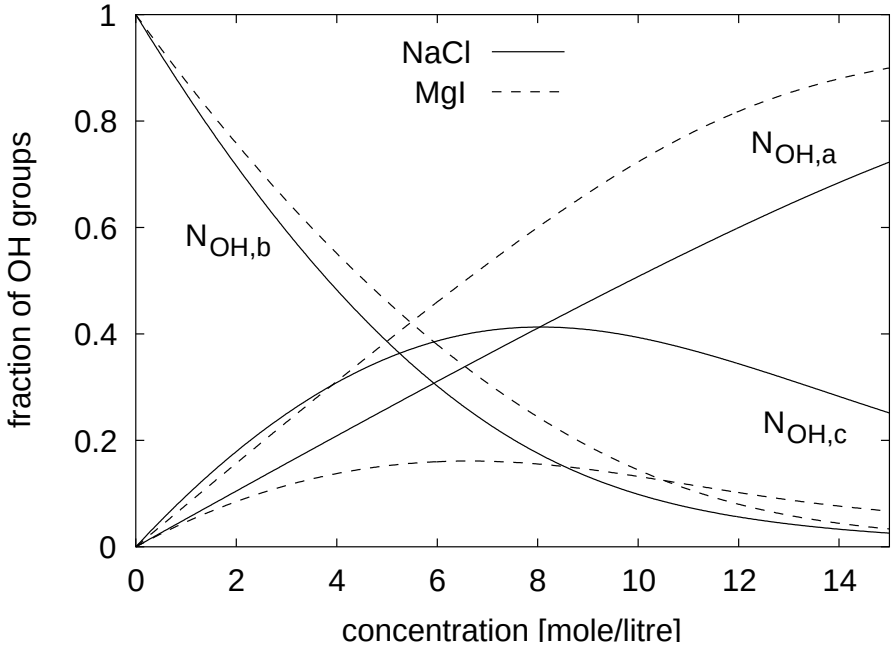

Figure 4.7. The functions $N_{\mathrm{OD,a}}(\epsilon)$, $N_{\mathrm{OD,b}}(\epsilon)$and $N_{\mathrm{OD,c}}(\epsilon)$, defined as the concentration of O–D groups that is involved in an anion-, cation-, or bulk hydrogen bond, for NaCl (solid lines) and MgI (dashed lines); see text (section 4.4) for details.

seen that with increasing concentration of dissolved salt, the fraction of O–D$\cdots$O hydrogen bonds decreases while the fraction of O–D$\cdots X^-$ hydrogen bonds increases. The fraction of cationic hydrogen bonds Y^+O-D$\cdots$O first increases with concentration because more ions are present, but at high concentration decreases again because an increasing part of the water molecules in the first solvation shell of the cation are simultaneously bound to an anion via an O–D$\cdots X^-$ hydrogen bond. In figure 4.8, the corresponding coefficients are shown for the same two salts. It is clearly seen that at low concentration the delocalized hydrogen bond is already dominated by the anionic hydrogen bond modes. With increasing concentration this character gets even stronger, making the hydrogen bond into an almost purely anionic hydrogen bond at high concentrations. Hence, the overall relaxation time T_1 increases with concentration because of the increase of the contribution of the long T_{1a} and the decrease of the contribution of the short T_{1b}.

The slope of the concentration dependence is largest for I^- salts. The slope of the concentration dependence of T_1 is mainly determined by the difference between T_{1a} and T_{1b}. This difference increases going from Cl^- to Br^- to I^-, thus largely explaining the observed increase in slope. In addition, the coordination number is higher for I^- than for Cl^- and Br^-. As a result, the fraction of anion-affected O–D groups increases faster with concentration for I^- than for Cl^- and Br^-. In figure 4.7, it is indeed seen that for MgI_2 the relative fraction of anionic hydrogen bonds rises much faster with anion concentration than for NaCl. The faster rise of the fraction of anionic hydrogen bonds for I^- leads to a

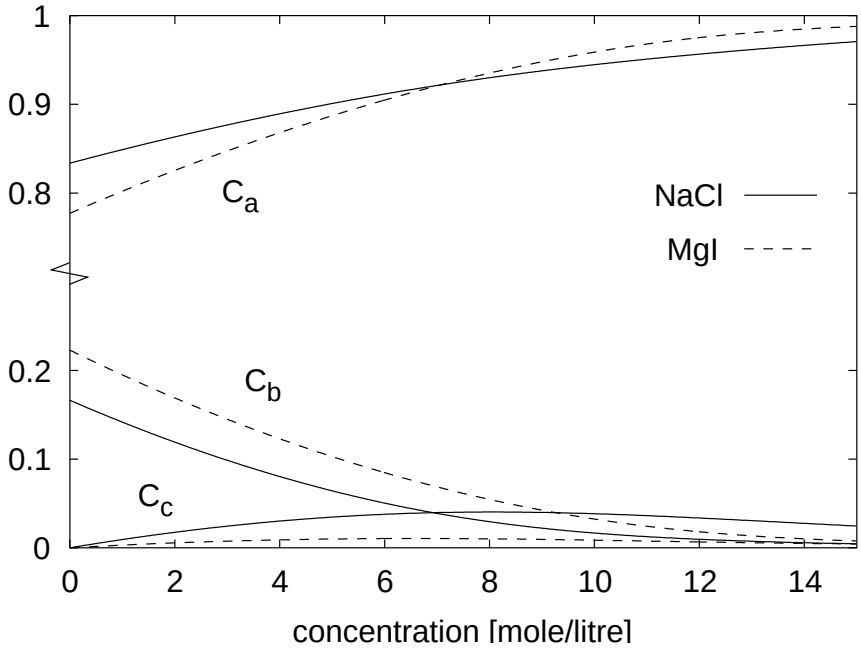

FIGURE 4.8. The functions $\sum_a C_a(\epsilon)$, $\sum_b C_b(\epsilon)$ and $\sum_c C_c(\epsilon)$, for NaCl (solid lines) and MgI (dashed lines). The functions depend on the functions $N_{\mathrm{OD,a}}(\epsilon)$, $N_{\mathrm{OD,b}}(\epsilon)$and $N_{\mathrm{OD,c}}(\epsilon)$, shown in figure 4.7, and are defined in equation 4.11; see text (section 4.4) for details.

faster rise of the contribution of the anionic hydrogen bonds to the delocalized hydrogen-bond wavefunctions $\varphi_{\mathrm{dhb,f}}$ and $\varphi_{\mathrm{dhb,i}}$, which in turn results in a faster increase of T_1.

Another important trend is the small but significant dependence of T_1 on the nature of the cation: the sodium salts have a longer T_1 than the magnesium and lithium salts. This results primarily from the difference in the value of T_{1c}. The different T_{1c} can be explained from the different strengths of the electric fields around the cations: Li^+ is smaller than Na^+, while Mg^{2+} has the same size as Na^+, but twice the charge. The electric field serves to polarize the hydrogen bonds of water molecules adjacent to the cation such that they are strengthened, thereby increasing the anharmonic interaction with the O–H vibration. The influence of the very short (0.5 ps) T_{1c} of lithium and magnesium is somewhat tempered by the fact that there are less cations around compared to sodium; for lithium because the coordination number is lower (4), for magnesium because of the double charge, halving its concentration with respect to the anion.

Finally, the influence of the cations on T_1 is much smaller for the iodide salts than for the bromide and chloride salts. In the model this effect is reflected in the relatively small contribution of the Li^+O–D$\cdots$O and $Mg^{2+}O$–D$\cdots$O hydrogen bonds to the delocalized $\varphi_{\mathrm{dhb,f}}$ and $\varphi_{\mathrm{dhb,i}}$ wavefunctions. This can be seen from the coefficients k_c of the iodide salts shown in table 4.1. A possible explanation for the small admixture of cationic hydrogen bonds is the large frequency difference between the Li^+O–D$\cdots$O and $Mg^{2+}O$–D$\cdots$O hydrogen bonds and the O–H$\cdots I^-$ hydrogen bond. The Li^+O–D$\cdots$O

and Mg^{2+}O–D···O hydrogen bonds are relatively strong and will have high frequencies, whereas the O–H···I^- hydrogen bond is relatively weak, resulting in a rather low frequency. Within a perturbative approach of the description of the wavefunction, the admixture is inversely proportional to the frequency difference, thus explaining why the Li^+O–D···O and Mg^{2+}O–D···O hydrogen bonds are only weakly contributing to the hydrogen bond of dominant O–H···I^- character.

From the above it is clear that the observed trends can be well explained from changes in the delocalized hydrogen-bond mode involving the hydrogen atom of the excited O–H vibration. However, this hydrogen bond is not the only accepting mode. The accepting combination tones likely also contain excitations of the bending mode and/or the O–D stretching vibration,[24] and other hydrogen-bond modes. These modes can also be affected by a change in concentration and nature of the dissolved cations and anions, and these effects can also contribute to the observed trends. However, the influence of the dissolved ions on the intramolecular modes will not be as strong as on the φ_{dhb} hydrogen-bond. Hence, the effects on the intramolecular modes are not expected to have a large influence on the overall relaxation rate. The other hydrogen bond modes certainly do depend on the nature and concentration of dissolved salt. These other hydrogen bonds are not expected to couple directly with the excited O–H stretch vibration, because they are shielded from the excited vibration by an oxygen atom or a heavy anion. The interaction with the bulk O–D···O and cationic Y^+O-D···O hydrogen bonds is therefore expected to occur mainly via the coupling of these modes with the local O–H···X^- mode, which forms the basis of the model of section 4.4.

4.7 Conclusions

We studied the mechanism of vibrational relaxation of water molecules in the solvation shells of Cl^-, Br^- and I^- halogenic anions. To this end we performed measurements on the vibrational relaxation of HDO:D_2O solutions of a series of salts formed by the cations Li^+, Na^+ and Mg^{2+}, and the anions Cl^-, Br^- and I^-. The concentration was varied between 0.5 M and 6 M (Cl^-), 9 M (Br^-), or 10 M (I^-). We found that the vibrational lifetime T_1 of HDO molecules in the solvation shell of the anions increases in the halogenic series Cl^-, Br^-, I^-, and with increasing concentration of dissolved salt. In addition, we found a small but significant dependence of T_1 on the nature of the cation: for the same type of anion and concentration, T_1 increases in the cationic series Mg^{2+}, Li^+, Na^+.

The observed trends in the relaxation can be well described with a model in which one of the accepting modes is the hydrogen bond involving the hydrogen atom of the excited O–H group. Due to the coupling between the hydrogen bonds in the liquid, this hydrogen bond is not a pure O–H···X^- (X=Cl^-, Br^-, or I^-) bond, but a delocalized mode showing admixture of other anionic O–D···X^- hydrogen bonds, bulk O–D···O hydrogen bonds and O–D···O hydrogen bonds of water molecules in the first solvation shells of the cations, denoted as Y^+O-D···O hydrogen bonds.

With increasing concentration, the O–D···X^- character of the delocalized hydrogen bond increases while the bulk O–D···O character decreases, leading to an increase of T_1 (slower relaxation), because the coupling to an O–D···O hydrogen bond is much stronger than to an O–D···X^- bond. For the iodide salts this difference in coupling is largest, thus

explaining the relatively steep increase of T_1 with concentration for solutions containing I^-. The value of T_1 is also affected by the coupling of the excited O–H stretch vibration to the part of the delocalized hydrogen-bond wavefunction representing the cationic $Y^+O\text{-}D\cdots O$ bonds. The strength of the cationic hydrogen bond increases going from $Na^+O\text{–}D\cdots O$ to $Li^+O\text{–}D\cdots O$ to $Mg^{2+}O\text{–}D\cdots O$. Hence, the anharmonic interaction increases in this series, thus explaining the observed decrease in T_1. The latter effect is small (maximum = 10%), because for all salt solutions the cationic hydrogen bonds only form a small contribution (<7%) to the delocalized hydrogen bond mode.

5 Comment on Laenen and Thaller

Comment on: *Water in the vicinity of solvated ions: modified dynamical and structural water properties resolved by sub-picosecond IR-spectroscopy*
by R. Laenen and A. Thaller, Chem. Phys. Lett. **349** (2001) 442

Recently, Laenen and Thaller published results on the vibrational lifetime of the O–H stretch vibration of aqueous salt solutions (LiCl, NaCl, KCl or NaI). They reported that the vibrational lifetime depends on the nature of the cation, and not on that of the anion. The variance of this finding with the results presented in chapter 3 and chapter 4, was attributed to differences in pulse characteristics. In this chapter, we present experimental results that show that the claims by Laenen and Thaller are wrong, and that the vibrational lifetime is influenced strongly by the anion, and only weakly by the cation, independent of the pulse characteristics.

5.1 Introduction

In the Letter published by Laenen and Thaller,[72] results were presented on the vibrational and orientational relaxation of water molecules in aqueous salt solutions containing LiCl, NaCl, KCl, or NaI. It was reported that the vibrational lifetime depends on the nature of the cation and not on that of the anion (see chapter 3 and chapter 4). Unfortunately, no comparative data were supplied to support these findings (only data for NaCl solutions were shown). Since the difference with our previously published work[66,67] was ascribed by Laenen and Thaller to differences in the pulse parameters, we repeated their measurements with laser pulses identical to the pulses they used. The results, which are presented in this chapter, show that the conclusions of Laenen and Thaller are incorrect.

5.2 Experiment

In order to reproduce the measurements of Laenen and Thaller, we changed our method of pulse generation slightly with respect to the previous chapters. By using two instead of only one KTP crystal in the pulse generation (section 2.3), we managed to obtain laserpulses with almost the same bandwidth, pulse duration and pump energy as the pulses used by Laenen. The spectral width of the pulses was reduced to 37 cm^{-1}, and the pulse duration was increased to 450 fs. The pump-pulse energy was limited to 10 μJ. The pump was tuned to 3420 cm^{-1}, the probe to 3150 cm^{-1} and 3420 cm^{-1}. The sample is contained in a rotating sample cell to obtain a fresh part of the sample at every laser shot. Hence, the temperature error is limited to the effect of a single pump pulse, and is less than 1 K. The only difference with the experiment of Ref. 72 is that the pulses used in the present study have a 1 kHz repetition rate, whereas the pulses used in Ref. 72 have a repetition rate of only 50 Hz.[71]

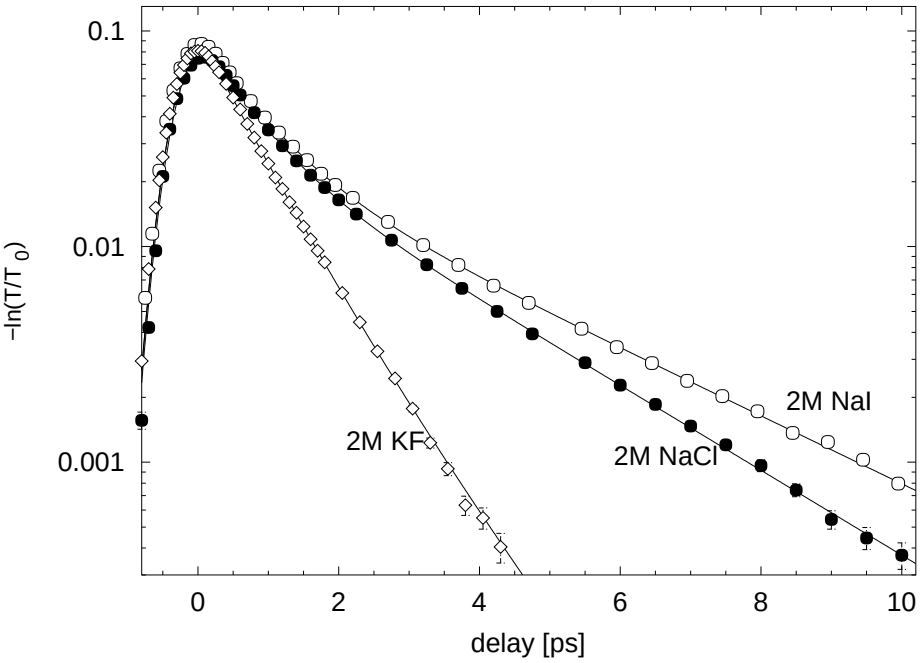

FIGURE 5.1. Isotropic transmission changes of solutions of HDO in D_2O and 2 M of NaI, NaCl, and KF. The pump was tuned to 3420 cm^{-1}, the probe to 3150 cm^{-1}.

5.3 RESULTS AND DISCUSSION

The pump–probe transients (isotropic transmission changes) of 2 M solutions of NaCl, KCl, KF, and NaI obtained with these pulse parameters are shown in figures 5.1 and 5.2.

First, we studied the dependence of the vibrational lifetime on the nature of the anion. In Ref. 72 it is reported that the vibrational relaxation is independent of the anion: the same time constant of 2.7±0.2 ps is reported for NaCl and NaI at all concentrations. In figure 5.1, we present data on these solutions using the same pulse parameters as Laenen and Thaller. It is clear that, contrary to the results of Ref. 72, the vibrational relaxation in the solutions containing 2 M NaCl or NaI is different. In the figure, we also added a measurement of 2 M KF, for which the absorption change decays much faster, approximately as fast as pure HDO:D_2O (0.74±0.1 ps). We used KF instead of NaF since the latter salt is poorly soluble in water. However, exchanging Na^+ for K^+ does not have a strong effect on the lifetime, as is illustrated in figure 5.2. It is clear from the measurements presented in figure 5.1 that the anion does have a strong effect on the vibrational lifetime and that this lifetime increases going from F^- to Cl^- to I^-.

Time constants for the relaxation can be obtained by performing a biexponential fit to the data (the fit function is the sum of two exponentials, multiplied with the Heavyside function and convolved with the gaussian cross-correlation trace). For all solutions, we

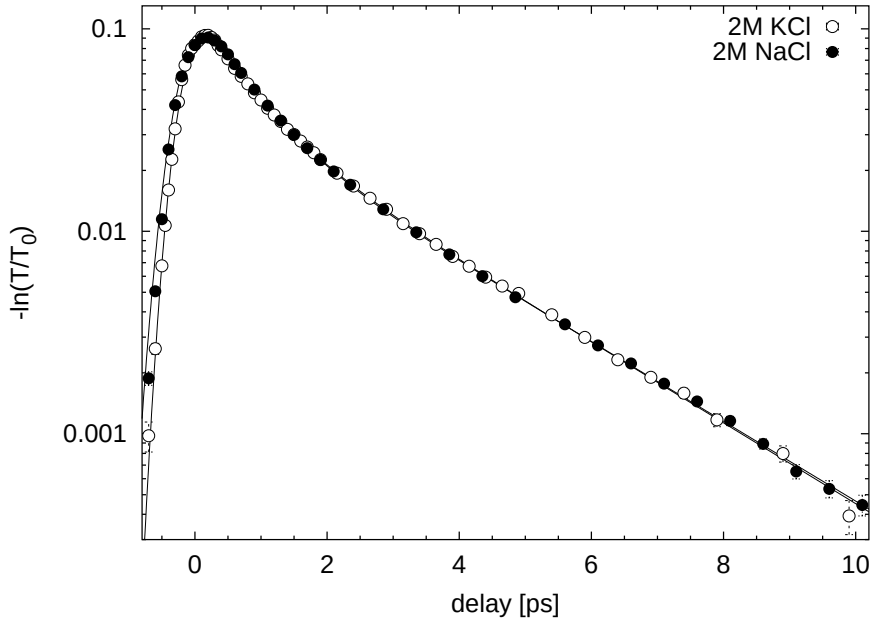

FIGURE 5.2. Isotropic transmission changes of solutions of HDO in D_2O and 2 M of NaCl, and KCl. The pump was tuned to 3420 cm^{-1}, the probe to 3150 cm^{-1}.

find a fast component similar to that of HDO:D_2O and slow decay-time constants of 2.21±0.1 ps (2 M NaCl) and 2.76±0.1 ps (2 M NaI). For higher concentrations, the decay times increase to 2.6±0.2 ps (6 M NaCl) and 3.7±0.2 ps (6 M NaI). The decay time of KF remains 0.74±0.1 ps at all concentrations. We found that the time constant of the slow component does not depend on the probe frequency: measurements on a 2 M NaCl solution using a pump frequency of 3420 cm^{-1} and probe frequencies of 3100, 3150, and 3200 cm^{-1} give the same result.

Second, we studied the dependence of the vibrational lifetime on the nature of the cation. Laenen and Thaller report a rather strong dependence of the vibrational lifetime on the cation, eg. 2.4 ps for KCl and 2.7 ps for NaCl (2 M solutions). We also performed measurements on these solutions; the results are presented in figure 5.2. The relaxation does not differ at all. Biexponential fits of the data reveal the following lifetimes: 2.21±0.1 ps (NaCl) and 2.18±0.1 ps (KCl) (2 M solutions, at 3150 cm^{-1} probe). At higher concentrations of salt, the vibrational relaxation of NaCl and KCl remain equal.

In these experiments on aqueous salt solutions, there is very little effect of spectral diffusion, at least at delay times >2 ps. Only if the 0→1 transition is excited in the wings of the absorption band, so that the initial distribution of excited molecules most strongly differs from the final equilibrium distribution, we observe a small effect (see chapter 6). In the experiments of figures 5.1 and 5.2, where the 0→1 transition is excited close to the

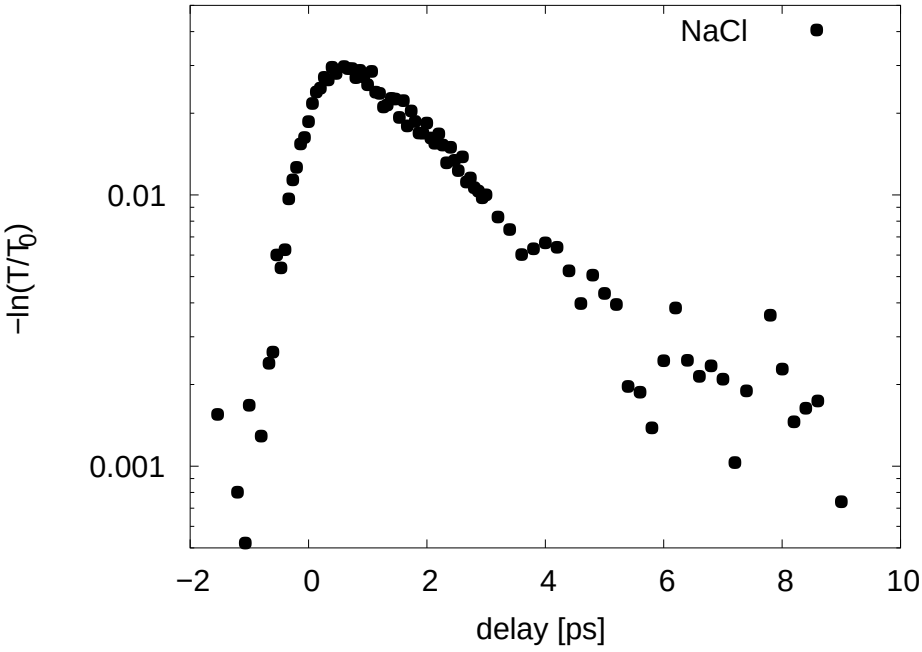

FIGURE 5.3. Experimental data published by Laenen and Thaller (figure 2 of Ref. 72). In the experiment, the pump was tuned to 3420 cm^{-1}, the probe to 3150 cm^{-1}. The sample was a solution of 5 M of NaCl.

center of the absorption band, the dynamics after 2 ps are not at all affected by spectral diffusion, which implies that the time constants directly represent the vibrational lifetimes T_1 of the O–H stretch vibration. This means that the differences between the time constants we find and those of Ref. 72 cannot be attributed to differences in modeling of the transient spectral response and of the spectral diffusion.

If not from the pulse parameters or from differences in spectral modeling, how can the qualitative differences between the present findings and those of Ref. 72 be explained? The answer to this question can be found in the quality of the data. For comparison of the data quality, similar experimental data from Laenen's work (figure 5.3) and measured with our setup (figure 5.4) are presented.

The difference in quality of the data can be quantized by calculating the value of χ^2. The value of χ^2 calculated from the data of figure 5.3 (figure 2 of Ref. 72) is 2×10^{-4} (with respect to their own fit), whereas for the data we obtained (figure 5.4), $\chi^2 = 3\times10^{-6}$ (with respect to a biexponential fit). The difference is almost two orders of magnitude. This difference in quality of the data leads to a large difference in dynamic range of the data: the data of figures 1 and 2 have a 20 times larger dynamic range than the measurements of Ref. 72. As a result, the uncertainties in the time constants reported in Ref. 72 must be quite substantial. As such, the statement of Ref. 72 that "increasing the size of the anion results in no measurable effect on T_1 for the investigated anions [...] within our measurement accuracy"is more informative on this accuracy than on the true physical

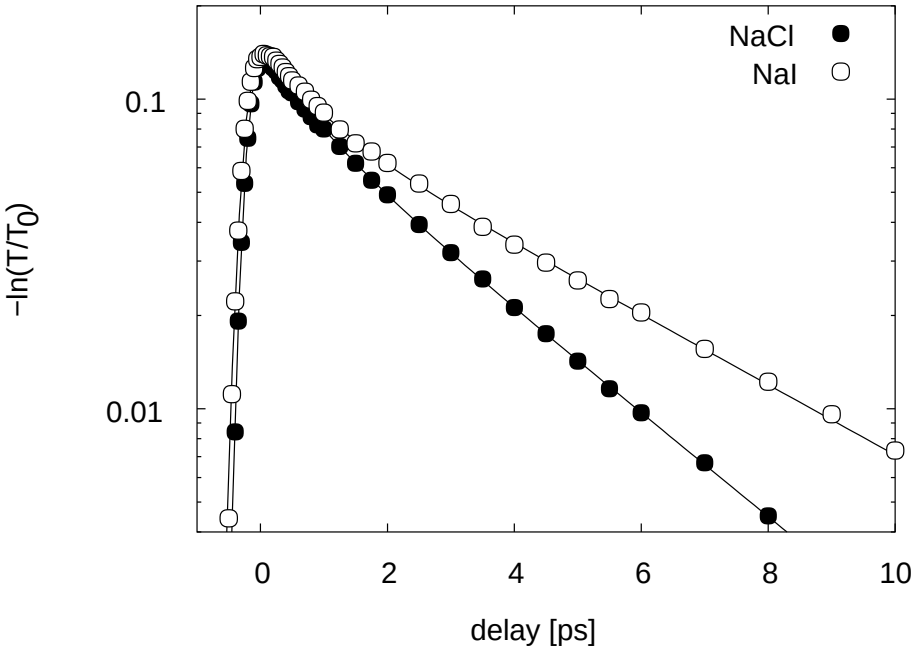

FIGURE 5.4. Data obtained at our setup, using the same sample and pulse characteristics as in the experiment of Laenen and Thaller, shown in figure 5.3. Comparison of the variances between the data set and its fitted curve leads to a value of χ^2 that is two orders of magnitude smaller in our case.

properties of these solutions. In view of the poor quality of the data, it is also questionable whether a decomposition of the absorption band in no less than six exchanging spectral components, as is done by Laenen and Thaller, is required and justified.

In their discussion of the data, Laenen and Thaller propose a correlation between the vibrational lifetime T_1 and the redshift of the O–H-stretch frequency with respect to the gas-phase value. This correlation is in agreement with experiment[85] and with theory, e.g. Ref 117, where the vibrational lifetime has been calculated as a function of O–H stretch frequency (hydrogen-bond strength) for an O–H$\cdots$O system. In Ref. 72 this correlation is illustrated with a figure in which T_1 is presented as a function of the redshift for three previously measured systems. Indeed, these results neatly fall on a straight line. This figure is used by Laenen and Thaller to explain the observed long vibrational lifetimes of solutions containing Cl^- and I^-. Curiously, however, the data measured for the salt solutions are not at all included in this figure. If one would include these data one would see that they are far above (larger T_1) the line representing the correlation between T_1 and the redshift.

The work in chapter 3 and chapter 4 provides a rather straightforward explanation for this observation. In short, the vibrational lifetime T_1 is indeed correlated to the O–H-stretch redshift via the empirical relation $T_1 \propto (\Delta\omega_{OH})^{-1.8}$;[117] for all hydrogen-bonded O–H groups, the vibrational lifetime will decrease with increasing redshift. However, the

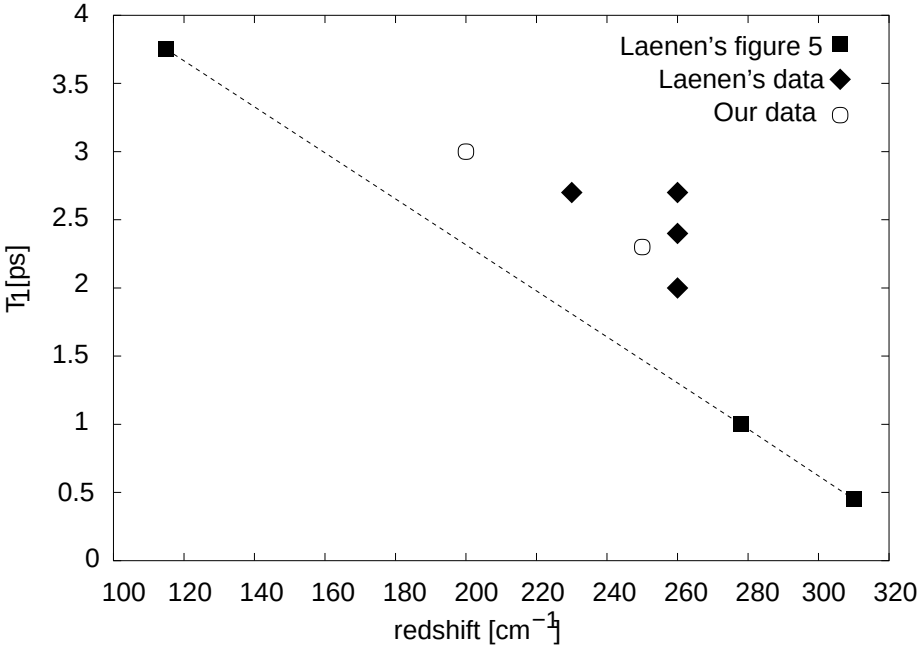

FIGURE 5.5. The data points connected by the straight line were used in Ref. 72, figure 5, to explain the lifetimes of the measured data, which we added here to show that these data are not at all on this line.

precise value of the lifetime will also depend on the nature of the hydrogen-bond acceptor, i.e. O, Cl^-, or I^-. In previous Raman[126] and infrared spectroscopic studies,[10] it was found that a substantial part of the O–H-stretch absorption spectrum of salt solutions containing X^- halogenic anions results from O–H$\cdots X^-$ hydrogen-bonded groups. The observed long vibrational lifetimes of solutions containing Cl^- and I^- can thus be well explained if these lifetimes represent the relaxation of O–H$\cdots Cl^-$ and O–H$\cdots I^-$ systems, and not of O–H$\cdots$O systems. The longer O–H-stretch vibrational lifetimes of O–H$\cdots Cl^-$ and O–H$\cdots I^-$ in comparison to O–H$\cdots$O at the same redshift can be well explained from the larger mass of the hydrogen-bond acceptor. This explanation also agrees with the observation that the O–H-stretch vibrational lifetime of O–H$\cdots F^-$ is comparable to that of O–H$\cdots$O, since the mass of F^- is very similar to that of a water molecule.

5.4 CONCLUSIONS

In this chapter, we presented experimental data on the salt solutions studied in Ref. 72 using the same experimental parameters, but with a much better signal-to-noise ratio. It is found that the vibrational lifetime strongly depends on the nature of the anion and only weakly on the nature of the cation, in strong contrast to the claims of Laenen and Thaller, and in agreement with the results of chapter 3 and chapter 4.

6 Hydrogen-bond dynamics of aqueous solvation shells

In the previous chapters, it was demonstrated that the lifetime of the O–H stretch vibration differs between those hydrogen bonded to an anion and those hydrogen bonded to another water molecule. This difference in vibrational lifetime allows for a clear separation of the response of the anion's solvation shell from that of the bulk liquid as well as from the cation's shell. In this chapter, we will use this property to specifically study the hydrogen-bond dynamics of the anion solvation shells. The hydrogen-bond dynamics is strongly related to the spectral dynamics, that can be studied by tuning the pump and probe frequencies through the absorption band. The results are interpreted using the Brownian-oscillator model. The spectral diffusion times thus obtained reveal that the hydrogen-bond dynamics of solvating molecules is much slower than the hydrogen-bond dynamics of bulk liquid water.

6.1 Introduction

The dynamics of chemical reactions in aqueous media are strongly dependent on the interactions between the reacting molecules and the solvating water molecules. In many cases, a chemical reaction can take place only after a water molecule has been removed from the solvation shell, opening the way for the molecules to approach each other and react.

The absorption band of the O–H stretch vibration is inhomogeneously broadened due to the variation in hydrogen-bond length. The hydrogen-bond lengths are not static, but vary in time. Averaged over a sufficiently long period of time, the absorption band of each individual molecule equals the total absorption band. These spectral dynamics cannot be measured with linear spectroscopy. With pump–probe saturation spectroscopy, however, this is possible: one can excite a specific set of molecules, characterized by their hydrogen-bond length, and follow the spectral evolution of this ensemble. Spectral diffusion has been studied for liquid water;[134,41,43,24] the correlation time of the absorption frequency of one HDO molecule in a solution of HDO:D_2O was measured to be 500 fs or 700 fs. To date, the experimental study of the hydrogen-bond dynamics in ionic solvation shells has been hindered by the fact that it is quite difficult to distinguish the response of the solvating water molecules from that of the other (bulk) water molecules.

The contribution of bulk water to the response of an aqueous solution can be eliminated by studying small clusters of an ion surrounded by a few water molecules in the gas phase.[4,6,5,7,16,20,110,128] Since the number of O–H groups is limited, the measured predissociation spectrum can be decomposed into separate absorption components, and a detailed picture of the structure of such a cluster can be obtained. However, no hydrogen-bond dynamics has been studied with this technique, and even if such a study were performed, the results cannot easily be applied to bulk solutions,[22] where collective modes largely drive the hydrogen-bond dynamics. Techniques like NMR, infrared absorption and Raman

scattering cannot be used either, because the time scales involved in these techniques are much longer than the time scale of the solvation dynamics.[96] Hence, the information on the hydrogen-bond dynamics in aqueous salt solutions is mainly theoretical in nature and originates from molecular-dynamics simulations.[17,22,47,114,143] In these studies strongly different time constants for the exchange of water molecules between the solvation shell and the bulk were reported, ranging from one picosecond up to hundreds of picoseconds.[47,114] Very recently an ab-initio molecular-dynamics study[105,106] was performed on the solvation of Br^-. For the average residence time of water in the solvation shell of Br^- a value of 19 ± 5 ps was found.

In the previous chapters it has been shown that the lifetime of the anion-bonded O–H groups is significantly longer than that of the other water molecules. This makes femtosecond mid-infrared saturation spectroscopy an ideal technique to study the spectral diffusion in solvation shells, since it allows for a distinction between the different O–H groups: after a few picoseconds, the only O–H groups that are still excited are those in the anionic solvation shells. In this chapter, we study the hydrogen-bond dynamics of water molecules in anionic solvation shells, in solutions of different salts, concentrations and temperatures.

6.2 EXPERIMENT

We performed femtosecond mid-infrared pump–probe experiments on the O–H stretch vibration of HDO molecules in an aqueous solution consisting of a low concentration of HDO (0.1 M) in D_2O and different concentrations (1 M, 2 M, 3 M, 6 M) of KF, NaCl, NaBr, NaI, and $MgCl_2$. The pump and probe pulses have a typical energy of 20 and 2 μJ, respectively, and a duration of approximately 200 femtoseconds. The spectral bandwidths of the pump and probe pulses are 80 and 60 cm^{-1}. The polarization of the probe pulse is at the magic angle (54.7°) with respect to the polarization of the pumping pulse in order to avoid the measurements to be affected by reorientation of the HDO molecules. In the experiments, both the pump and probe frequencies are tuned through the absorption band of the O–H stretching mode of the HDO molecules.

6.3 RESULTS

In figure 6.1, delay scans are presented measured at a pump frequency of 3400 cm^{-1} and six different probe frequencies for a solution of 6 M NaI in HDO:D_2O. At frequencies $\geq$3350 cm^{-1}, a bleaching ($\ln(T/T_0) > 0$, with T the transmission of the probe and T_0 the transmission of the probe in absence of the pump) of the $v = 0 \rightarrow 1$ transition is observed. At frequencies $\leq$3300 cm^{-1}, an induced absorption ($\ln(T/T_0) < 0$) is observed, which can be assigned to the induced $v = 1 \rightarrow 2$ transition. With increasing delay, the bleaching and induced absorption decay due to the energy relaxation of the $v = 1$ state of the O–H stretch vibration of the excited HDO molecules.

In figures 6.2–6.4, transients measured for three different salts are presented. The transients are shown on a vertical logarithmic scale to illustrate that at all frequencies the decay is non-exponential and consists of a rapid decay followed by a much slower decay. The curves are scaled with respect to each other for clarity. The amplitude of

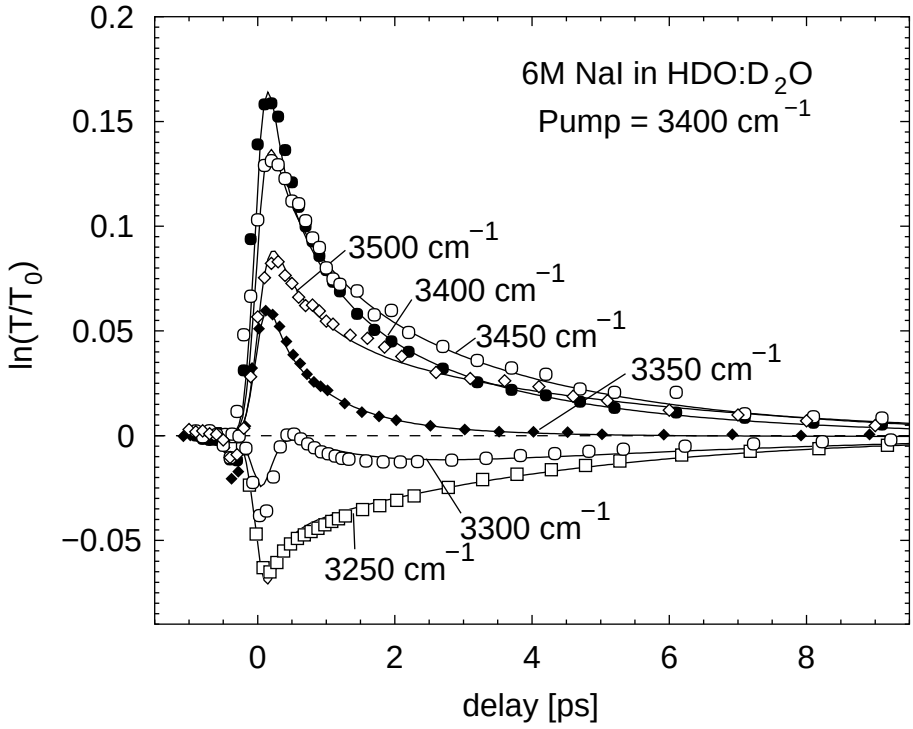

FIGURE 6.1. Pump–probe transients measured for an aqueous solution of 6 M NaI in HDO:D_2O. The transients are measured at six different probe frequencies and a pump frequency of 3400 cm^{-1}. The solid curves are calculated with the Brownian-oscillator model described in the text.

the signals depends on both the pump and probe frequencies. For a solution of NaCl, the largest amplitude is observed for pump and probe frequencies of approximately 3450 cm^{-1}, whereas for solutions of NaBr and NaI, the largest amplitude is observed for pump and probe frequencies of approximately 3500 cm^{-1}. All transients can be described as a sum of two exponentials, one with a time constant of 800 femtoseconds and one with a longer time constant that depends on salt and probe frequency. The amplitude of the slow component depends linearly on the concentration of dissolved salt.

The time constant of the slow component shows a small but significant dependence on the probe frequency. To illustrate this more clearly, figures 6.2–6.4 contain calculated dashed curves that run parallel at large delay times (> 3 ps). The time constant of the slow component is observed to increase with increasing frequency difference between pump and probe. If the pump is at 3575 cm^{-1} (figures 6.2 and 6.3), the fastest decay is observed at 3600 cm^{-1} and the slowest decay at 3500 cm^{-1}. If the pump is at 3525 cm^{-1} (figure 6.4), the fastest decay is observed at 3500 cm^{-1} and the slowest decay at 3600 cm^{-1}. These observations show that the decay time constant of the slow component is affected by a slow spectral-diffusion process with a time constant of approximately 10 picoseconds. Due to this spectral-diffusion process, excited molecules (spectrally) diffuse away from the

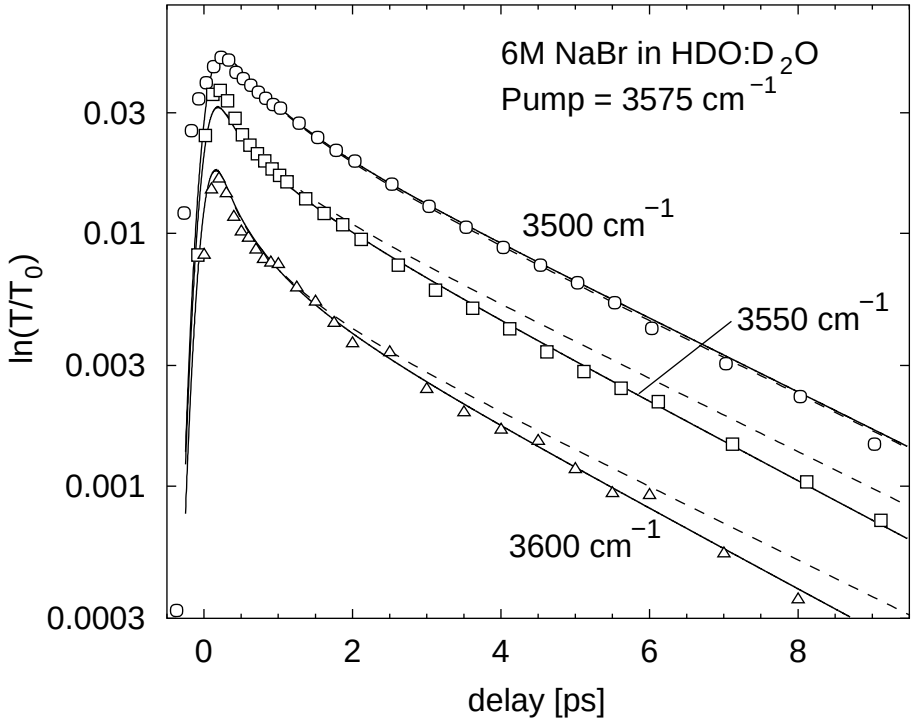

FIGURE 6.2. Pump–probe transients measured for an aqueous solution of 6 M NaBr in HDO:D_2O. The transients are scaled with respect to each other and are plotted on a logarithmic scale to clarify the presence of two absorption components and the difference in time constant The solid curves are calculated with the Brownian-oscillator model of the slow component using a τ_c of the modulation of the O–H$\cdots$$Br^-$ hydrogen bond of 25 picoseconds. The dashed curves are calculated with the same model using $\tau_c = \infty$.

excitation frequency, which leads to a faster decay at probe frequencies close to the pump frequency and a slower decay at probe frequencies that significantly differ from the pump frequency.

In figure 6.5, transients are presented that are measured for a solution of 3 M NaCl in HDO:D_2O at three different temperatures. At all three temperatures, the transient measured at 3600 cm^{-1} is observed to decay faster than the transient at 3450 cm^{-1}, as a result of the above mentioned spectral diffusion. An interesting observation is that the difference in decay rate of the two transients decreases with temperature: at a temperature of 85 °C the two transients show a more similar decay than at room temperature. This observation indicates that the spectral diffusion becomes slower when the temperature increases.

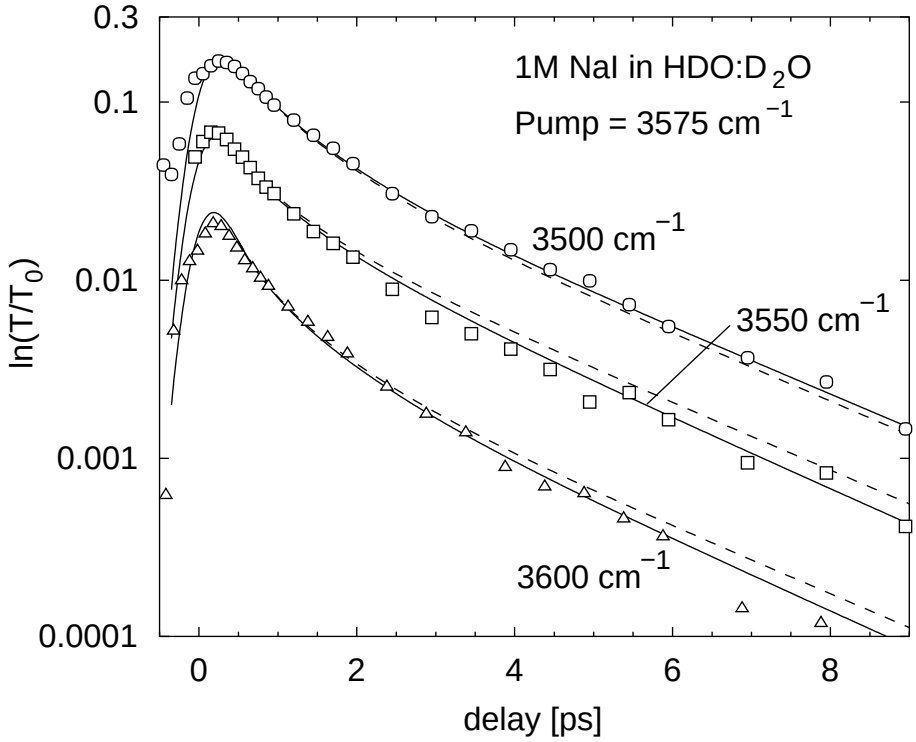

FIGURE 6.3. As figure 6.2, but for a solution of 1 M NaI in HDO:D_2O. The solid curves are calculated using a τ_c of the modulation of the O–H$\cdots$I$^-$ hydrogen bond of 18 picoseconds. The dashed curves are calculated with $\tau_c = \infty$.

6.4 SPECTRAL DIFFUSION AND THE BROWNIAN-OSCILLATOR MODEL

In an aqueous solution of a salt in HDO:D_2O, three different types of HDO molecules can be distinguished: HDO molecules in the first solvation shell of the anion, HDO molecules in the first solvation shell of the cation and HDO molecules that are only surrounded by D_2O molecules. In the following, these latter molecules will be denoted as bulk HDO molecules. The three different types of HDO molecules give rise to the fast and the slow component observed in the transient spectral data of figures 6.1–6.5.

The pump- and probe-frequency dependence of the dynamics of the slow component (figures 6.1–6.5) shows that the response of this component is affected by a slow spectral-diffusion process with a time constant of approximately 10 picoseconds. This spectral diffusion reflects the (stochastic) modulation of the hydrogen-bond length because the transition frequency of the O–Hstretch vibration and the length of the hydrogen bond are strongly correlated for directional hydrogen bonds.[94,83,84]

For a bulk solution of HDO in D_2O, the spectral diffusion of the O–H stretch ab-

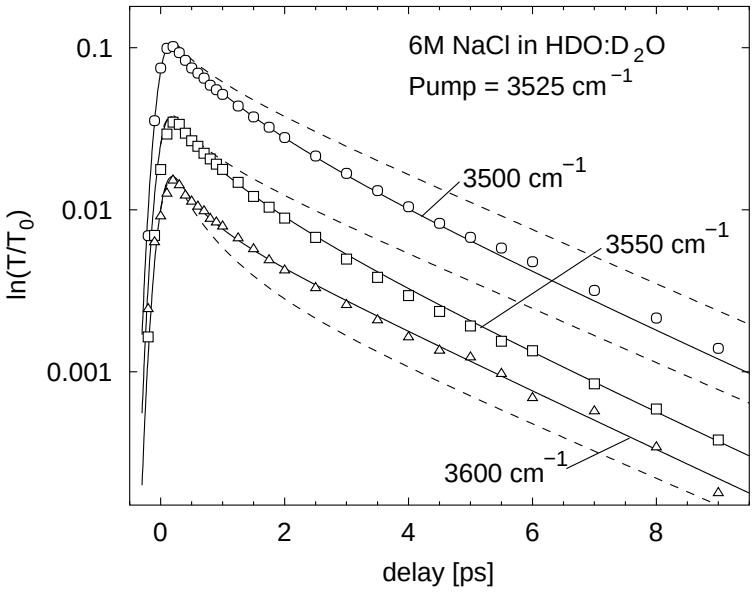

FIGURE 6.4. As figure 6.2, but for a solution of 6 M NaCl in HDO:D_2O. The solid curves are calculated using a τ_c of the modulation of the O–H$\cdots$$Cl^-$ hydrogen bond of 12 picoseconds, The dashed curves are calculated with $\tau_c = \infty$.

sorption band was observed to be very fast, having a correlation time constant τ_c of approximately 500 femtoseconds [41,134]. As a result, the excited spectrum (spectral hole) of the O–H stretch vibration of HDO dissolved in D_2O was observed to acquire the shape of the linear absorption spectrum within a few picoseconds [41]. The much longer time scale of the spectral diffusion of the slow absorption component observed for the aqueous salt solutions indicates that the stochastic modulation of the O–H$\cdots$$X^-$ hydrogen-bond length is significantly slower than the stochastic modulation of the O–H$\cdots$O hydrogen-bond length in bulk liquid water.

In order to determine the precise value of the correlation time constant τ_c of the stochastic modulation of the O–H$\cdots$$X^-$ hydrogen bond, we modeled the data of figures 6.1–6.5 with the Brownian-oscillator model.[88] Recently, it was shown that this model works well in describing the spectral dynamics of the O–H stretching mode of HDO dissolved in D_2O induced by the interactions with the O–H$\cdots$O hydrogen bond.[134] The determination of τ_c of the O–H$\cdots$$X^-$ hydrogen bond is greatly facilitated by the large difference in vibrational lifetime between the O–H$\cdots$O and the O–H$\cdots$$X^-$ component (X^- = Cl^-, Br^-, I^-).

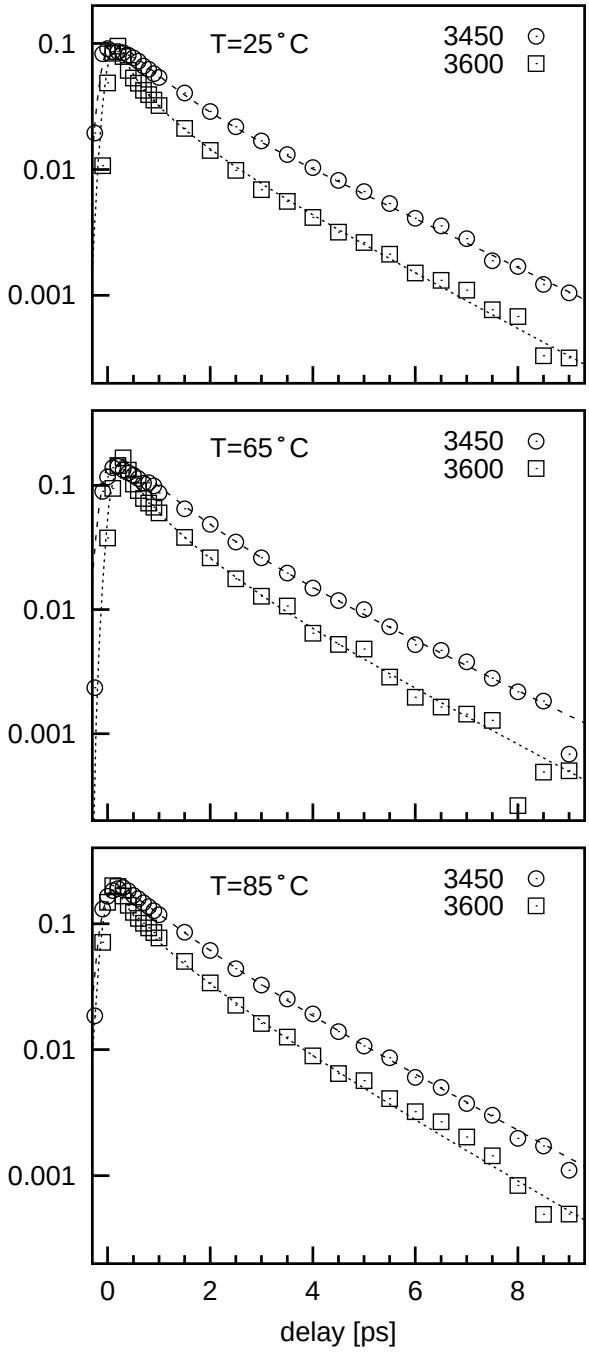

FIGURE 6.5. Pump–probe transients measured for a solution of 3 M NaCl in HDO:D_2O at three different temperatures. The difference in final decay time of the slow component decreases with increasing temperature which means that the value of τ_c of the modulation of the O–H$\cdots$$Cl^-$ hydrogen bond increases. The solid curves are calculated using τ_c =14 ps (25 °C), τ_c =24 ps (65 °C) and τ_c =30 ps (85 °C).

The Brownian-oscillator model assumes harmonic potential energy functions for the low-frequency mode (hydrogen bond) that are displaced with respect to each other in the ground and excited state of the O–H stretch oscillator (see figure 6.6). In case the hydrogen bond is a strongly overdamped mode, this results in a Gaussian absorption spectrum for the O–H stretch vibration, in quite good agreement with the experimental observations. Within the Brownian-oscillator model, the spectral dynamics of the transition of the O–H stretch vibrational transition is described with two parameters: the correlation time constant τ_c, representing the time scale at which the hydrogen-bond length is stochastically modulated, and the width Δ of the Gaussian absorption line shape $e^{-\omega^2/2\Delta^2}$ of the O–H stretch vibration. This width increases with increasing displacement of the harmonic potential energy functions. An explicit expression for the pump–probe signal $ln(T/T_0)$ as a function of delay τ and pump and probe frequency can be found in the literature:[88]

$$\begin{aligned} ln(T/T_0)(\omega_1,\omega_2,\tau) &= \frac{2\pi e^{-\tau/T_1}}{\sqrt{(\Delta^2+\delta_1^2)\alpha^2(\tau)}} e^{(-\omega_1-\omega_{eg})^2/2(\Delta^2+\delta_1^2)} \\ &\quad \times \left\{ e^{-[\omega_2-\omega_g(\tau)]^2/2\alpha^2(\tau)} + e^{-[\omega_2-\omega_e(\tau)]^2/2\alpha^2(\tau)} \right\}, \end{aligned} \tag{6.1}$$

with

$$\omega_g(\tau) = \omega_{eg} + e^{-\tau/\tau_c}(\omega_0 - \omega_{eg}) \tag{6.2}$$

$$\omega_e(\tau) = \omega_{eg} - 2\lambda + e^{-\tau/\tau_c}(\omega_0 - \omega_{eg} + 2\lambda) \tag{6.3}$$

$$\lambda = \hbar\Delta^2/2k_BT \tag{6.4}$$

$$\omega_0 = \omega_1 \frac{\Delta^2}{\Delta^2+\delta_1^2} + \omega_{eg}\frac{\delta_1^2}{\Delta^2+\delta_1^2} \tag{6.5}$$

$$\alpha^2(\tau) = \Delta^2\left[1 - \frac{\Delta^2}{\Delta^2+\delta_1^2}e^{-\tau/\tau_c}\right] + \delta_2^2 \tag{6.6}$$

where ω_1, δ_1 and ω_2, δ_2 are the centre frequencies and the spectral widths of pump and probe, respectively. The frequency ω_{eg} is the maximum of the linear absorption spectrum and T_1 is the vibrational lifetime. The parameter λ represents the Stokes shift (=2λ) that results from the fact that the position of the minimum of the hydrogen-bond potential of the excited state of the O–H stretch vibration differs from that of the ground state. Hence, excitation of the O–H stretch vibration results in a shift of the hydrogen-bond length to a new equilibrium position and an associated redshift of 2λ of the stimulated emission out of the $v = 1$ potential to the $v = 0$ potential. For harmonic potentials, the Stokes shift is directly related to the width Δ of the absorption band. λ itself does not depend on temperature, since it is only determined by the shape and displacement of the harmonic potentials. Nevertheless, in expression (6.4) the temperature T enters, because the width Δ of the absorption band depends on the thermal occupation of the ground-state potential. The two terms between the braces in equation (6.1) correspond to the bleaching (depletion of the $v = 0$) and to the stimulated emission $v = 1 \rightarrow 0$ contribution to the transmission change $ln(T/T_0)$, respectively.

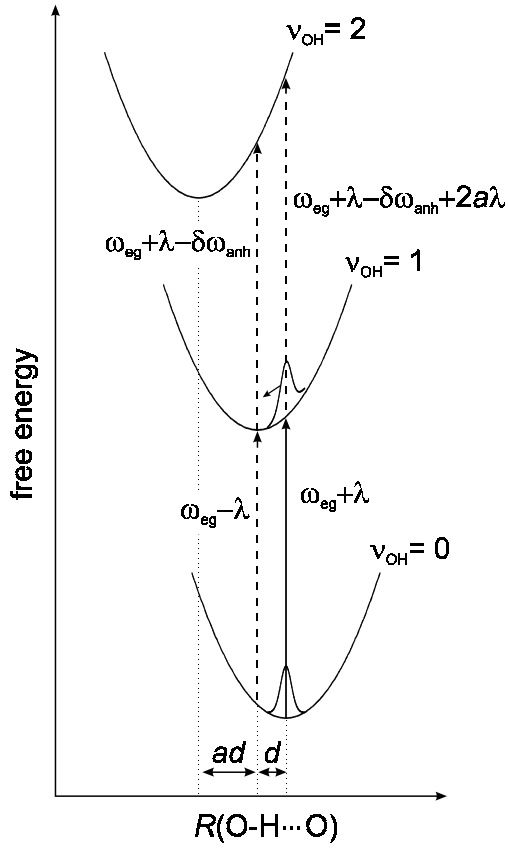

FIGURE 6.6. Harmonic potential energy functions for the O–H stretch vibration (ground state and the first two excited states), as a function of the O–H···O distance. $\omega_{eg} + \lambda$ is the ground state absorption centre frequency, 2λ the Stokes shift, $\delta\omega_{anh}$ the anharmonic frequency shift; d is the displacement of the potential minimum between $\nu_{OH} = 0$ and $\nu_{OH} = 1$; ad is the displacement of the minima of $\nu_{OH} = 1$ and $\nu_{OH} = 2$.

For all transients, we find an excellent fit using two Brownian oscillators that represent the O–H···O and O–H···X^- components. The signals of each component can simply be added, similar to equation 2.8. In table 6.1, the central frequency ω_{eg}, the spectral width $\Delta\omega$ (full width at half maximum: $\Delta\omega = \sqrt{8 \ln 2}\Delta$), the vibrational lifetime T_1 and the correlation time τ_c that result from these fits are presented for the different absorption components.

For all solutions, we find the same set of parameters for the O–H···O component. The parameters of this oscillator are quite similar to those of HDO dissolved in D_2O. Only the width of the absorption band appears to be slightly larger, which can be explained from the contribution of HDO molecules solvating the cations. The results of the calculations are shown in figures 6.1–6.5 by the solid curves. The measurements are sensi-

	ω_o	$\Delta\omega$	T_1	τ_c
O–H···O	3420±10 cm^{-1}	280±20 cm^{-1}	0.8±0.1 ps	0.5±0.2 ps
O–H···Cl^-	3440±15 cm^{-1}	160±15 cm^{-1}	2.6±0.2 ps	12±3 ps
O–H···Br^-	3470±15 cm^{-1}	130±15 cm^{-1}	3.0±0.2 ps	25±5 ps
O–H···I^-	3490±15 cm^{-1}	105±15 cm^{-1}	3.7±0.3 ps	18±5 ps

TABLE 6.1. The central frequency ω_o, width $\Delta\omega$, vibrational lifetime T_1 and spectral-diffusion time τ_c of the O-H stretch vibration of different hydrogen-bonded O-H groups, obtained by fitting the data using a two-component Brownian-oscillator model, described in the text. The values are obtained for 6 M solutions of NaCl, NaBr, and NaI. For all solutions, the same set of values for the O–H···O component was used.

tive to the value of the correlation time constant τ_c. We find τ_c=12±3 for Cl^-, τ_c=25±5 for Br^-, and τ_c=18±5 for I^-. For comparison, in figures 6.2–6.4 also results obtained with $\tau_c = \infty$ are shown (dashed curves). The calculated dashed curves run parallel at large delays, because for $\tau_c = \infty$ the transients are no longer affected by spectral diffusion. This behaviour is in in clear contrast to the experimental observations and the calculated solid curves. The value of τ_c of 25±5 ps for Br^- is in good agreement with recent Car–Parrinello simulations,[105,106] in which a value for the residence time of a water molecule in the solvation shell of Br^- of 19±5 ps was found.

The frequencies of the O–H···Cl^-, O–H···Br^- and O–H···I^- absorption components are in quite good agreement with the results from a study in which a double-difference spectroscopic technique was used to obtain the change in O–D stretch frequency due to salt addition.[10] After multiplying by 1.36 to convert O–D into O–H stretch frequencies,[131] the central absorption frequencies they found are 3441 cm^{-1} (O–H···Cl^-), 3476 cm^{-1} (O–H···Br^-) and 3495 cm^{-1} (O–H···I^-).

The central frequency of the absorption band of the O–H···X^- component increases in the halogenic series Cl^-, Br^-, I^-, whereas the width of the absorption band decreases within this series. Both trends reflect the decrease of the strength of the hydrogen-bond interaction between the solvating HDO molecule and the anion in the halogenic series. The relation between the O–H stretch vibrational frequency and the length of the O–H···X^- has been measured for many hydrogen-bond acceptors X including the halogenic anions.[83,84] This relation can be used to determine the distribution of O–H···X^- hydrogen-bond lengths from the width of the O–H···X^- absorption components. For the O–H···Cl^-, O–H···Br^-, and O–H···I^- hydrogen-bonds, we obtain widths of the length distribution of 0.20±0.05 *Å*, 0.21±0.05 *Å* and 0.12±0.04 *Å*, respectively. These widths are relatively small compared to the width of the O–H···O absorption band of HDO:D_2O of 0.36±0.02 *Å*. It should be noted that, because of additional homogeneous broadening, the widths of the obtained distributions form upper limits; the true widths may be even narrower. Homogeneous broadening can be expected to be significant, since for pure water it is between 60 and 120 cm^{-1}.[121,120] The narrow width and long τ_c of the O–H···X^- absorption component imply that the water molecules that directly bind to the X^- halogenic anion form a relatively stable and well-defined structure. The solvation shells of F^- and of the cations likely show similar dynamics as the solvation shells of Cl^-, Br^- and I^-, but unfortunately these dynamics could not be measured because the O–H

stretch vibrational lifetime of the water molecules in these solvation shells is comparable to that of bulk HDO:D_2O.

The value of τ_c is observed to be somewhat longer for the solvation shells of Br^- and I^- than for the solvation shell of Cl^- and τ_c is observed to increase with temperature from 12±3 ps at 25 °C, to 24±5 ps at 65 °C, to 30±6 ps at 85 °C (figure 6.5). These observations can be well explained within the framework of the Brownian-oscillator model, in which the time constant τ_c is related to the frequency ω_{HB} of the hydrogen-bond stretch vibration via $\tau_c = \gamma/\omega_{HB}^2$,[109] with γ the damping of the hydrogen-bond stretch vibration. The dependence of τ_c on ω_{HB} can be understood from the fact that tight bonds (high ω_{HB}) show faster dynamics than weak bonds (low ω_{HB}), leading to a faster decay of $\langle R_{HB}(\tau)R_{HB}(0)\rangle \propto e^{-\tau/\tau_c}$.[12] The scaling of τ_c with the damping parameter γ reflects the fact that the motion in the hydrogen-bond coordinate R_{HB} will slow down when γ increases. Exchanging Cl^- for Br^- or I^- leads to a decrease of ω_{HB},[6] because the hydrogen bond becomes weaker and because the reduced mass of the hydrogen-bond vibration increases. An increase in temperature also leads to a decrease of ω_{HB}, because the hydrogen-bond interaction decreases with temperature. Hence, if the damping γ of the hydrogen-bond stretch vibration is similar for O–H···Cl^-, O–H···Br^- and O–H···I^- hydrogen bonds, and if γ does not depend strongly on temperature, the observed increase of τ_c with temperature and variation of the anion from Cl^- to Br^- or I^-, can be well explained from a decrease of the hydrogen-bond stretch frequency ω_{HB}.

The large difference between the values of τ_c of the O–H···O and the O–H···X^- oscillators cannot simply be explained from a difference in ω_{HB}, because the frequency ω_{HB} of the O–H···X^- hydrogen-bond stretch vibration is only 1–2 times lower than the frequency of the O–H···O hydrogen-bond stretch vibration,[6,140] which can account for an increase of τ_c of almost a factor of 4. Hence, the difference in τ_c must be explained from differences in microscopic structure.

For a solvation shell, the value of the hydrogen-bond coordinate R_{HB} will be largely determined by strongly damped deformational vibrations of this shell. The frequency of these deformations will be much lower than ω_{HB} of the O–H···X^- hydrogen-bond stretch vibration between a single water molecule and the X^- halogenic ion, because, in the liquid phase, the deformation of a relatively large solvation structure requires a reorganization of a large part of the local liquid structure. These deformational modes effectively take the role of the Brownian oscillator in the above described model. Because the deformations are slow, the autocorrelation function $\langle R_{HB}(t)R_{HB}(0)\rangle$ will decay slowly, i.e. τ_c is large. Bulk liquid water possesses a disordered 3-dimensional structure and the fluctuations that affect a local O–H···O hydrogen-bond length will involve a reorganization of only a small part of the local liquid structure. As a result, the time scale of these fluctuations will be much shorter, leading to a much faster decay of $\langle R_{HB}(t)R_{HB}(0)\rangle$.

6.5 CONCLUSIONS

In this chapter, we presented two-color femtosecond mid-infrared spectroscopic measurements of the dynamics of the aqueous solvation shells of the halogenic anions Cl^-, Br^- and I^-. A few picoseconds after excitation, only HDO molecules in the solvation shells of the anions remain excited, which allows for a highly selective study of the spectral dynamics of these molecules.

The spectral dynamics was studied by measuring pump–probe transients at different probe frequencies. From this study, we found that the stochastic modulation of the length of the hydrogen bond between the water molecules and the halogenic anions has a characteristic time constant τ_c of 15–25 ps which is 30–50 times longer than the τ_c of the O–H$\cdots$O hydrogen bonds of bulk liquid water. In addition, the distribution of lengths of the hydrogen bond between the water molecules and the halogenic anions was observed to be relatively narrow. Both the long τ_c and the narrow distribution of hydrogen-bond lengths indicate that the aqueous solvation shell forms a relatively long-living, well-defined structure. The value of τ_c is larger for the aqueous solvation shells of Br^- and I^- than for the solvation shell of Cl^- and was observed to increase with temperature. These observations can be well explained from the dependence of τ_c on the frequency of the hydrogen-bond vibrations between the HDO molecules and the solvated anions.

The large difference between the values of τ_c of aqueous solvation shells and bulk liquid water likely results from a strong difference in the time scale of the fluctuations that affect the length of the hydrogen bond. For an aqueous solvation shell, these fluctuations can be identified with slow deformations of the solvation shell that involve a relatively large reorganization of the local liquid structure. For bulk liquid water, the fluctuations that affect the hydrogen-bond length likely are more local in nature which makes them much faster.

7 Orientational dynamics of aqueous solvation shells

In this chapter, we present a study of the orientational dynamics of aqueous solvation shells of halogenic anions in bulk water solution with femtosecond two-color mid-infrared spectroscopy. The reorientational motion was studied by simultaneously monitoring the pump–probe signals at parallel and perpendicular pump and probe polarizations. The orientational dynamics has time constants between 2.5 and 12 picoseconds, depending on the type of anion and the temperature. We find that the solvation shell of I^- shows faster orientational dynamics than the shells of the smaller ions Cl^- and Br^-.

7.1 Introduction

In the previous chapter, it was found that water molecules around the anions Cl^-, Br^- and I^- form relatively rigid structures, compared to the more rapidly fluctuating structures that exist in pure liquid water. The relative stiffness of the anionic hydrogen bonds in these shells was revealed by the slow spectral diffusion. The residence time of water molecules in the solvation shell must at least equal the spectral-diffusion time. Therefore, the residence time is at least 10 ps, but possibly much longer. In the present chapter, we aim to study the motion of the entire solvation structure in the solvent. We can measure the orientational-correlation time of an excited O–H group with polarization-resolved pump–probe spectroscopy (see section 2.2.4).

Recently, the reorientational motion of water molecules in pure water ($HDO:D_2O$) has been studied with non-linear spectroscopy. In a first study,[137] two time constants were found in the reorientation of water molecules, 0.7 and 13 ps. In a second study,[90] in which also the frequency and temperature dependence was studied, a more comprehensive treatment was provided. According to the latter work, a water molecule can reorient only when one of its donated hydrogen-bonds is broken. The spectral-diffusion time was thus found to be important for the orientational dynamics. The results were in general agreement with NMR and dielectric relaxation studies.

The anionic solvation structure, that is assumed to consist of at least six water molecules, can form many hydrogen bonds with the surrounding water, that hinder the reorientational motion. Therefore, long rotational-correlation times should be expected for the solvation shells. For salt solutions, the reorientational motion has been studied with NMR. The results of a large number of studies are summarized in Ref. 96. For the halide ions, the rotational-correlation times found with NMR are of the same order of magnitude as for pure liquid water. One disadvantage of NMR is that the frequency of the applied magnetic pulses is at most 100 MHz,[96] which limits the time resolution to nanoseconds. Within this time, the water molecules exchange numerous times between

bulk and solvation shell.[47,114,105] Therefore, the measured rotation is in fact an average over all molecules in the liquid.

7.2 EXPERIMENT

The experiments are polarization-resolved two-color femtosecond mid-infrared pump-probe experiments on a dilute (<1 M) solution of HDO dissolved in D_2O that contains a high concentration (1–3 M) of salt (NaCl, NaBr, or NaI). The generated mid-infrared pulses have a pulse energy up to 30 μJ, and a pulse duration of approximately 200 fs. The pump and probe pulses were tuned to 3450 cm^{-1} and 3200 cm^{-1}, with bandwidths of 80 and 60 cm^{-1}, respectively.

To study the orientational relaxation of the excited HDO molecules, we rotated the polarization of the probe pulse by 45 degrees with respect to the pump polarization using a zero-order $\lambda/2$ plate. The transmission changes of the probe parallel to the pump ($\ln(T/T_0)_{\parallel}$) and perpendicular to the pump ($\ln(T/T_0)_{\perp}$) are measured as a function of the delay τ with respect to the pump. These signals are used to calculate the anisotropy parameter R. Details about the setup and the experiment can be found in chapter 2.

To prevent Förster energy transfer between nearby O–H groups, which could influence the anisotropy decay,[135] the HDO concentration was relatively low: only 0.5 % of the solvent molecules were HDO molecules, the other 99.5 % of the solvent molecules were D_2O. The 'safe' concentration was determined by measuring at different HDO concentrations. Below 0.5 %, there was no measurable dependence of the decay of R on the HDO concentration.

7.3 RESULTS

In figure 7.1, the anisotropy parameter R is presented as a function of delay for a solution of 3 M NaCl in HDO:D_2O at different temperatures. Also shown are exponential fits to the data in the delay-time window from 3 to 8 picoseconds in which the observed transients only represent the orientational dynamics of the HDO molecules in the first solvation shell of the Cl^- ion (it will be shown. At 27 °C, the orientational-relaxation time constant τ_{or} of these HDO molecules is 9.6±0.6 ps, which is longer than the value of τ_{or} of 2.6 ps of HDO molecules in a solution of HDO in D_2O.[90] With increasing temperature, the orientational relaxation becomes much faster: τ_{or} decreases to 4.2±0.4 ps at 106 °C.

If an anion-bonded water molecule leaves the solvation shell while it is still excited, it will rapidly form a new hydrogen bond with another water molecule, and decay with a time constant of 740 fs. The exchange of water molecules between shell and solvent will therefore not have a great effect on the measurements of the anisotropy. In addition, it was shown in chapter 6 that the residence time of a water molecule in the solvation shells of the studied anions is at least on the order of 20 ps, much longer than τ_{or}.

The same series of measurements has been performed for solutions of NaBr and NaI. The fitted orientational diffusion time constants τ_{or} are shown in figure 7.3 for all three salts and for several temperatures in the range between room temperature and 106 °C. At all temperatures, $\tau_{or}(I^-) < \tau_{or}(Cl^-) < \tau_{or}(Br^-)$.

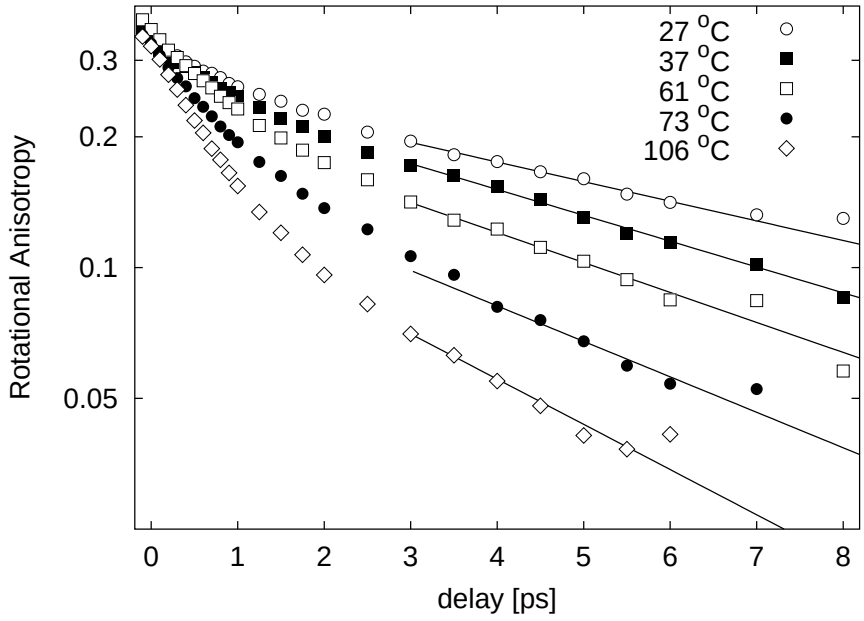

FIGURE 7.1. Anisotropy parameter R as a function of delay τ for a solution of 3 M NaCl in HDO:D_2O at five different temperatures. The pump frequency is 3450 cm^{-1} and the probe frequency is 3200 cm^{-1}. Also shown are exponential fits to the transients in the delay-time range from 3 to 8 picoseconds (solid curves).

7.4 DISCUSSION

The question arises whether the observed reorientation of HDO molecules results from reorientation within the solvation shell of the anion or from reorientation of the complete shell. In the case of reorientation of individual molecules within the shell, the O–H stretch frequency should be subject to a spectral-diffusion process that is at least as fast as the reorientation, because such a reorientation inevitably affects the bond angle or bond length of the O–H$\cdots X^-$ hydrogen-bond, that are both strongly correlated to the O–H stretch frequency.[83,74] It was shown in chapter 6 that the dynamics of the spectral diffusion can be measured by probing the induced isotropic bleaching of the $0\rightarrow1$ transition at different probe frequencies. As the hydrogen-bond length of a molecule changes, the molecule spectrally diffuses away from the frequency at which it was excited, resulting in a faster decay if pump and probe have the same frequency and in a slower decay if the probe frequency differs from that of the pump.

The time constant τ_c of this modulation can be obtained by fitting the measurements to a Brownian-oscillator model.[134,88] In chapter 6, we found that the time constant τ_c of the modulation of the O–H$\cdots Cl^-$ hydrogen-bond length increases from 14±2 ps at 25 °C, to 24±5 ps at 65 °C, to 30±6 ps at 85 °C. This increase of τ_c could be well explained within the framework of the Brownian oscillator model, in which the time constant τ_c is related

to the frequency ω_{HB} of the hydrogen-bond stretch vibration via $\tau_c = \gamma/\omega_{HB}^2$,[109] with γ the damping of the hydrogen-bond stretch vibration. An increase in temperature leads to a decrease of ω_{HB}, and thus to an increase of τ_c, because the hydrogen-bond vibration is anharmonic[12] and because the hydrogen-bond interaction decreases with temperature.[37]

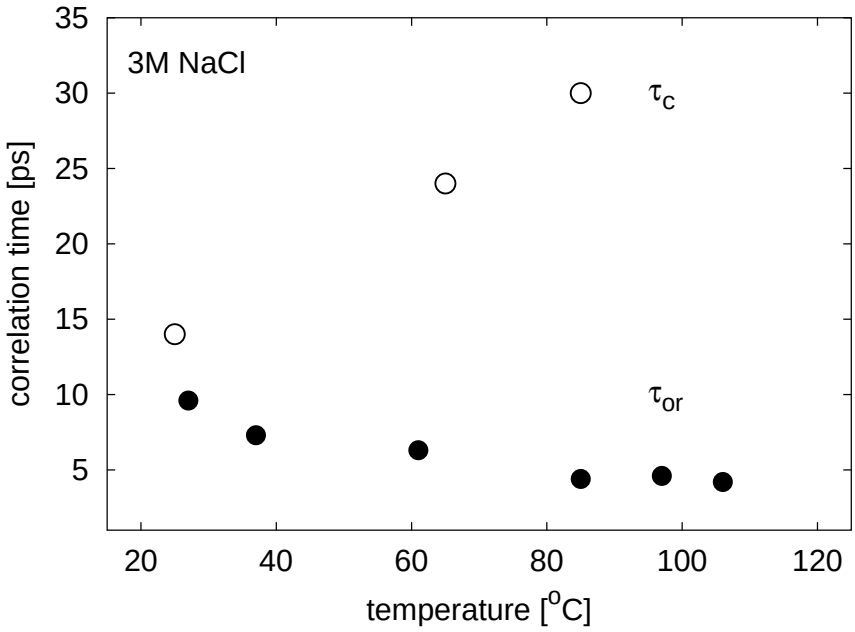

FIGURE 7.2. Orientational and spectral-diffusion time constants τ_{or} and τ_c of the first solvation shell of Cl^-, as a function of temperature. The spectral-diffusion times were obtained in chapter 6. The values of τ_{or} are the same as in figure 7.3. Comparison of τ_{or} and τ_c leads to the conclusion that τ_{or} represents the reorientation of the entire solvation structure rather than an individual water molecule.

The values of τ_{or} and τ_c for a 3 M solution of NaCl in water are displayed in figure 7.2. From the observation that τ_c is longer than τ_{or}, and from the reversed temperature dependence, it follows that the orientational dynamics of the HDO molecules in the first solvation shell of the Cl^- ion must result from motions that do not contribute to the spectral diffusion, i.e. that do not affect the O–H$\cdots$$Cl^-$ hydrogen bond. Hence, the observed reorientation represents the orientational diffusion of the complete solvation structure. The long-living excitation of the anion-bound HDO molecule thus forms a label that, like a flag on a sphere, enables one to follow the orientational motion of the complete anionic solvation structure in the time domain. We would like to stress again that the cation's solvation shell is expected to be similar to the anion's shell[28] and that it likely shows similar dynamics; however, due to the shorter O–H stretch lifetime of the former, we cannot distinghuish its reorientational motion from that of the bulk water.

In figure 7.3, the orientational diffusion time constants τ_{or} of the first solvation shell of the halogenic anions Cl^-, Br^- and I^- are presented as a function of temperature.

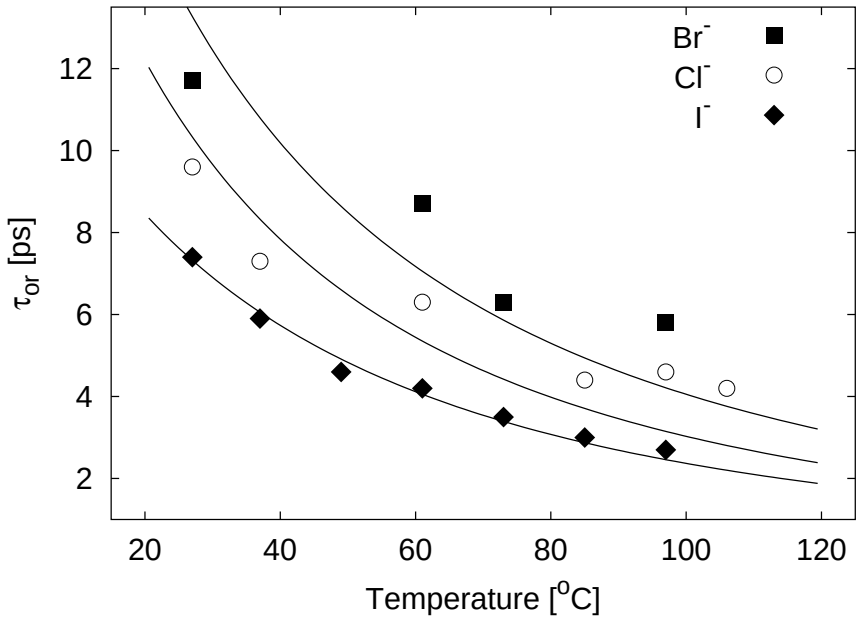

FIGURE 7.3. Orientational diffusion time constants τ_{or} of the solvation shells of Cl^-, Br^- and I^- as a function of temperature. The solid curves represent fits of the data using equation (7.4).

Surprising is the order of τ_{or} for the different anions: $\tau_{or}(I^-) < \tau_{or}(Cl^-) < \tau_{or}(Br^-)$ at all temperatures. It seems to be in contradiction with the fact that the bare I^- ion is larger than Br^- and Cl^-. In the NMR measurements listed in Ref 96, the order was $\tau_{or}(I^-) < \tau_{or}(Br^-) < \tau_{or}(Cl^-)$. Thus, the NMR results are also in contradiction with the intuitive notion that it should be more difficult to rotate the larger ion than to rotate the smaller. Yet, similar anomalous behavior was observed for the ionic mobility, which is related to translational diffusion [3,65]. We will come back to this at the end of the Discussion, after modeling the data.

The orientational diffusion of the ensemble of aqueous solvation shells that are excited by the pump pulse is described by the equation

$$\frac{\partial n(\theta,t)}{\partial t} = \frac{D_\theta}{\sin\theta}\frac{\partial}{\partial\theta}\left(\sin\theta\frac{\partial n(\theta,t)}{\partial\theta}\right), \tag{7.1}$$

with θ the angle with respect to the pump-pulse polarization, $n(\theta,t)d\Omega$ the number of particles in a solid angle $d\Omega$ ($d\Omega = d\phi d\theta \sin\theta$), ϕ the azimuth angle, and D_θ the orientational diffusion constant. Equation (7.1) does not contain any dependence on the azimuth angle ϕ, because the excitation is symmetric around the pump-pulse polarization axis. The solution of this equation can be written as a sum of exponentially decaying Legendre polynomials P_l:

	$r_{h,solv}$	r_{HB}	r_h	r_{ion}
Cl^-	2.13 Å	3.23 Å	1.20 Å	1.81 Å
Br^-	2.37 Å	3.40 Å	1.18 Å	1.96 Å
I^-	2.05 Å	3.60 Å	1.20 Å	2.20 Å

TABLE 7.1. Values of $r_{h,solv}$ obtained from our fit and the hydrogen-bond length, and of r_h from the ionic mobility using the Stokes-Einstein relation for translational diffusion, the ionic radius.

$$n(\theta, t) = \sum_{l \geq 0} a_l P_l(\cos\theta) e^{-D_\theta l(l+1)t}, \tag{7.2}$$

with a_l the coefficients that are determined by the distribution of $n(\theta, t)$ at t=0. Because the measured anisotropy $R(\tau)$ equals $\langle P_2(\cos\theta)\rangle$, the time constant τ_{or} of the decay of $R(\tau)$ is related to D_θ by $\tau_{or} = 1/(6D_\theta)$. The orientational diffusion constant D_θ can be related to the viscosity of the liquid using the Stokes-Einstein relation for orientational diffusion of a sphere [30]:

$$D_\theta = \frac{kT}{8\pi\eta(T) r_{h,solv}{}^3}, \tag{7.3}$$

with k Boltzmann's constant, T the temperature in Kelvin, $\eta(T)$ the temperature-dependent viscosity, and $r_{h,solv}$ the hydrodynamic radius of the solvation structure. Combining this equation with $\tau_{or} = 1/(6D_\theta)$ gives:

$$\tau_{or}(T) = \frac{4\pi\eta(T) r_{h,solv}{}^3}{3kT}. \tag{7.4}$$

In figure 7.3, fits of equation (7.4) to the data are shown (solid curves). The only fit parameter is the radius $r_{h,solv}$. The temperature-dependent viscosities were obtained from temperature-dependent Jones-Dole A [112] and B [97] coefficients. The Jones-Dole calculation of the viscosity is valid for low concentrations; however, we verified for NaCl[60] and for NaBr[53] that the difference between the calculated curve and experimental data was less than 10 % over the whole temperature range, which gives a deviation of $r_{h,solv}$ of only 3 %.

The temperature dependence of the orientational diffusion is well described by $\eta(T)/T$. For the hydrodynamic radii we find $r_{h,solv}(Cl^-)$ = 2.1 Å, $r_{h,solv}(Br^-)$ = 2.4 Å, and $r_{h,solv}(I^-)$ = 2.1 Å (precise values are in table 7.1, together with other radii that will appear in the text). These radii can be compared to the hydrodynamic radii r_h obtained from the Stokes-Einstein relation for translational diffusion. From the ionic mobility[3], related to translational diffusion, we find r_h = 1.2 Å for all anions. r_h is significantly smaller than $r_{h,solv}$ for all anions. If $r_{h,solv}$ would have been equal to r_h, the reorientation would be about 8 times as fast, τ_{or} being on the order of 1 ps. This suggests that the (translational) diffusion steps take place for a significant part without the solvation shell, thus reducing its effective size.

It seems surprising that we find similar values for the hydrodynamic radii r_h of the different ions. From the orientational diffusion times, it follows that the hydrodynamic

radius $r_{h,solv}$ of I^- is even smaller than that of Br^- and Cl^-. These observations may lead to the straightforward interpretation that the size of the diffusing structure, i.e. the ion with its solvation shell, is smaller for I^- than for Cl^- and Br^-. Since I^- is a bigger ion, the electrostatic field felt by the molecules in the solvation shell is weaker, and the anionic hydrogen bonds are weaker. Possibly, the water molecules in the solvation shell have more freedom to go in and out of the shell, creating moments in which the ion is able to displace with a smaller number of molecules attached. Another possible explanation is that the dielectric friction between the ion and its surroundings could be smaller for the larger ions,[65] or that the Cl^- ion, more than I^-, forms short-living clusters of two or more ions,[26] that hinder the diffusive motion.

Both radii obtained, r_h from the ionic mobilities and $r_{h,solv}$ from the rotational-anisotropy data, are much smaller than expected. The values of r_h should be at least as large as the ionic radii: $r_{ion}(Cl^-) = 1.8\,\mathring{A}$, $r_{ion}(Br^-) = 2.0\,\mathring{A}$, and $r_{ion}(I^-) = 2.2\,\mathring{A}$.[3] For $r_{h,solv}$ one should expect values of at least the anion–water hydrogen-bond length: $r_{HB}(Cl^-) = 3.2\,\mathring{A}$, $r_{HB}(Br^-) = 3.4\,\mathring{A}$, and $r_{HB}(I^-) = 3.6\,\mathring{A}$.[83] This deviation is probably caused by the fact that the Stokes–Einstein relation, in particular the viscosity, is defined for macroscopic objects. In the present case, however, the moving objects are of the same length scale as the molecules of the viscous liquid. In this regime, the concept of viscosity loses its meaning, and the orientational mobility becomes closely connected to the specific interactions between the solvation shell and its surroundings, mainly electrostatic interactions with other ions and hydrogen bonding.

7.5 CONCLUSIONS

In this chapter, direct time-resolved measurements of the orientational dynamics of HDO molecules in the first solvation shell of Cl^-, Br^-, and I^- in bulk aqueous solution are presented. The selective study of anion-bound water molecules is enabled by their exceptionally long vibrational lifetime. We find that the orientational diffusion is about twice as fast for I^- as for Br^-; for Cl^- it is in between. From the temperature dependence of the reorientation rate and the comparison with spectral-diffusion data, we conclude that the observed reorientation of the HDO molecules results from the orientational diffusion of the complete solvation structure. The O–H group of the HDO molecule in the solvation shell thus acts as a label that enables the direct measurement of the orientational diffusion of the solvation structure in the time domain.

8 The influence of ions on the hydrogen-bond structure of water

The effects of ions on bulk properties of liquid water, such as viscosity and ionic mobility, suggest that ions alter the hydrogen-bond network of liquid water. In this chapter, measurements of the orientational-correlation time of water molecules in solutions of $NaClO_4$, $Mg(ClO_4)_2$, and Na_2SO_4 are presented. The measurements show that, even for high concentrations of ions that are believed to strongly enhance the hydrogen-bond network, there is no influence on the rotational dynamics of water molecules outside the first solvation shell. The results described in this chapter oppose the prevailing notion of structure-making or structure-breaking ions, that has been held for decennia.

8.1 Introduction

After having studied several aspects of solvations shells, we turn our attention in this final chapter to the behaviour of the bulk solvent. It is generally assumed that ions can enhance or weaken the hydrogen-bond structure in water;[29,35,39,40] as a result, ions are categorized as either 'structure makers' or 'structure breakers'. The concept of structure making and breaking was probably introduced in the 1930's.[21] The central idea of this concept is that the hydrogen-bond structure and dynamics of water in the direct environment, usually over a distance of several molecules, are changed by the electrostatic field exerted by the ion. To quote Engel in Ref. 35, 'the word structure breaking is synonymous with the characterization "causing faster motions of the water molecules".' Therefore, ions with strong electric-field density, i.e. small or highly-charged ions, will be structure makers, while larger ions will likely be structure breakers. For polyatomic ions, it is not always a priori obvious whether they will belong to the one or the other group: SO_4^{2-} is a strong structure maker, while ClO_4^- is a structure breaker. Structure breaking is sometimes called 'negative hydration'.

The concept of structure making and breaking has gained recognition when more anomalous phenomena could be explained by these ideas. First, there are the anomalous mobilities of many ions in water. The usual models use Stokes' law, that describes friction due to viscosity, and/or dielectric friction, as described by Zwanzig.[144] These models provide a poor description of the mobility. In general, ions with low charge densities (e.g. large univalent ions) move less hindered and therefore have a larger mobility than predicted by the Stokes/Zwanzig models,[40] while ions with high charge densities generally have smaller mobilities. The large tetra-alkylammonium ions also have an unexpected low mobility. The effect is much stronger if these ions are dissolved in water than if they are dissolved in some aprotic solvent, which can be explained when the tetra-alkylammonium ions are assumed to promote the degree of hydrogen bonding between the solvent molecules in the case of water.

A second argument that supports the concept of a changed hydrogen-bond structure in water due to ions, is provided by the effect of the presence of ions on the viscosity of water.[45] The phenomenological Jones–Dole expression[56] relates the viscosity of an aqueous ionic solution to the ion concentration:

$$\frac{\eta}{\eta_0} \approx 1 + A\sqrt{c} + Bc. \tag{8.1}$$

In this equation c is the ion concentration, η is the viscosity of the solution, η_0 is the viscosity of pure water, and A and B are the 'Jones–Dole constants'. Equation (8.1) is valid for concentrations up to about 1 M, but this range can be extended by including higher-order terms in the concentration.[97] The second term on the right-hand side, $A\sqrt{c}$, results from electrostatic interactions between the ions. The constant A is due to the electrostatic interaction between the ions and can be derived from theory.[36] The third term, Bc is attributed to the influence on the hydrogen-bond structure by the ion: the ions that are considered strong structure makers have positive B coefficients, while ions with negative B coefficients are structure-breaking, since structured water, with stronger hydrogen bonds, is expected to be more viscous than nonstructured water.

The vibrational spectra of electrolyte solutions have also been studied in order to get insight in the influence of ions on the hydrogen-bond structure in liquid water.[40] Some cations with high charge density (like Al^{3+} [82] or Mg^{2+} [125]) are considered to be strong structure makers and cause a slight redshift of the spectrum, indicative of an enhanced hydrogen-bonding (see figure 8.1). However, aqueous tetra-alkylammonium solutions do not show this redshift,[40] although the tetra-alkylammonium ions would be even stronger structure makers than Mg^{2+}.

The above described effects all constitute rather indirect probes of the effect of ions on the hydrogen-bond structure of liquid water, relating macroscopic quantities to microscopic behaviour. A better way would be to probe the hydrogen-bonded network in ionic solutions directly at a microscopic level, as was done for the solvating molecules in the experiments presented in the previous chapters. The orientational-correlation time of the water molecules can be viewed as a probe for the stiffness of the hydrogen-bond network, because it is more difficult for water molecules to change their orientation if the hydrogen-bond network is more rigid.[90] Based on the hypothesis that ions influence the hydrogen-bond network, one would expect the 'bulk' water molecules around a structure-making ion to have a relatively long orientational-correlation time (compared to pure liquid water with no ions present), and those surrounding a structure-breaking ion to have a relatively short orientational correlation time. The orientational-correlation time of water molecules in ionic solutions has been measured with NMR.[96] However, as has been mentioned before, for ionic solutions NMR lacks specificity, since the pulses used in this method are very long (microseconds) compared to the time scale on which water molecules exchange between the solvation shell and the bulk solution. Hence, only the average reorientation time of all water molecules is measured.

The properties of ionic solutions have also been studied with MD simulations, but the results obtained are inconclusive as to the long-range effect of ions on the hydrogen bonding of the water molecules. A number of MD results have been supportive of the concept of structure making and structure breaking,[18,95,123] but other MD studies do not confirm this picture.[19,143,130,75]

Until recently, it was not possible to study the very fast hydrogen-bond dynamics of water molecules experimentally. Since a few years, however, this has become possible with femtosecond nonlinear spectroscopy.[24,44,41,78,137,134] It was shown in the previous chapters that with this technique, the behaviour of O–H groups of water molecules hydrogen bonded to an anion can be distinguished from the behaviour of O–H groups of water molecules hydrogen bonded to a water molecule. Consequently, the solvation shells of negative ions and the bulk water molecules can be studied separately from each other.

8.2 EXPERIMENTAL

The experiments are similar to the ones in the previous chapter. They are polarization-resolved two-color femtosecond mid-infrared pump-probe experiments on a dilute (<1 M) solution of HDO dissolved in D_2O and several concentrations (0–6 M) of salt ($NaClO_4$, $Mg(ClO_4)_2$ or Na_2SO_4). The generated mid-infrared pulses have a pulse energy of 20 μJ and a duration of approximately 200 fs.

To study the orientational relaxation of the excited HDO molecules, the polarization of the probe pulse was rotated by 45 degrees with respect to the pump polarization using a zero-order $\lambda/2$ plate. The transmission changes of the probe parallel to the pump ($\ln(T/T_0)_{\parallel}$) and perpendicular to the pump ($\ln(T/T_0)_{\perp}$) were measured as a function of the delay τ with respect to the pump. These signals are used to calculate the anisotropy parameter R. Details about the setup and the experiment can be found in chapter 2.

8.3 RESULTS

SEPARATION OF ABSORPTION BANDS The absorption spectra of the O–H stretch vibration of solutions of 6 M $NaClO_4$ and 3 M $Mg(ClO_4)_2$ in HDO:D_2O solution is shown in figure 8.1. For both solutions, two distinct peaks are seen. The peak in the $NaClO_4$ spectrum. which is centred at 3400 cm^{-1}, is attributed to O–H groups hydrogen-bonded to D_2O molecules, whereas the peak at 3575 cm^{-1} is attributed to O–H groups bonded to ClO_4^-.[40] By fitting two Gaussian functions to the absorption spectrum of $NaClO_4$, we determined the approximate centre and width (FWHM) of the O–H$\cdots ClO_4^-$ band to be 3575 cm^{-1} and 90 cm^{-1}, respectively, and of the O–H$\cdots$O band 3400 cm^{-1} and 270 cm^{-1}.

We performed pump–probe measurements to study the dynamics of these two bands. The decay of the isotropic signal is shown in figure 8.2. First, we pumped at 3575 cm^{-1} (0$\rightarrow$1 transition of ClO_4^- bonded O–H groups) and probed at 3325 cm^{-1} (1$\rightarrow$2 transition). The decay is clearly biexponential, where the fast component (0.8 ps) results from O–H groups that are hydrogen-bonded to D_2O, and the slow component (1.7 ps) is due to the decay of the excitation of O–H groups bonded to ClO_4^-. Then, we pumped at 3400 cm^{-1} (0$\rightarrow$1 transition of water-bonded O–H groups) and probed at 3150 cm^{-1} (1$\rightarrow$2 transition). At this frequency, practically no anion-bonded O–H groups are observed: the decay is fast and almost monoexponential with a time constant of about 0.8 ps (the same as observed for O–H groups in the pure liquid.[91])

Since the water band at 3400 cm^{-1} is much broader (270 cm^{-1} compared to 90 cm^{-1}), these bulk-water molecules still can absorb at 3575 cm^{-1}. The reverse is not the case:

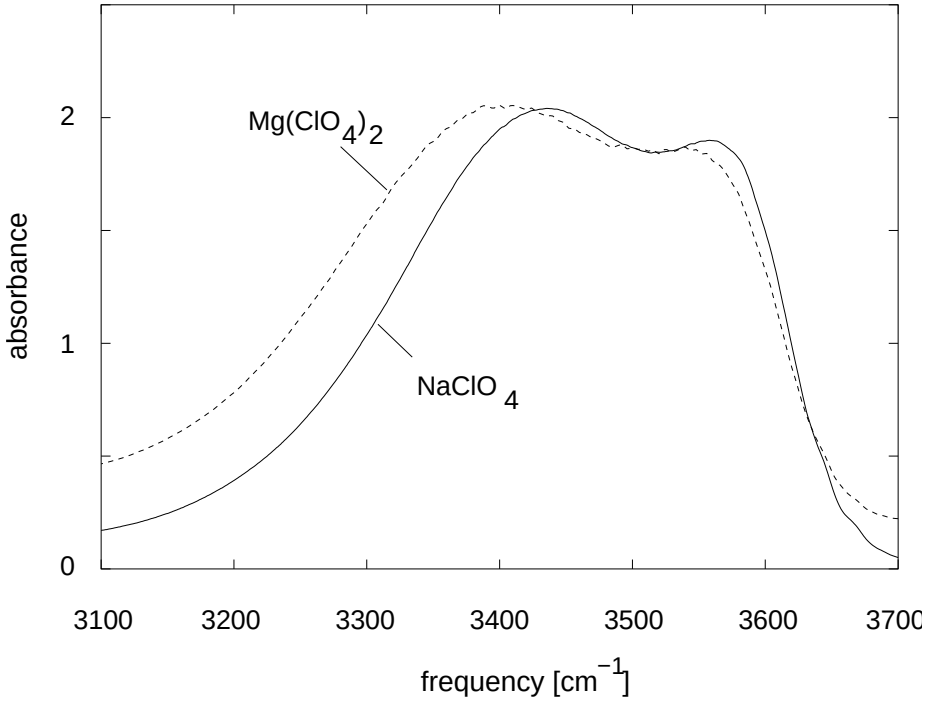

Figure 8.1. Absorption band of the O–H stretching vibration in a 6 M $NaClO_4$ and in a 3 M $Mg(ClO_4)_2$ ($\equiv$ 6 M ClO_4^-) in HDO:D_2O solution. For both solutions there are two distinct peaks meaning that the O–H$\cdots ClO_4^-$ band is well separated from the O–H$\cdots$O band. Therefore, the O–H$\cdots$O band could be pumped and probed selectively.

pumping at 3400 cm^{-1} will not excite anion-bound water molecules. The difference in vibrational relaxation times of the two absorption bands confirm what was already concluded from the linear spectra, namely that the high-frequency absorption peak corresponds to the O–H$\cdots ClO_4^-$ groups, while the rest of the molecules, all forming O–H$\cdots$O hydrogen bonds to other water molecules, give rise to the broad absorption at 3400 cm^{-1}.

Orientational mobility In the previous chapter, we studied the anisotropy decay of the anion-bound water molecules. The specificity was obtained by the difference in vibrational lifetime. We could not look in detail to the dynamics of the other water molecules, since all pump–probe responses were dominated by the response of the anion-bound molecules. In the case of ClO_4^-, the absorption frequencies are well separated, which enables the study of the other molecules, i.e. all molecules with the exception of the anion-bound ones. These include pure bulk molecules and water molecules in the cations' solvation shells, that may show some redshift (stronger hydrogen bonds) in the absorption spectrum (chapter 4). It is known that the stiffness of the hydrogen bonds affects the orientational-correlation time.[90] Since we are interested in the hydrogen-bond network outside the anion's solvation shell, we performed measurements of the anisotropy

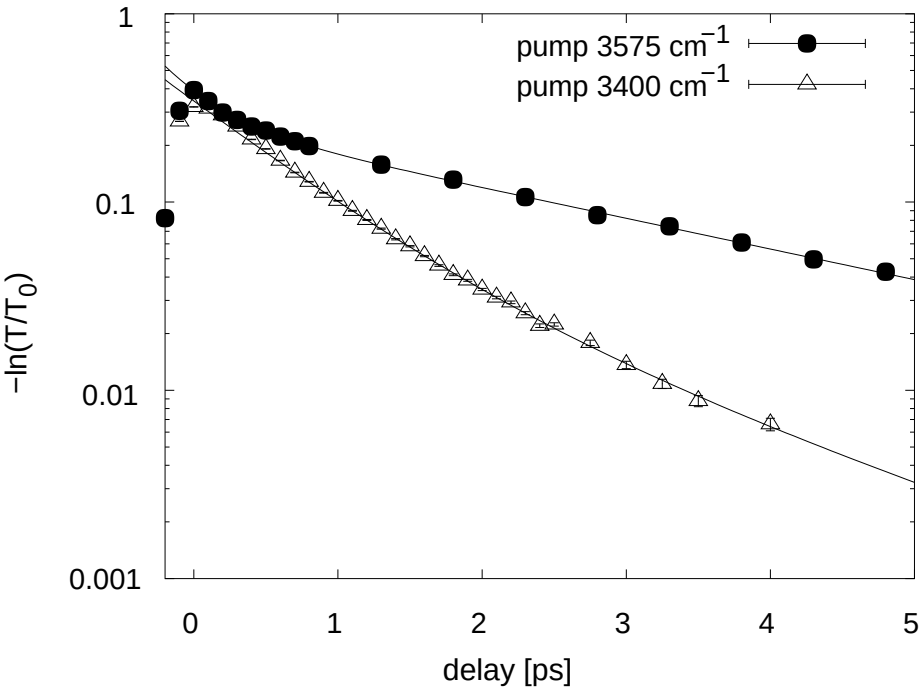

FIGURE 8.2. A logarithmic plot of the induced absorption measured as a function of time delay for a 6 M $NaClO_4$ solution for two different pump and probe frequencies. The decay has been fitted biexponentially. When the pump frequency is 3575 cm^{-1} and the probe frequency is 3325 cm^{-1}, the decay is biexponential, whereas the decay is almost monoexponential when the pump frequency is 3400 cm^{-1} and the probe frequency is 3150 cm^{-1}.

decay in several solutions known for their structure-making quality.

First, we performed two anisotropy measurements on a solution of $NaClO_4^-$ in $HDO{:}D_2O$. In the first, we pumped the 'water' peak at 3400 cm^{-1}, in the second, the 'anion' peak at 3575 cm^{-1}. In both experiments, the $1\rightarrow2$ induced absorption was probed, by tuning the probe frequency 250 cm^{-1} redshifted with respect to the pump. By pumping the different subbands, mostly O–H groups of one type are excited. However, since the water band is quite broad, it is inevitable that these O–H groups are also excited when pumping at 3575 cm^{-1}. Fortunately, the latter O–H groups have a shorter vibrational lifetime, and the ratio between excited O–H$\cdots$$ClO_4^-$ and O–H$\cdots$O groups rapidly decreases. Thus, by analyzing the anisotropy at delays larger than 2.5 ps, only O–H$\cdots$$ClO_4^-$ groups are probed. The results of the two experiments are shown in figure 8.3. The anisotropy clearly decays at different rates. For the O–H$\cdots$O groups, a decay of 3.2$\pm$0.3 ps is measured, similar to pure liquid water. For the O–H$\cdots$$ClO_4^-$ groups, a slower decay is observed, 7.6$\pm$0.3 ps. This is in qualitative agreement with the results of chapter 7. In this case, separation between O–H$\cdots$O and O–H$\cdots$$ClO_4^-$ groups has been achieved by 'spectral selection', rather than separation based on vibrational lifetime.

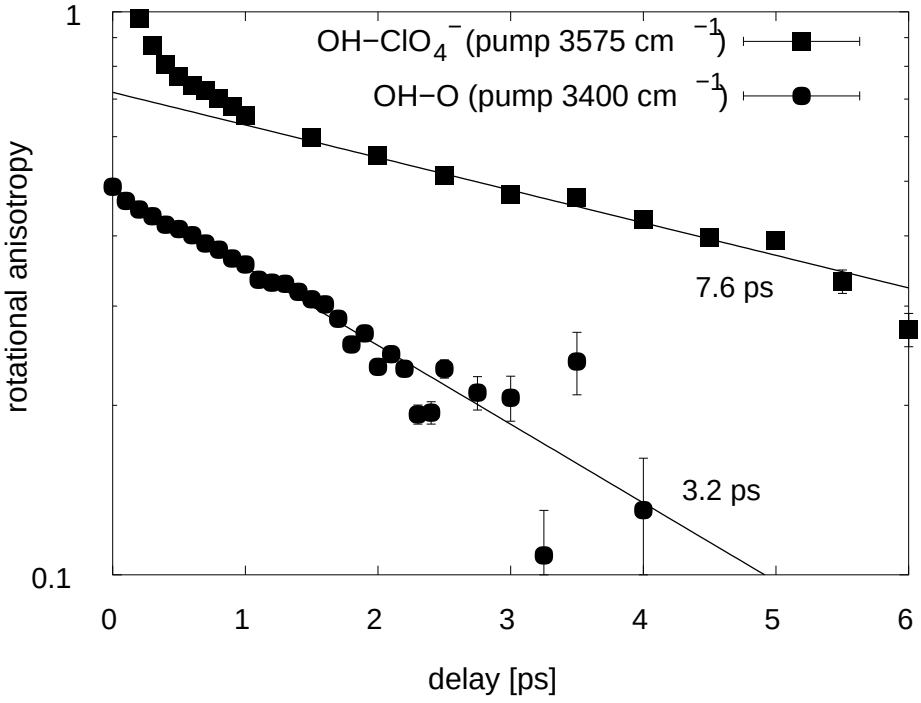

Figure 8.3. A logarithmic plot of the anisotropy parameter R as a function of time delay for a solution of 6 M $NaClO_4$ in HDO:D_2O for two different pump and probe frequencies. When the pump frequency is 3575 cm^{-1} and the probe frequency is 3325 cm^{-1}, the anisotropy decay is much slower than if the pump frequency is 3400 cm^{-1} and the probe frequency is 3150 cm^{-1}. In the former case, initially a rapid decay is seen, which can be attributed to O–H$\cdots$O groups. After a few picoseconds, these molecules have relaxed and the anisotropy is purely determined by the solvation shell water molecules, forming O–H$\cdots ClO_4^-$ hydrogen bonds that have a much longer orientational-correlation time. The 3575 cm^{-1} pump data have been fitted monoexponentially between 2.5 ps and 6 ps delay, the 3400 cm^{-1} pump data have been fitted monoexponentially between 0.5 ps and 3 ps delay.

In contrast to the solutions of chapter 7, we can now study the bulk O–H$\cdots$O groups separate from the anion-bound O–H groups.

To investigate the influence of ions on the hydrogen-bond network in bulk liquid water, we determined the orientational-correlation time of bulk water molecules in aqueous solutions of $NaClO_4$, $Mg(ClO_4)_2$ and Na_2SO_4. We performed measurements of the decay of the anisotropy parameter R at different concentrations of $NaClO_4$ in which the O–H$\cdots$O band was pumped at 3400 cm^{-1} and probed at 3150 cm^{-1}.

The measured anisotropy decay for 0 M, 0.5 M, 1 M, 3 M and 6 M $NaClO_4$ in HDO:D_2O solutions is shown in figure 8.4, where R is plotted against the time delay between the pump and probe pulses. The anisotropy decay, at pump and probe frequencies of 3400 cm^{-1} and 3150 cm^{-1} respectively, turns out to be independent of the $NaClO_4$

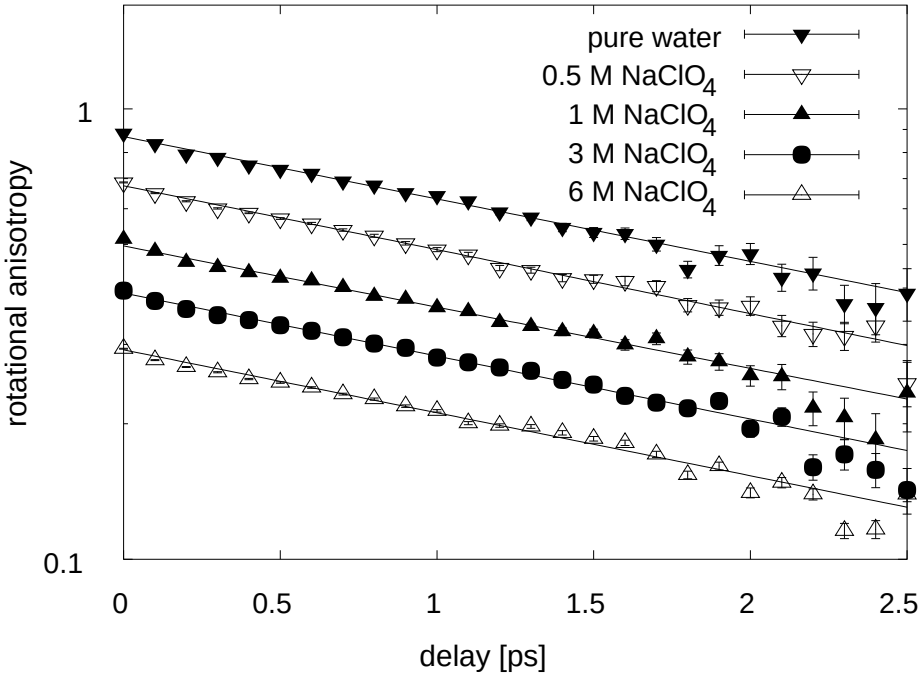

FIGURE 8.4. A logarithmic plot of the anisotropy parameter R measured as a function of delay for different concentrations of $NaClO_4$. The pump frequency was tuned to 3400 cm^{-1}, the probe to 3150 cm^{-1}. The data have been fitted monoexponentially and shifted vertically with respect to each other for clarity. As can be seen, the orientational correlation time is the same for each concentration.

concentration, which means that the orientational correlation time τ_{or} for the bulk water molecules is independent of the salt concentration, its value is 3.4±0.1 ps.

Na^+ is known as a very weak structure maker and ClO_4^- is known as a weak structure breaker,[40,81] so maybe there *is* an effect of ions on the hydrogen-bond network of bulk water but for $NaClO_4$ the effect is just too small to have a measurable effect on the orientational-correlation time. Therefore, we also performed measurements on solutions that contained supposed strong structure makers, like Mg^{2+} and SO_4^{2-}. Thus, anisotropy measurements were performed for bulk water molecules in $Mg(ClO_4)_2$ and Na_2SO_4 solutions. The Jones–Dole B coefficients at room temperature of $Mg(ClO_4)_2$ and Na_2SO_4 solutions are 0.3 and 0.4 respectively.[81] With these values, the viscosity of 1 M $Mg(ClO_4)_2$ is about 30 % higher than the viscosity of pure water and the viscosity of 1 M Na_2SO_4 is even about 40 % higher.[1] Because the O–H···O and O–H···ClO_4^- bands are also well separated in the $Mg(ClO_4)_2$ solution (see figure 8.1), the O–H···O groups can be studied selectively in a $Mg(ClO_4)_2$ solution as well. In the case of Na_2SO_4, the anion-bonded O–H groups absorb near 3400 cm^{-1}, like the bulk water molecules, but at low concentrations, the contribution of the water-bonded O–H groups will be much larger. Therefore, even for a solution of Na_2SO_4, mainly the water-bonded O–H···O groups are probed as

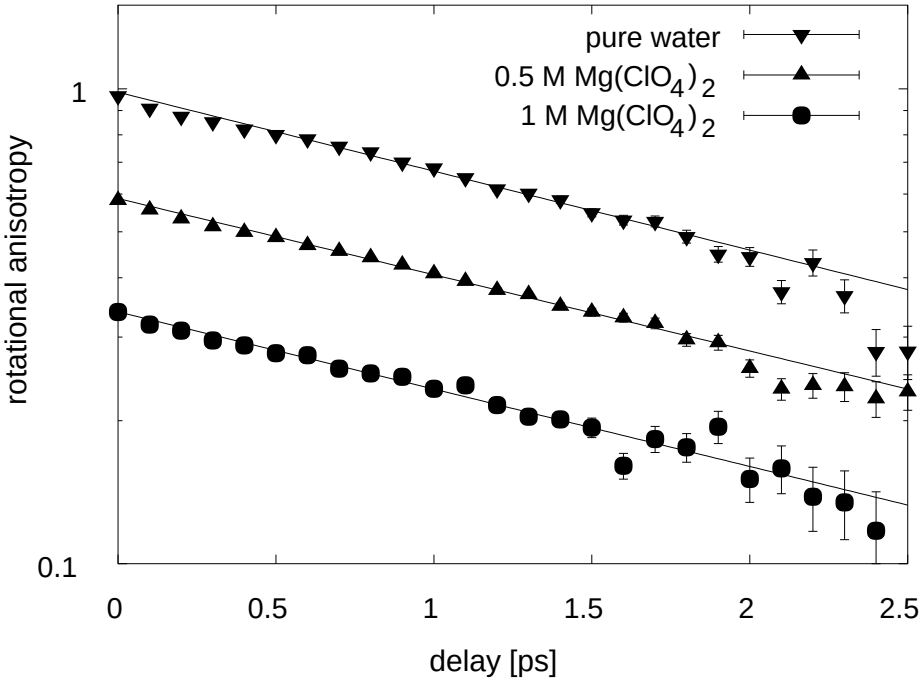

Figure 8.5. A logarithmic plot of the anisotropy parameter R as a function of time delay for different concentrations of $Mg(ClO_4)_2$. Again, the data have been fitted monoexponentially and are shifted vertically with respect to each other for clarity.

long as the salt concentration is sufficiently low. The results for $Mg(ClO_4)_2$ are shown in figure 8.5, for Na_2SO_4 in figure 8.6. Again, the decay of R turns out to be independent of the salt concentration (at least for concentrations up to 1 M): the orientational-correlation time is 3.2 ± 0.2 ps for each solution. The difference with the $NaClO_4$ solutions of figure 8.4 is within the experimental error.

Now it is still possible that some of the water molecules can rotate freely in some directions while being hindered in others. This would lead to relaxation of R to some permanent or longer-living end level. Unfortunately, the anisotropy decay of the bulk O–H$\cdots$O oscillators can only be followed during a few picoseconds, because of the short relaxation time of the O–H stretch vibration. To investigate the possible presence of such a small slow component in the anisotropy, we also probed the O–D stretch vibration of salt solutions using HDO:H_2O as solvent. The vibrational-relaxation time of the O–D stretch vibration in HDO:H_2O is 1.7 ± 0.3 ps,[68] which is more than twice as long as the vibrational-relaxation time of the O–H stretch vibration. Consequently, the anisotropy decay can be followed twice as long (over 5 ps instead of 2.5 ps). We performed measurements on the anisotropy decay in solutions of different concentrations (1 M and 3 M) of $Mg(ClO_4)_2$ in HDO:H_2O. The O–D stretch vibration is pumped and probed at

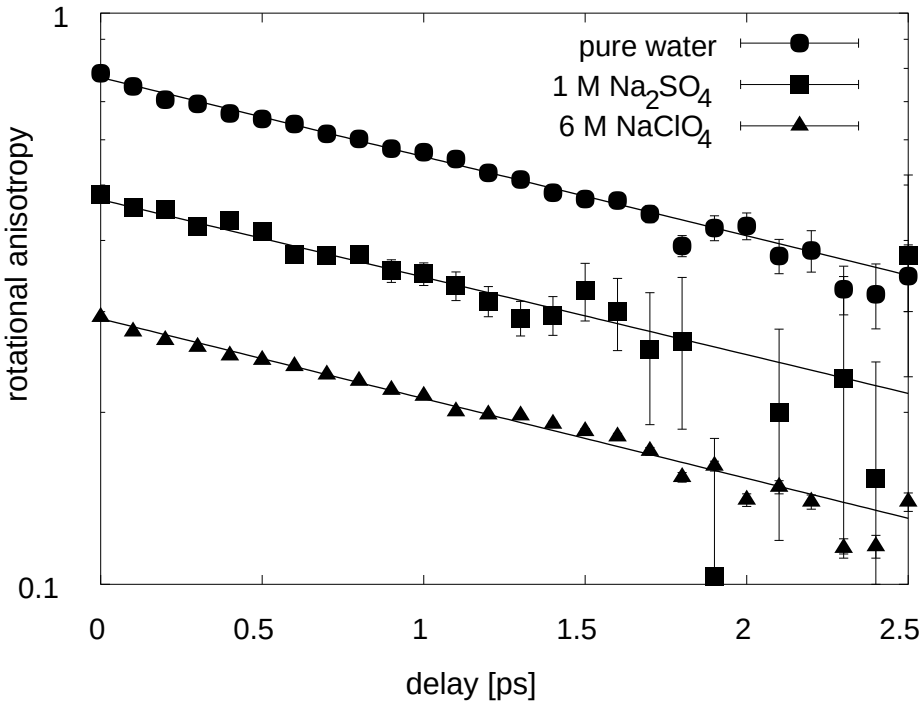

FIGURE 8.6. A logarithmic plot of the anisotropy parameter R as a function of time delay for pure water, for 1 M Na_2SO_4 and for 6 M $NaClO_4$. The data have been fitted monoexponentially and are shifted vertically with respect to each other for clarity.

2500 cm^{-1} (0→1 transition).* The results are shown in figure 8.7. Again, no concentration dependence is found, which shows once more that the addition of $Mg(ClO_4)_2$ has a negligible effect on the orientational dynamics of bulk water molecules. For each solution, the orientational-correlation time of the bulk water molecules is 2.5±0.1 ps. This orientational-correlation time agrees well with the orientational-correlation time of 2.6 ps found by Nienhuys et al.[90] for pure HDO:D_2O, with NMR measurements,[50,115] and with terahertz spectroscopy.[61,111] The difference between τ_{or} of 3.4 ps of figures 8.4, 8.5, and 8.6 and the τ_{or} of 2.5 ps of figure 8.7 can be understood in the following way. When the 0→1 transition is probed as in figure 8.7, the signal is caused partly by a depletion of the ground state ('hole contribution') and partly by a population of the first excited state ('particle contribution'). The hydrogen bond in the first excited state of the O–H (O–D) stretch vibration is stronger than in the vibrational ground state.[134] Hence, when probing the 0→1 transition relatively weakly hydrogen-bonded O–H (O–D) groups in the ground state as well as relatively strongly hydrogen-bonded O–H (O–D) groups in the

*To generate these pulses, the KTP crystal was exchanged for a $LiNbO_3$ crystal in figure 2.3.5, and all other crystals were adjusted to a slightly different frequency. Since $LiNbO_3$ starts to absorb below 2500 cm^{-1}, we could not make the laser pulses necessary to probe the 1→2 transition without rather drastically changing the pulse-generation setup.

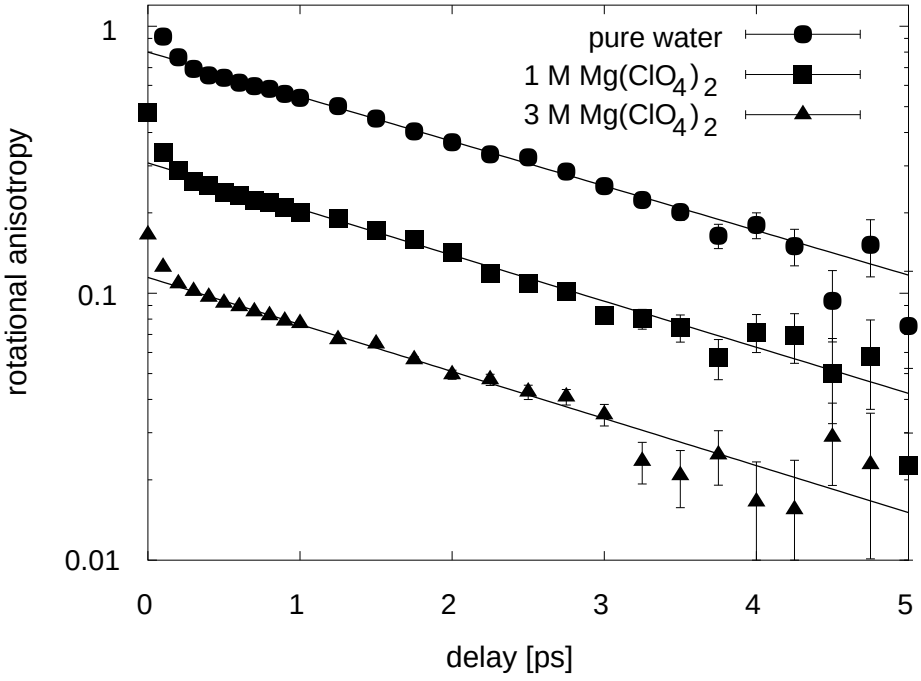

Figure 8.7. A logarithmic plot of the anisotropy parameter R as a function of time delay for different concentrations of $Mg(ClO_4)_2$ dissolved in H_2O with 4 % HDO. The data have been fitted with a mono-exponential function and are shifted vertically with respect to each other for clarity.

excited state contribute to the observed (orientational) dynamics. However, if the $1 \rightarrow 2$ transition is probed as in figures 8.4, 8.5, and 8.6, the signal is caused by a population of the first excited state only, and therefore only stronger hydrogen-bonded O–H (O–D) groups contribute to the measured dynamics.

8.4 Discussion

The measurements of the orientational mobility of water molecules in salt solutions oppose the idea of enhanced or weakened hydrogen bonds around ions, outside their first solvation shell: no structure-making or structure-breaking effect of ions on the hydrogen-bond structure could be found, even for ions that are particularly known for their supposed structure-making capacity. With respect to reorientation rate, i.e. average hydrogen-bond strength, there are only two types of water molecules: anion-bonded or water-bonded. This result indicates that an aqueous salt solution should not be viewed as a homogeneous liquid with a modified hydrogen-bond structure, but rather as a colloidal suspension of inert particles (hard spheres) in pure liquid water, that consist of the ion and its first hydration shell. The viscosity at low concentration can then be described by the Einstein equation:[51]

$$\frac{\eta}{\eta_0} \approx 1 + 2.5\phi,$$

with ϕ the volume fraction of the spheres.

It follows from this equation that a 30 % increase of the viscosity, as observed for a 1 M $Mg(ClO_4)_2$ solution, can be obtained with a solution of 1 M suspended spheres that have a radius of about 3.6 Å. This radius is surprisingly similar to the radius of an ion and its first solvation shell of water molecules. Hence, the increase in viscosity upon adding small spherical ions to liquid water can indeed be fully explained from the rigid nature of the solvation structure formed by the ion and its first solvation shell.

8.5 Conclusions

The orientational-correlation time was measured for O–H groups of bulk water molecules in various ionic solutions [$NaClO_4$, $Mg(ClO_4)_2$ and Na_2SO_4 in $HDO:D_2O$ and $Mg(ClO_4)_2$ in $HDO:H_2O$] at different salt concentrations with femtosecond pump–probe spectroscopy. It is found that the addition of ions has no influence on the rotational dynamics of the bulk water molecules, even at very high concentrations (up to 6 M). For all the ionic solutions the orientational-correlation time of the bulk water molecule (measured at the $1\rightarrow2$ transition) is 3.4 ± 0.2 ps. Only for the O–H groups in the first solvation shell of the ClO_4^- ion, a different orientational-correlation time was found, its value is 7.6 ± 0.3 ps. Therefore, we conclude that ions do not enhance or break the hydrogen-bond network outside their direct vicinity (probably only their first solvation shell). As a result, there is no long-range structure-making effect or structure-breaking effect. The origin of the strong influence on the viscosity of water is not the ability of the ions to enhance the bulk hydrogen-bond network, but rather the rigidity of the first solvation shell, that increases the effective radius of the dissolved ion.

Bibliography

1. M. Afzal, M. Saleem, and M. T. Mahmood. Temperature and concentration dependence of viscosity of aqueous electrolytes from 20 to 50 °C. Chlorides of Na^+, K^+, Mg^{2+}, Ca^{2+}, Ba^{2+}, Sr^{2+}, Co^{2+}, Ni^{2+}, Cu^{2+}, Cr^{3+}. *J. Chem. Eng. Data* **34**, 339–346 (1989).

2. T. Asada and K. Nishimoto. Monte-Carlo simulations of $M^+Cl^-(H_2O)_n$ (M=Li, Na) clusters and the dissolving mechanism of ion-pairs in water. *Chem. Phys. Lett.* **232**, 518–523 (1995).

3. P. W. Atkins. *Physical Chemistry*. Oxford University Press, Oxford, 1990.

4. P. Ayotte, C. G. Bailey, G. H. Weddle, and M. A. Johnson. Vibrational spectroscopy of small $Br^-\cdot(H_2O)_n$ and $I^-\cdot(H_2O)_n$ clusters: infrared characterization of the ionic hydrogen bond. *J. Phys. Chem. A* **102**, 3067-3071 (1998).

5. P. Ayotte, G. H. Weddle, and M. A. Johnson. An infrared study of the competition between hydrogen-bond networking and ionic solvation: Halide-dependent distortions of the water trimer in the $X^-\cdot(H_2O)_3$ (X = Cl, Br, I) systems. *J. Am. Chem. Soc.* **120**, 12361-12362 (1998).

6. P. Ayotte, G. H. Weddle, J. Kim, and M. A. Johnson. Vibrational spectroscopy of the ionic hydrogen bond: Fermi resonances and ion–molecule stretching frequencies in the binary $X^-\cdot H_2O$ (X = Cl, Br, I) complexes via Argon predissociation spectroscopy. *J. Am. Chem. Soc.* **120**, 12361-12362 (1998).

7. C. G. Bailey, J. Kim, C. E. H. Dessent, and M. A. Johnson. Vibrational predissociation spectra of $I^-\cdot(H_2O)$: Isotopic labels and weakly bound complexes with Ar and N_2. *Chem. Phys. Lett.* **269**, 122-127 (1997).

8. H. J. Bakker and H.-K. Nienhuys. Delocalization of protons in liquid water. *Science* **297**, 587–590 (2002).

9. H. J. Bakker, P. C. M. Planken, L. Kuipers, and A. Lagendijk. Ultrafast saturation spectroscopy of chloroform, bromoform and iodoform. *J. Chem. Phys.* **94**, 1736 (1991).

10. P.-Å. Bergström and J. Lindgren. An IR study of ClO_4^-, NO_3^-, I^-, Br^-, Cl^-, and SO_4^- anions in aqueous solution. *J. Phys. Chem.* **95**, 8575-8580 (1991).

11. N. Bloembergen, E. M. Purcell, and R. V. Pound. Relaxation effects in Nuclear Magnetic Resonance absorption. *Phys. Rev.* **73**, 679–712 (1948).

12. M. Bonn, M. J. P. Brugmans, A. W. Kleyn, R. A. van Santen, and H. J. Bakker. Vibrational dephasing mechanisms in hydrogen-bonded systems. *Phys. Rev. Lett.* **76**, 2440 (1996).

13. T. A. Boyd. *Nonlinear Optics*. Academic Press, London, 1992.

14. B. H. Bransden and C. J. Joachain. *Introduction to Quantum Mechanics*. Longman, Harlow.

15. M. J. P. Brugmans, M. Bonn, H. J. Bakker, and A. Lagendijk. Multiphonon decay of stretch vibrations in zeolites. *Chem. Phys.* **201**, 215–225 (1995).

16. O. M. Cabarcos, C. J. Weinheimer, J. M. Lisy, and S. S. Xantheas. Microscopic hydration of the fluoride ion. *J. Chem. Phys.* **110**, 5-8 (1999).

17. A. Chandra. Effects of ion atmosphere on hydrogen-bond dynamics in aqueous electrolyte solutions. *Phys. Rev. Lett.* **85**, 768 (2000).

18. J. Chandrasekhar and W. L. Jorgensen. The nature of dilute solutions of sodium ion in water, methanol, and tetrahydrofuran. *J. Chem. Phys.* 77, 5080–5089 (1982).

19. J. Chandrasekhar, D. C. Spellmeier, and W. L. Jorgensen. *J. Am. Chem. Soc.* **106**, 903 (1984).

20. J.-H. Choi, K. T. Kuwata, Y.-B. Cao, and M. Okumura. Vibrational spectroscopy of the $Cl^-(H_2O)_n$ anionic clusters, n = 1–5. *J. Phys. Chem. A* **102**, 503-507 (1998).

21. W. M. Cox and J. H. Wolfenden. The viscosity of strong electrolytes measured by a differential method. *Proc. of the Royal Society A* **145**, (1934).

22. L. X. Dang, J. E. Rice, J. Caldwell, and P. A. Kollman. Ion solvation in polarizable water: molecular dynamics simulations. *J. Am. Chem. Soc.* **113**, 2481-2486 (1991).

23. J. J. Dannenberg, L. Haskamp, and A. Masunov. Are hydrogen bonds covalent or electrostatic? A molecular orbital comparison of molecules in electric fields and H-bonding environments. *J. Phys. Chem. A.* **103**, 7083–7086 (1999).

24. J. C. Deàk, S. T. Rhea, L. K. Iwaki, and D. D. Dlott. Vibrational energy relaxation and spectral diffusion in water and deuterated water. *J. Phys. Chem. A* **104**, 4866–4875 (2000).

25. L. Degrève, A. C. Borin, F. M. Mazzé, and A. L. G. Rodrigues. Molecular simulation of a phase separation in a non-primitive electrolyte solution. *Chem. Phys.* **265**, 193–205 (2001).

26. L. Degrève and F. L. B. da Silva. Large ionic clusters in concentrated aqueous NaCl solution. *J. Chem. Phys.* **111**, 5150 (1999).

27. L. Degrève and F. L. B. da Silva. Structure of concentrated aqueous NaCl solution: a Monte Carlo study. *J. Chem. Phys.* **110**, 3070 (1999).

28. L. Degrève, V. M. de Pauli, and M. A. Duarte. Simulation study of the role and structure of monatomic ions multiple hydration shells. *J. Chem. Phys.* **106**, 655 (1997).

29. G. R. Desiraju and T. Steiner. *The weak hydrogen bond in structural chemistry and biology*. Oxford university press, New York, 1999.

30. J. K. G. Dhont. *An Introduction to Dynamics of Colloids*. Elsevier Science B.V., Amsterdam, 1996.

31. S. R. Dillon and R. C. Dougherty. Raman studies of the solution structure of univalent electrolytes in water. *J. Phys. Chem. A* **106**, 7647–7650 (2002).

32. M. Diraison, Y. Guissani, J.-Cl Leicknam, and S. Bratos. Femtosecond solvation dynamics of water: solvent response to vibrational excitation of the solute. *Chem. Phys. Lett.* **258**, 348–351 (1996).

33. H. J. Eichler, P. Günter, and D. W. Pohl. *Laser-induced dynamic gratings*. Springer Verlag, Berlin, 1986.

34. U. Emmerichs, S. Woutersen, and H. J. Bakker. Generation of intense femtosecond optical pulses near 3 μm with a kilohertz repetition rate. *J. Opt. Soc. Am. B* **14**, 1478 (1997).

35. G. Engel and H. G. Hertz. On the negative hydration. A Nuclear Magnetic Relaxation study. *Berichte der Bunsengesellschaft für physikalische chemie* **72**, 807–834 (1968).

36. H. Falkenhagen and M. Dole. *Phys. Z.* **30**, 611 (1929).

37. T. A. Ford and M. Falk. Hydrogen bonding in water and ice. *Can. J. Chem.* **46**, 3579 (1968).

38. H. S. Frank and M. W. Evans. Free volume and entropy in condensed systems. *J. Chem. Phys.* **13**, 507 (1945).

39. F. Franks. *Water, a comprehensive treatise*. Plenum Press, New York, 1972.

40. F. Franks. *Water*. Royal Society of Chemistry, London, 1983.

41. G. M. Gale, G. Gallot, F. Hache, N. Lascoux, S. Bratos, and J.-Cl. Leicknam. Femtosecond dynamics of hydrogen bonds in liquid water: a real time study. *Phys. Rev. Lett.* **82**, 1068–1071 (1999).

42. G. M. Gale, G. Gallot, and N. Lascoux. Frequency-dependent vibrational population relaxation of the OH stretching mode in liquid water. *Chem. Phys. Lett.* **311**, 123–125 (1999).

43. G. Gallot, N. Lascoux, G. M. Gale, J.-Cl. Leicknam, S. Bratos, and S. Pommeret. Non-monotonic decay of transient infrared absorption in dilute HDO/D_2O solutions. *Chem. Phys. Lett.* **341**, 535-539 (2001).

44. H. Graener, T. Q. Ye, and A. Laubereau. Ultrafast dynamics of hydrogen bonds directly observed by time-resolved infrared spectroscopy. *J. Chem. Phys* **90**, 3413 (1988).

45. R. W. Gurney. *Ionic processes in solution*. McGraw–Hill, New York, 1953.

46. K. Hashimoto and K. Morokuma. Ab-initio theoretical study of surface and interior structures of the $(NaH_2O)_4$ cluster and its cation. *Chem. Phys. Lett.* **223**, 423-430 (1994).

47. K. Hermansson and M. Wojcik. Water exchange around Li^+ and Na^+ in LiCl(aq) and NaCl(aq) from MD simulations. *J. Phys. Chem. B* **102**, 6089-6097 (1998).

48. H. G. Hertz. *in: The chemical physics of solvation Part B, Spectroscopy of solvation*.

49. G. Herzberg. *Molecular spectra and molecular structure*. D. van Nostrand, New York, 1950.

50. J. C. Hindman, A. Svirmickas, and M. Wood. Relaxation processes in water. A study of the proton spin-lattice relaxation time. *J. Chem. Phys.* **59**, 1517–1522 (1959).

51. A. Holtzer and M. F. Emerson. On the utility of the concept of water structure in the rationalization of the properties of aqueous solutions of proteins and small molecules. *J. Phys. Chem.* **73**, 26–33 (1969).

52. S. Irle and J. M. Browman. Direct ab-initio variational calculation of vibrational energies of the $H_2O\cdots Cl^-$ complex and resolution of experimental differences. *J. Chem. Phys.* **113**, 8401–8403 (2000).

53. T. Isono. Density, viscosity and electrolytic conductivity of concentrated aqueous electrolyte solutions at several temperatures. alkaline-earth chlorides, $LaCl_3$, Na_2SO_4, $NaNO_3$, NaBr, KNO_3, KBr and $Cd(NO_3)_2$. *J. Chem. Eng. Data* **29**, 45–52 (1984).

54. S. Izvekov and M. R. Philpott. Ab initio molecular dynamics simulation of LiBr association in water. *J. Chem. Phys.* **113**, 10676–10684 (2000).

55. R. Jimenez, G. R. Fleming, P. V. Kumar, and M. Maronncelli. Femtosecond solvation dynamics of water. *Nature* **369**, 471 (1994).

56. G. Jones and M. Dole. *J. Am. Chem. Soc.* **51**, 2950 (1929).

57. H. Kanno. Raman study of aqueous HX solutions (X = F, Cl, Br and I) in both liquid and glassy states. *J. Raman Spectrosc.* **24**, 689–693 (1993).

58. Z. Kęcki, P. Dryjański, and E. Kozłowska. Effect of electrolytes on the intensity of the infrared bands of water. *Roczniki Chem.* **42**, 1749 (1968).

59. V. M. Kenkre, A. Tokmakoff, and M. D. Fayer. Theory of vibrational relaxation of polyatomic molecules in liquids. *J. Chem. Phys.* **101**, 10618–10629 (1994).

60. J. Kestin, H. E. Khalifa, Y. Abe, C. E. Grimes, H. Sookiazian, and W. A. Wakeham. Effect of pressure on the viscosity of aqueous NaCl solutions in the temperature range 20–150 °C. *J. Chem. Eng. Data* **23**, 328–336 (1978).

61. J. T. Kindt and C. A. Schuttenmaer. Far-infrared dielectric properties of polar liquids probed by femtosecond terahertz pulse spectroscopy. *J. Phys. Chem.* **100**, 10373–10379 (1996).

62. M. Kiselev and K. Heinzinger. Molecular dynamics simulation of a chloride ion in water under the influence of an external electric field. *J. Chem. Phys.* **105**, 650–657 (1996).

63. J. T. Knudtson and J. C. Stephenson. Vibrational relaxation of HCl in dilute CCl_4 and CCl_3 solutions. *Chem. Phys. Lett.* **107**, 385 (1984).

64. S. Koneshan and J. C. Rasaiah. Computer simulation studies of aqueous sodium chloride solutions at 298 K and 683 K. *J. Chem. Phys.* **113**, 8125–8137 (2000).

65. S. Koneshan, J. C. Rasaiah, R. M. Lynden-Bell, and S. H. Lee. Solvent structure, dynamics, and ion mobility in aqueous solutions at 25 °C. *J. Phys. Chem. B* **102**, 4193–4202 (1998).

66. M. F. Kropman and H. J. Bakker. Dynamics of water molecules in aqueous solvation shells. *Science* **291**, 2118-2120 (2001).

67. M. F. Kropman and H. J. Bakker. Femtosecond mid-infrared spectroscopy of aqueous solvation shells. *J. Chem. Phys.* **115**, 8942-8949 (2001).

68. M. F. Kropman, H.-K. Nienhuys, S. Woutersen, and H. J. Bakker. Vibrational relaxation and hydrogen-bond dynamics of HDO:D_2O. *J. Phys. Chem. A* **105**, 4622-4626 (2001).

69. R. Laenen, C. Rauscher, and A. Laubereau. Transient hole burning in the infrared in an ethanol solution. *J. Phys. Chem. A.* **101**, 3201-3206 (1997).

70. R. Laenen, C. Rauscher, and A. Laubereau. Dynamics of local substructures in water observed by ultrafast infrared hole burning. *Phys. Rev. Lett.* **80**, 2622–2625 (1998).

71. R. Laenen, K. Simeonidis, and A. Laubereau. Parametric generation of synchronized, independently tunable subpicosecond pulses in the mid-infrared with adjustable pulse duration. *J. Opt. Soc. Am. B* **15**, 1213-1217 (1997).

72. R. Laenen and A. Thaller. Water in the vicinity of solvated ions: modified dynamical and structural water properties resolved by sub-picosecond IR-spectroscopy. *Chem. Phys. Lett.* **349**, 442-450 (2001).

73. A. Laubereau, L. Greiter, and W. Kaiser. Intense tunable picosecond pulses in the infrared. *Appl. Phys. Lett.* **25**, 87 (1974).

74. C. P. Lawrence and J. L. Skinner. Vibrational spectroscopy of HOD in liquid D_2O. III. Spectral diffusion, and hydrogen-bonding and rotational dynamics. *J. Chem. Phys.* **118**, 264–272 (2003).

75. F. C. Lightstone, E. Schwegler, R. Q. Hood, F. Gygi, and G. Galli. A first principles molecular dynamics simulation of the hydrated magnesium ion. *Chem. Phys. Lett.* **343**, 549–555 (2001).

76. J. Lindgren, K. Hermansson, and M. J. Wójcik. Theoretical simulation and experimental determination of OH and OD stretching bands of isotopically diluted HDO molecules in aqueous electrolyte solutions. *J. Phys. Chem.* **97**, 5254–5259 (1993).

77. A. J. Lock and H. J. Bakker. Temperature dependence of vibrational relaxation in liquid H_2O. *J. Chem. Phys.* **117**, 1708–1713 (2002).

78. A. J. Lock, S. Woutersen, and H. J. Bakker. Ultrafast energy equilibration in hydrogen-bonded liquids. *J. Phys. Chem. A* **105**, 1238-1243 (2001).

79. R. Loudon. *The quantum theory of light, 2nd edition*. Oxford university press, New York, 1983.

80. M. I. Lubin, E. J. Bylaska, and J. H. Weare. Ab initio molecular dynamics simulations of aluminium ion solvation in water clusters. *Chem. Phys. Lett.* **322**, 447–453 (2000).

81. Y. Marcus. *Ion solvation*. John Wiley & Sons, New York, 1985.

82. J. F. McIntyre, R. T. Foley, and B. F. Brown. Infrared spectra of aluminium salt solutions. *Appl. Spectroscopy* **36**, 128–136 (1982).

83. W. Mikenda. Stretching frequency versus bond distance correlation of O—D(H)$\cdots$Y (Y = N, O, S, Se, Cl, Br, I) hydrogen bonds in solid hydrates. *J. of Mol. Struct.* **147**, 1–15 (1986).

84. W. Mikenda and S. Steinböck. Stretching frequency vs. bond distance correlation of hydrogen bonds in solid hydrates: A generalized correlation function. *J. of Mol. Struct.* **384**, 159–163 (1996).

85. R. E. Miller. The vibrational spectroscopy and dynamics of weakly bound neutral complexes. *Science* **240**, 447 (1988).

86. P. Moore, A. Tokmakoff, T. Keyes, and M. D. Fayer. The low frequency density of states and vibrational population dynamics of polyatomic molecules in liquids. *J. Chem. Phys* **103**, 3325–3334 (1995).

87. T. S. Moore and T. F. Winmill. The state of amines in aqueous solution. *J. Chem. Soc.* **101**, 1635–1676 (1912).

88. S. Mukamel. *Nonlinear optical spectroscopy*. Oxford university press, New York, 1995.

89. H.-K. Nienhuys. *Femtosecond mid-infrared spectroscopy of water*. PhD thesis, Technische Universiteit Eindhoven, 1998.

90. H.-K. Nienhuys, R. A. van Santen, and H. J. Bakker. Orientational relaxation of liquid water molecules as an activated process. *J. Chem. Phys* **112**, 8487-8494 (2000).

91. H.-K. Nienhuys, S. Woutersen, R. A. van Santen, and H. J. Bakker. Mechanism for vibrational relaxation in water investigated by femtosecond infrared spectroscopy. *J. Chem. Phys* **111**(4), 1494 (1999).

92. M. Nisoli, S. De Silvestri, O. Svelto, R. Szipöcs, K. Ferencz, Ch. Spielmann, S. Sartania, and F. Krausz. Compression of high-energy laser pulses below 5 fs. *Opt. Lett.* **22**, 522 (1997).

93. A. Nitzan and J. Jortner. Vibrational relaxation of a molecule in a dense medium. *Mol. Phys.* **25**, 713–734 (1973).

94. A. Novak. *Struct. Bonding (Berlin)* **18**, 177 (1974).

95. S. Obst and H. Bradaczek. Molecular dynamics study of the structure and dynamics of the hydration shell of alkaline and alkaline-earth metal cations. *J. Phys. Chem.* **100**, 15677–15687 (1996).

96. H. Ohtaki and T. Radnai. Structure and dynamics of hydrated ions. *Chem. Rev.* **93**, 1157–1204 (1993).

97. D. J. P. Out and J. M. Los. Viscosity of aqueous solutions of univalent electrolytes from 5 to 95 °C. *J. Sol. Chem.* **9**, 19–35 (1980).

98. P. M. Paul, E. S. Toma, P. Breger, G. Mullot, F. Augé, Ph. Balcou, H. G. Muller, and P. Agostini. Observation of a train of attosecond pulses from high-harmonic generation. *Science* **292**, 1689–1692 (2001).

99. L. Pauling. The structure and entropy of ice and of other crystals with some randomness of atomic arrangement. *J. Am. Chem. Soc.* **57**, 2680–2684 (1935).

100. L. Pauling. *The nature of the chemical bond*. Cornell university press, New York, 1939.

101. G. Peslherbe, B. M. Ladanyi, and J. T. Hynes. Free energetics of NaI contact and solvent-separated ion pairs in water clusters. *J. Phys. Chem. A* **104**, 4533-4548 (2000).

102. C. P. Petersen and M. S. Gordon. Solvation of sodium chloride: an effective fragment study of $NaCl(H_2O)_n$. *J. Phys. Chem. A* **103**, 4162–4166 (1999).

103. M. S. Pshenichnikov, K. Duppen, and D. A. Wiersma. Time-resolved femtosecond photon echo probes bimodal solvent dynamics. *Phys. Rev. Lett.* 74, 674-677 (1995).

104. L. M. Ramaniah, M. Bernasconi, and M. Parrinello. Density-functional study of hydration of sodium in water clusters. *J. Chem. Phys.* **109**, 6839–6843 (1998).

105. S. Raugei and M. L. Klein. Dynamics of water molecules in the Br^- solvation shell: an ab initio molecular dynamics study. *J. Am. Chem. Soc.* **123**, 9484-9485 (2001).

106. S. Raugei and M. L. Klein. An ab initio study of water molecules in the bromide ion solvation shell. *J. Chem. Phys.* **116**, 196–202 (2002).

107. S. B. Rempe and L. R. Pratt. The hydration number of Na^+ in liquid water. *Fluid Phase Equilibria* **183**, 121–132 (2001).

108. R. Rey and J. T. Hynes. Vibrational energy relaxation of HOD in liquid D_2O. *J. Chem. Phys.* **104**, 2356 (1996).

109. G. N. Robertson and J. Yarwood. Vibrational relaxation of hydrogen-bonded species in solution. *Chem. Phys.* **32**, 267–282 (1978).

110. W. H. Robertson, G. H. Weddle, J. A. Kelley, and M. A. Johnson. Solvation of the $Cl^- \cdot H_2O$ complex in CCl_4 clusters: the effect of solvent-mediated charge redistribution on the ionic H-bond. *J. Phys. Chem. A* **106**, 1205–1209 (2002).

111. C. Rønne, L. Thrane, P.-O. *Å*strand, A. Wallqvist, and S. R. Keiding. Investigation of the temperature dependence of dielectric relaxation in liquid water by THz spectroscopy and molecular dynamics simulation. *J. Chem. Phys.* **107**, 5319–5331 (1997).

112. A. Sacco, A. de Giglio, and A. Dell'atti. Ionic B coefficients in water at 30, 40 and 50 °C. *J. Chem. Soc., Faraday Trans. I* 77, 2693–2699 (1981).

113. Y. R. Shen. *The Principles of Nonlinear Optics*. John Wiley & Sons, New York, 1984.

114. D. E. Smith and L. X. Dang. Computer simulations of NaCl association in polarizable water. *J. Chem. Phys.* **100**, 3757 (1994).

115. D. W. G. Smith and J. G. Powles. *Mol. Phys.* **10**, 451 (1966).

116. D. E. Spence, P. N. Kean, and W. Sibbett. 60-fsec pulse generation from a self-mode-locked Ti-Sapphire laser. *Opt. Lett.* **16**, 42–44 (1991).

117. A. Staib and J. T. Hynes. Vibrational predissociation in hydrogen bondend OH$\cdots$O complexes via OH stretch–OO stretch energy transfer. *Chem. Phys. Lett.* **204**(1,2), 197–205 (1993).

118. J. Stangret and T. Gampe. Ionic hydration behavior derived from infrared spectra in HDO. *J. Phys. Chem. A* **106**, 5393–5402 (2002).

119. J. Stenger. *Ultrafast response of inter- and intramolecular hydrogen bonds in liquids: vibrational quantum beats and dephasing*. PhD thesis, Humboldt Universität, Berlin, 2002.

120. J. Stenger, D. Madsen, P. Hamm, E. T. J. Nibbering, and T. Elsaesser. A photon echo peak shift study of liquid water. *J. Phys. Chem. A* **106**, 2341–2350 (2002).

121. J. Stenger, D. Madsen, E. T. J. Nibbering, and T. Elsaesser. Ultrafast vibrational dephasing of liquid water. *Phys. Rev. Lett.* **87**, 7401-7404 (2001).

122. L. Stryer. *Biochemistry, third edition*. W. H. Freeman and Co., New York, 1988.

123. A. Tongraar, K. R. Liedl, and B. M. Rode. Born-Oppenheimer ab initio QM/MM dynamics simulations of Na^+ and K^+ in water: From structure making to structure breaking effects. *J. Phys. Chem. A* **102**, 10340–10347 (1998).

124. T. Ujike, Y. Tominaga, and K. Mizoguchi. Dynamical structure of water in alkali halide aqueous solutions. *J. Chem. Phys.* **110**, 1558–1568 (1999).

125. R. D. Waldron. Infrared spectra of HDO in water and ionic solutions. *J. Chem. Phys.* **26**, 809 (1957).

126. G. E. Walrafen. Raman spectral studies of the effects of electrolytes on water. *J. Chem. Phys.* **36**, 1035-1042 (1962).

127. G. E. Walrafen. Raman spectral studies of the effects of perchlorate ion on water structure. *J. Chem. Phys.* **52**, 4176 (1970).

128. J. M. Weber, J. A. Kelley, S. B. Nielsen, P. Ayotte, and M. A. Johnson. Isolating the spectroscopic signature of a hydration shell with the use of clusters: superoxide tetrahydrate. *Science* **287**, 2461–2463 (2000).

129. A. Werner. Ueber Haupt- und Nebenvalenzen und die Constitution der Ammoniumverbindungen. *Liebig's Annalen der Chemie* **322**, 261–297 (1902).

130. J. A. White, E. Schwegler, G. Galli, and F. Gygi. The solvation of Na^+ in water: First-principles simulations. *J. Chem. Phys.* **113**, 4668–4673 (2000).

131. M. J. Wójcik, J. Lindgren, and J. Tegenfeldt. Note on a theoretical interpretation of the isotopic ration ν_{oh}/ν_{od} versus ν_{oh}. *Chem. Phys. Lett.* **99**, 112–115 (1983).

132. P. G. Wolynes. Dynamics of electrolyte solutions. *Ann. Rev. Phys. Chem.* **31**, 345–376 (1980).

133. S. Woutersen. *Femtosecond vibrational dynamics in hydrogen-bonded systems*. PhD thesis, Universiteit van Amsterdam, 1999.

134. S. Woutersen and H. J. Bakker. The hydrogen bond in liquid water as a Brownian oscillator. *Phys. Rev. Lett.* **83**, 2077–2080 (1999).

135. S. Woutersen and H. J. Bakker. Resonant intermolecular transfer of vibrational energy in liquid water. *Nature* **402**, 507–509 (2000).

136. S. Woutersen, U. Emmerichs, and H. J. Bakker. A femtosecond mid-infrared pump–probe study of hydrogen bonding in ethanol. *J. Chem. Phys.* **107**, 1483 (1997).

137. S. Woutersen, U. Emmerichs, and H. J. Bakker. Femtosecond mid-IR pump–probe spectroscopy of liquid water: Evidence for a two-component structure. *Science* **278**, 658–660 (1997).

138. S. Woutersen, U. Emmerichs, H.-K. Nienhuys, and H. J. Bakker. Anomalous temperature dependence of vibrational lifetimes in water and ice. *Phys. Rev. Lett.* **81**, 1106–1109 (1998).

139. H. R. Wyss and M. Falk. Infrared spectrum of HDO in water and in NaCl solution. *Can. J. Chem.* **48**, 607 (1970).

140. S. S. Xantheas. Quantitative description of hydrogen bonding in chloride–water clusters. *J. Phys. Chem.* **100**, 9703–9713 (1996).

141. S. Yeremenko, A. Baltuška, F. de Haan, M. S. Pshenichnikov, and D. A. Wiersma. Frequency-resolved pump-probe characterization of femtosecond infrared pulses. *Opt. Lett.* **27**, 1171–1173 (2002).

142. S. Yeremenko, M. S. Pshenichnikov, and D. A. Wiersma. Hydrogen-bond dynamics in water explored by heterodyne-detected photon echo. *Chem. Phys. Lett.* **369**, 107–113 (2003).

143. S-B Zhu and G. Wilse Robinson. Molecular-dynamics computer simulation of an aquous NaCl solution: structure. *J. Chem. Phys.* **97**, 4336 (1992).

144. R. Zwanzig. Dielectric friction on a moving ion. *J. Chem. Phys.* **38**, 1603–1605 (1963).

Summary

In this thesis, experimental studies are described on the dynamics of water molecules in ionic solvation shells. Although knowledge of the properties of water and aqueous solutions are of great importance to chemistry and biology, and despite centuries of experimental and theoretical studies, by far not everything is yet known. Some information on the structure of liquid water was obtained from X-ray diffraction and infrared spectroscopy, in the beginning of the twentieth century. In spectroscopic studies, usually the O–H stretch vibration is probed. The usefulness of this vibration in the study of the structure of water is based on the influence on its frequency of the hydrogen-bond it forms with adjacent (water) molecules; the relation between the O–H stretch frequency and hydrogen-bond length is approximately linear. However, the time resolution of both spectroscopic and diffraction techniques is by far not sufficient to discern any solvation dynamics. Only recently, the dynamics on sub-picosecond time scales has become accessible for experimental study.

The experiments that are described in this thesis are two-colour mid-infrared femtosecond pump–probe spectroscopic studies. In this type of study, the O–H stretch vibration of a number of water molecules, characterized by their absorption frequency, is vibrationally excited. The pump pulse has a duration of approximately 200 fs, and is tuned to the O–H stretch frequency. As a result of the excitation by the pump pulse, the transmission of the sample changes, which is measured by the probe pulse. A detailed description of the experiment is given in chapter 2. In this thesis, concentrated salt solutions have been studied. The solutions consist of a low concentration of HDO ($<$1 M) in D_2O and a high concentration (0.5 to 10 M) of a particular salt: NaCl, NaBr, NaI.

In chapter 3, the isotropic transmission change was measured as a function of delay for several salt solutions. For a solution containing KF, the decay is single-exponential with a time constant of about 800 fs, identical to that of the neat liquid, i.e. HDO dissolved in D_2O. For the solutions containing NaCl, NaBr or NaI, the relaxation becomes strongly non-exponential and contains a fast component and a slow component of which the amplitude is observed to correlate with the concentration of the dissolved anion. The slow component represents the vibrational lifetime T_1 of the anion-bonded O–H groups. The longer vibrational lifetime can be understood from the fact that the O–H stretch frequency and its relaxation rate are strongly determined by the hydrogen-bond interaction. One of the O–H groups of a water molecule in the solvation shell of an anion X^- will form an O–H$\cdots X^-$ hydrogen bond, that is different from an O–H$\cdots$O hydrogen bond in bulk water and in a cationic solvation shell. The time constant of the slow component increases with the anion's mass, and decreases with temperature. The decrease with temperature is expected on theoretical grounds and observed for most molecular vibrations, except for bulk water. The opposite behaviour of bulk water and ionic solutions can be explained from the much stronger temperature dependence of the hydrogen-bond interaction for bulk water.

At high concentrations (at concentrations of 6 M, there are about 5 water molecules per ion), the anions and cations are quite close to each other and both will probably have an influence on the vibrational relaxation of the anion-bonded O–H groups. In chapter 4, we compared the vibrational relaxation of solutions of a series of salts consisting of the cations Li^+, Na^+ and Mg^{2+}, and the anions Cl^-, Br^- and I^-. The concentration was varied between 0.5 M and 6 M (Cl^-), 9 M (Br^-) or 10 M (I^-). It was found that the vibrational lifetime increases in the halogenic series Cl^-, Br^-, I^-, and with increasing concentration of dissolved salt. In addition, we found a small but significant dependence of the lifetime on the nature of the cation: for the same type of anion and concentration, it increases in the cationic series Mg^{2+}, Li^+, Na^+.

Chapter 5 is a response to an article published by Laenen et al., who claimed that the vibrational relaxation in salt solutions depends on the *cation* content, not on the anion's, opposing the results of chapter 4. The difference was attributed to differences in the applied laser pulses. Additional experiments, using laser pulses modified to have Laenen's pulse characteristics, are presented, reaffirming our previous conclusions, and showing that Laenen's signal-to-noise ratio was not sufficient to draw sound conclusions.

From chapters 3, 4 and 5, it is concluded that the vibrational lifetime of anion-bonded O–H groups is significantly longer than of the other O–H groups in the solution. This has the great advantage that after a few picoseconds only HDO molecules remain excited that are hydrogen bonded to an anion, which enables a very selective study of the dynamics of the aqueous anionic solvation shell.

In chapter 6, we used different pump and probe frequencies to measure the rate at which the frequency of an excited O–H group changes, resulting from variation of the O–H$\cdots$X$^-$ hydrogen-bond length. It was observed that the isotropic transmission change decays at different rates for different probing frequencies. The difference in decay rates results from a spectral diffusion process, that produces an 'outflow' of molecules that vibrate at a frequency near the pump frequency, and an 'inflow' at frequencies away from the pump. The data have been modeled using two Brownian oscillators, one for the water-bound O–H groups (O–H$\cdots$O) and one for the anion-bound (O–H$\cdots$X$^-$). We obtained values for the O–H stretch frequency (hydrogen-bond length) correlation time of several anions, that are approximately 30 times as long as for the bulk water molecules. Thus, the solvation shell is a stable, well-ordered structure compared to bulk liquid water.

In chapter 7, the reorientational motion of the anionic solvation shells is studied by measuring the dynamics of the rotational anisotropy. The anisotropy decays slower than for pure liquid water, but is faster than the hydrogen-bond motion. This means that the orientational motion stems from a rotation of the complete solvation structure, not of the individual solvent-shell molecules. The temperature dependence of the anisotropy decay can be related to the temperature dependence of the viscosity using the Stokes-Einstein equation for rotational diffusion of a sphere.

In the final chapter, an old hypothesis is tested, according to which some ions would be able to change the hydrogen-bond structure of the solvating water molecules. If this structure would be enhanced (by the so-called 'structure-making ions'), these water molecules should be hindered in their reorientational motion. This was tested in chapter 8 for a series of 'structure-making' ions, ClO_4^-, Mg^{2+}, and SO_4^-. Even for strong 'structure makers', no change in reorientational motion could be measured. This implies that the long-held belief in 'structure making' and 'structure breaking' should be abandoned, and a new ex-

planation must be found to explain the phenomena that gave rise to these ideas.

The experiments in this thesis may add to the understanding of the important phenomenon of ion solvation, providing information on the structure and dynamics of solvation shells. The picture promoted by the results is the following: The ion is surrounded by a shell of solvating water molecules. The whole structure is characterized by an average diameter that in most cases corresponds to approximately one layer of solvent molecules. The structure is rigid compared to the bulk solvent, being preserved during rotation and changing shape relatively slowly. The influence of the ion does not extend beyond this shell, at least not to the extent that it has a measurable influence on the hydrogen-bond network.

Samenvatting

Zout water Dit proefschrift gaat over zout water. Zout water is natuurlijk van groot belang in de wereld: ruim twee derde van het aardoppervlak is bedekt met oceanen, die tezamen een zoutoplossing vormen van 10^{21}, ofwel duizendmaal een miljard maal een miljard, liter. Gemiddeld over het hele aardoppervlak is dit een laag water met een diepte van bijna 3 kilometer. Een ander voorbeeld is het menselijk lichaam, dat eveneens voor een groot deel bestaat uit water met daarin allerlei opgeloste zouten en mineralen. Het is van belang om precies te weten hoe de watermoleculen zich gedragen ten opzichte van de opgeloste deeltjes omdat dit gedrag een grote invloed heeft op de chemische reacties die in het lichaam plaatsvinden.

Een zoutmolecuul bestaat uit een kation en een anion: positief, respectievelijk negatief geladen deeltjes. De ionen worden bijeengehouden door een sterke electrostatische aantrekking: de ionische binding. Het oplossen van zout in water vereist het verbreken van deze binding, zodat de ionen los van elkaar in de vloeistof verblijven. Dit proces wordt gedreven door de interacties tussen ionen en watermoleculen en de toename van de entropie.

Solvatatieschillen Al vanaf het begin van de twintigste eeuw werden zoutoplossingen bestudeerd. De eerste theorieën hielden geen rekening met de moleculaire structuur van het water, maar beschreven de oplossing simpelweg als puntladingen in een homogeen medium met een karakteristieke dielectrische constante. Hierin kwam verandering in de jaren twintig en dertig, toen nieuwe technieken werden gebruikt voor de studie van water, zoals Röntgen diffractie en infrarood spectroscopie. Er kon worden aangetoond dat vloeibaar water wel degelijk een structuur bezit, en dat die structuur verandert als er deeltjes in worden opgelost. De watermoleculen bevinden zich bij voorkeur op specifieke afstanden van het deeltje, zodat een of meer schillen van watermoleculen worden gevormd, zogenaamde solvatatieschillen. De dynamica van deze schillen speelt een essentiële rol in chemische reakties: op zijn minst zullen eerst de watermoleculen aan de kant moeten. Daarnaast blijken de watermoleculen ook een actieve rol in de reaktie te kunnen spelen.

De waterstofbrug Tussen watermoleculen bestaat een specifieke binding, de waterstofbrug. Deze binding kan alleen bestaan tussen een waterstofatoom enerzijds en een sterk electronegatief atoom, zoals O, N, F, Cl, Br of I anderzijds. De binding is zwakker dan een covalente of 'chemische' binding, maar sterk genoeg om watermoleculen bijeen te houden, zodat water bij kamertemperatuur niet verdampt. Vloeistoffen die geen waterstofbruggen kunnen vormen vervliegen wel bij kamertemperatuur, bijvoorbeeld ether.

Een waterstofbrug is directief, of gericht: bij een brug tussen een O–H groep en een zuurstofatoom liggen alle atomen bij voorkeur op een lijn: O–H$\cdots$O. Dit feit maakt dat ijs, waarbij alle watermoleculen vier waterstofbruggen vormen met andere moleculen, een lagere dichtheid heeft dan water van 0 °C. De watermoleculen in ijs zouden dichter

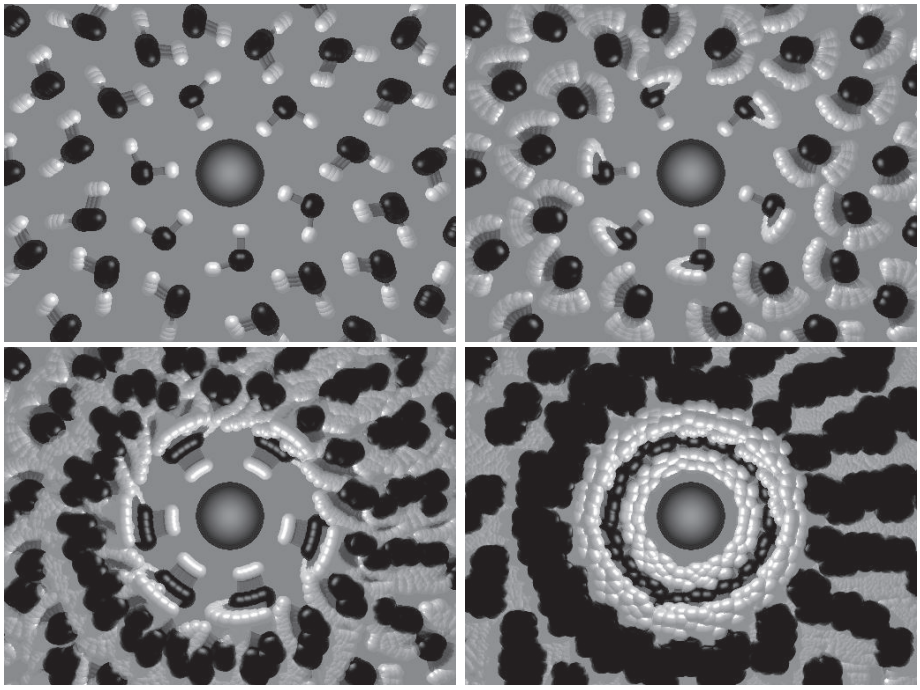

Figuur 8.8. Gesimuleerde foto's van een jodide ion, gesolvateerd door watermoleculen. De experimenten tonen aan dat de watermoleculen in de eerste solvatatieschil van het ion langzamer bewegen dan de moleculen buiten deze schil. De translationele en rotationele dynamica van watermoleculen in de schil vindt plaats met tijdsconstanten van respectievelijk 18 en 10 picoseconden. Buiten de schil is dat 0.5 resp. 2.6 ps. De figuren zijn "artist's impressions" van foto's van de vloeistof, genomen met sluitertijden van respectievelijk 1, 4, 10 en 30 ps.

op elkaar kunnen zitten, maar zouden daartoe een of meer waterstofbruggen moeten verbreken.

Wat bepaalt de solvatatiestructuur? De structuur van water rond een ion wordt bepaald door een drietal interacties. Ten eerste, watermoleculen kunnen een waterstofbrug vormen met een anion. Ten tweede, watermoleculen zijn van zichzelf een klein beetje polair: het zuurstofatoom is licht negatief, terwijl beide waterstofatomen een beetje positief geladen zijn, en omdat het middelpunt van beide waterstofatomen niet samenvalt met het zuurstofatoom heeft het molecuul een dipoolmoment, dat zich wil richten naar het electrisch veld dat van het ion uitgaat. Ten slotte vormen watermoleculen ook nog waterstofbruggen met elkaar. De tweede schil van watermoleculen rond een ion zal zich richten naar de eerste schil, om zoveel mogelijk profijt te hebben van de waterstofbrug-interacties. Van de andere kant zal de waterstofbrug-structuur die in de vloeistof bestaat zich willen voortzetten tot bij het ion.

ULTRASNELLE SPECTROSCOPIE De drie genoemde interacties moeten samen de structuur van watermoleculen rond een ion bepalen. Lange tijd bestond er eigenlijk geen techniek waarmee we de moleculen dichtbij een ion konden waarnemen los van de verder van het ion verwijderde moleculen. En als dat wel kon, zoals met Röntgen diffractie, was de meetmethode zo traag dat het vergeleken zou kunnen worden met een foto van een scrum in een rugbywedstrijd, genomen met een sluitertijd van een uur. Als de camera gedurende die tijd steeds op de bal gericht is geweest is deze nog wel te zien, maar de individuele spelers zullen niet meer te onderscheiden zijn. Omdat ondertussen ook nog van speelhelft is gewisseld, kan men uit de foto van de scrum vrijwel niets over de spelers te weten komen. Als wij willen weten wie er aan de scrum deelnemen, hoe lang iedere speler is, of hij zich langer of korter dan zijn medespelers in het strijdgewoel staande houdt, en of hij zich van ontoelaatbare trucs bedient om de bal te bemachtigen, hebben we dus een fotocamera nodig met een korte sluitertijd. Waar een gewone camera sluitertijden van ongeveer een milliseconde haalt, ruim voldoende voor zelfs de snelste rugbyspeler, is voor het bestuderen van watermoleculen een sluitertijd van minder dan een picoseconde (1 ps = 10^{-12} s ofwel een miljoenste van een miljoenste seconde) vereist; een miljard maal korter dus dan van een gewone camera.

Onze 'fotocamera' is een woud van laserapparatuur, spiegels, lenzen en speciale kristallen, die samen een oppervlak van ongeveer 8 vierkante meter beslaan. Hiermee maken we zeer korte laserpulsen, lichtflitsen van ongeveer 100 femtoseconde (1 fs = 10^{-15} s, ofwel een duizendste picoseconde), die met een frequentie van 1 kHz (dus duizend per seconde) worden geproduceerd. De golflengte van dit licht is ongeveer 3 μm ; dit is infrarood licht dat wij met onze ogen niet kunnen zien. Licht met deze golflengte wordt door water geabsorbeerd: ieder geabsorbeerd foton brengt een watermolecuul in trilling. Het watermolecuul kan op verschillende manieren trillen; de specifieke trilling die wij bestuderen is de vibratie van het waterstofatoom ten opzichte van het zuurstof atoom, de O–H strek vibratie. Gedurende de tijd dat het molecuul trilt —de "levensduur" van de vibratie— kan het geen licht van deze frequentie absorberen; door de absorptie te meten weten we dus hoeveel moleculen er (nog) in trilling zijn.

Ik zal nu uitleggen hoe we deze trilling kunnen gebruiken om de eigenschappen van watermoleculen rondom ionen te bestuderen. De frequentie van deze O–H strek vibratie wordt bepaald door de sterkte van de waterstofbrug die deze O–H groep vormt met een naburig watermolecuul, of met een anion (het kation kan geen waterstofbrug vormen). Hoe korter en sterker de waterstofbrug, hoe lager de frequentie van de aangeslagen trilling. De trilling leeft iets minder dan een picoseconde voor O–H groepen die aan water zijn gebrugd, maar veel langer, enkele picoseconden, als het molecuul aan een anion is gebrugd. Dit is zeer gunstig, omdat we nu de moleculen die de solvatatieschil van het anion vormen kunnen onderscheiden van de andere watermoleculen. Als we met onze laserpulsen op het zoute water schieten, brengen we in eerste instantie alle watermoleculen in trilling. Als we vervolgens korte tijd wachten, zijn de gewone watermoleculen reeds uitgetrild, terwijl die in de schil rond het anion nog trillen. Aangezien we specifiek willen kijken naar de watermoleculen rond de anionen, gebruiken we in onze experimenten alleen de gegevens die zijn verkregen na voldoende lang (ongeveer 3 ps) te hebben gewacht.

In de figuur worden vier "foto's" getoond van watermoleculen rond een anion, genomen met verschillende sluitertijden, variërend van 0.2 tot 10 ps (1 ps = 10^{-12} s). De "foto's" zijn niet werkelijk en kunnen de werkelijkheid ook niet exact weergeven,

maar ze geven wel een impressie van de dynamica van watermoleculen rond een anion, gebaseerd op de resultaten van onze experimenten. In de rest van deze samenvatting zal ik verschillende aspecten van de bewegingen van de watermoleculen uitleggen, en hoe we ze hebben kunnen meten.

BEWEGINGEN VAN DE SOLVATATIESCHIL In vloeistof bewegen de moleculen op allerlei manieren: alles beweegt door elkaar, draait om elkaar en om zijn eigen as, en wordt heen en weer geduwd, net als de rugbyspelers in de scrum. Dit is zichtbaar gemaakt in de figuur, met name in de foto met een sluitertijd van 4 ps. Met Röntgen diffractie was eerder al waargenomen dat watermoleculen zich op specifieke afstanden rond ionen bevinden, maar met deze techniek kon men niet zien hoe deze moleculen bewegen. In de vergelijking met de scrum: de coach weet wel dat er bijvoorbeeld twee rijen van spelers om de bal staan (daartoe heeft hij bovendien zelf opdracht gegeven), en of zijn team na de scrum de bal meestal al dan niet in zijn bezit heeft. Nu wil hij echter met betrekking tot het vergroten van de stootkracht van zijn team in dergelijke situaties bepalen welke spelers het langst standhouden en zich het minst door de tegenpartij aan de kant laten duwen. Dat doet hij door verschillende foto's te maken, waarop de afzonderlijke spelers steeds duidelijk te zien zijn. Door verschillende van deze foto's achter elkaar te plaatsen verkrijgt hij een filmpje van het verloop van de scrum, en de rol daarin van iedere speler. Terug naar water: we maken "foto's" van watermoleculen door gebruik te maken van het feit dat de trillingsfrequentie varieert als de afstand tussen het watermolecuul en het anion verandert. De karakteristieke tijd dat de frequentie gelijk blijft noemen we de correlatietijd, of, omdat het gaat om een frequentieverandering ten gevolge van de diffusieve beweging van moleculen, de spectrale diffusie tijd. Deze tijd blijkt ongeveer 10 tot 25 ps te zijn, afhankelijk van het ion. Dit lijkt kort, maar eigenlijk waren we juist verbaasd dat het zo *lang* is; het is namelijk veel langer dan de correlatietijd tussen twee watermoleculen in bulk water, die minder dan 1 ps bedraagt. In de figuur is te zien dat de afstand van de zuurstofatomen tot het anion niet erg sterk verandert gedurende 10 ps.

ROTATIE VAN SOLVATATIESTRUCTUREN Als we water exciteren met gepolariseerd laserlicht, zullen we vooral die moleculen in trilling brengen, waarvan de O–H groep parallel staat aan de polarisatie van het licht. Eerder is al gezegd dat we het aantal nog in trilling zijnde moleculen kunnen meten doordat de trillende moleculen geen licht meer kunnen absorberen. Dit moet ik eigenlijk iets preciezer formuleren; de absorptieverandering ten gevolge van de excitatie is namelijk alleen meetbaar met licht dat is gepolariseerd langs de as waarin de moleculen trillen. We gebruiken dit effect om de rotatie van watermoleculen in solvatatieschillen te meten. Weer wachten we tot de 'gewone' watermoleculen zijn uitgetrild, en kijken dan naar de oriëntatie van de nog in trilling zijnde moleculen in de solvatatieschillen van anionen. De tijd dat een watermolecuul in de schil van een anion in dezelfde richting wijst wordt de oriëntationele correlatietijd genoemd; hoe korter de correlatietijd, hoe groter de draaisnelheid. Volgens onze metingen is deze correlatietijd ongeveer 10 ps voor de bestudeerde anionen (Cl^-, Br^- en I^-). Ter vergelijking: in puur water roteren de moleculen met een tijdsconstante van ongeveer 2.7 ps. In de figuur, vooral die met een sluitertijd van 4 ps, is te zien dat de watermoleculen veel sneller roteren dan degene die aan het anion gebonden zijn. Op een tijdschaal van 10 ps echter roteert ook de solvatatieschil.

Interessant is verder dat de oriëntationele correlatietijd korter is dan de spectrale diffusietijd. Met andere woorden: een watermolecuul in de solvatatieschil van een anion draait sneller dan dat het zich van het anion af beweegt. De rotatie die we meten betreft dus de rotatie van de gehele solvatatieschil, en niet van een enkel molecuul dat even de schil verlaat en daardoor gemakkelijker roteert. Het vreemde is dat de schil van het grootste ion, I^-, het snelste draait. Hetzelfde zien we bij de mobiliteit van deze ionen, de snelheid waarmee een ion zich door het oplosmiddel kan verplaatsen (dit hebben wij niet gemeten maar in een tabel opgezocht). Vermoedelijk is de reden hiervoor dat I^- zo groot is, dat de watermoleculen niet meer zo sterk aan het ion binden, en er gemakkelijk even van losraken. Hierdoor is de effectieve grootte van de schil tijdelijk afgenomen, en kan de schil vrijer roteren.

STRUCTUUR VAN WATER BUITEN DE EERSTE SOLVATATIESCHIL Ik heb al laten zien dat de structuur van water verandert door de aanwezigheid van ionen: een stabiele solvatatieschil wordt gevormd. Het traditionele beeld van de solvatatie van ionen is echter dat sommige ionen de structuur van watermoleculen ook *buiten* deze solvatatieschil beïnvloedt, en deze structuur sterker maakt dan de structuur in puur water, dus zonder ionen; andere ionen zouden de structuur verzwakken. Een van de redenen van het ontstaan van dit idee is het vreemde gedrag van de viscositeit van zoutoplossingen: bij het oplossen van bepaalde ionen, zoals Mg^{2+}, neemt de viscositeit veel sterker toe dan voor bijvoorbeeld Na^+. Dit microscopische beeld van een veranderde waterstofbrugstructuur blijkt echter uiterst moeilijk te verifiëren.

Tot nu toe was het niet mogelijk om direct naar deze moleculen te kijken om te zien of ze zich daadwerkelijk anders gedragen. Met onze techniek kunnen we echter meten hoe snel deze moleculen roteren. In alle eerder besproken metingen konden we specifiek naar de moleculen in de solvatatieschillen van anionen kijken, doordat deze moleculen langer dan de andere trilden. Nu willen we juist naar die andere moleculen kijken, en kunnen we dus niet meer dezelfde truc toepassen. Er is gelukkig een anion waarvoor de moleculen in de solvatatieschil met een zodanig andere frequentie trillen, dat we door de golflengte van het laserlicht goed te kiezen, deze laatste moleculen links kunnen laten liggen, en alleen moleculen exciteren die zich ofwel vrij in de vloeistof, ofwel in de solvatatieschil van een kation bevinden. We kiezen bij dit anion speciaal een kation dat er om bekend staat een sterke 'structure maker' te zijn: Mg^{2+}.

Wanneer we dit doen, en dus specifiek kijken naar de watermoleculen die de 'structure-making' invloed van dit kation zouden moeten ondergaan, zien we ... niets! Er is geen enkele invloed waarneembaar op de structuur van water rond ionen, althans niet buiten de eerste solvatatieschil. Dit betekent dat de 'structure making' en 'structure breaking' effecten die al minstens 70 jaar wordt verondersteld de waterstofbrugstructuur te bepalen waarschijnlijk helemaal niet bestaan! We stellen een andere verklaring voor het effect van het oplossen van zouten op de viscositeit voor. Wanneer we aannemen dat een ion met een solvatatieschil kan worden beschouwd als een harde bol, kunnen we uit de diffusiviteit van het ion de viscositeit van de oplossing berekenen met de Stokes–Einstein formule die al in het begin van de twintigste eeuw is afgeleid. De aldus berekende viscositeit blijkt aardig goed te kloppen met de waarnemingen. In dit beeld komt het verschil tussen ionen tot uitdrukking in een verschillende diameter van de harde bol, dat wil zeggen de effectieve grootte van het ion met zijn solvatatieschil.

We weten nog lang niet alles over water en de interacties van water met verschillende erin opgeloste stoffen, maar er begint toch een beeld te ontstaan van de dynamica van solvatatieschillen. Wij hopen met het werk beschreven in dit proefschrift bij te dragen aan de kennis over solvatatieschillen. Kort samengevat luiden de belangrijkste conclusies als volgt: de structuur van een zoutoplossing in water is er een van ionen met een solvatatieschil, die met niet-lineaire spectroscopie bestudeerd kan worden als gevolg van de langere vibrationele levensduur van de watermoleculen uit deze schillen. De schil verandert slechts langzaam van vorm, en kan als geheel roteren. De invloed van het ion op de sterkte van de waterstofbrugstructuur blijft beperkt tot een enkele solvatatieschil, en strekt zich niet uit, zoals lang werd gedacht, over verschillende lagen van watermoleculen.

Dankwoord

Tot slot wil ik een aantal mensen bedanken die van groot belang zijn geweest bij de uitvoering van het onderzoek en de totstandbrenging van het verslag ervan in dit proefschrift. Het grootste deel van mijn dank gaat uit naar mijn promotor Huib, die mij na mijn afstudeeronderzoek in zijn groep aanspoorde een promotieonderzoek te beginnen. Hoewel ik aanvankelijk niet van plan was in de wetenschap te blijven, heb ik er absoluut geen spijt van zijn raad te hebben opgevolgd, want het zijn uiterst plezierige en leerzame jaren geworden, terwijl het onderzoek, grotendeels dankzij de inspirerende inbreng van Huib, veel resultaten heeft gebracht. De samenwerking is steeds uitstekend geweest, mede door de gedeelde liefde voor Ajax, fietsen en hardlopen, en de gelijkopgaande haaruitval. Zijn raadgevingen omtrent de interpretatie van nieuwe data, verbeteringen aan de experimentele opstelling, en het schrijven van artikelen waren altijd zeer doordacht en doeltreffend. Ik kan mij in alle eerlijkheid geen betere promotor voorstellen.

Ook van grote invloed is geweest mijn Eerste Leermeester op de laseropstelling, de onvergelijkelijke Han-Kwang Nienhuys, die mij wegwijs maakte in de niet-lineaire spectroscopie, het onderzoek aan water en het computerbesturingssysteem Linux, en die, door zijn oude racefiets voor een schappelijke prijs aan mij te verkopen, mij aan het fietsen heeft gebracht. Zijn wetenschappelijke activiteiten hebben een spoor van programmatuur achtergelaten: bovenal het prachtprogramma Irismeet waarmee de metingen zijn verricht, maar ook programma's om de data te verwerken, met één commando in het beveiligingssysteem in te loggen, of om posters of proefschriften in latex te schrijven. Tot en met het schrijven van dit proefschrift was hij een vraagbaak voor het werkend houden van mijn computer, en voor het installeren van het Garamond font dat voor dit proefschrift is gebruikt.

Dan dank ik Sander Woutersen voor alle hulp bij het ontwerpen en uitvoeren van experimenten, het schrijven van artikelen en het opdrinken van flessen wijn (hiervoor dank ik tevens zijn vrouw Saskia). Anne Willem Omta bedank ik hartelijk voor de prettige samenwerking gedurende zijn afstudeeronderzoek in onze groep. De experimenten van hoofdstuk 8 zijn door hem met groot enthousiasme en volharding uitgevoerd. Ook de samenwerkingen met Ingrid Giebels en Frederik van den Broek waren zeer vruchtbaar en plezierig. Frederik bedank ik daarnaast voor computerhulp: na het vertrek van Han-Kwang heeft hij het vaandel van groeps-computergoeroe overgenomen. Hinco Schoenmaker is als perfectionistische technicus met een enorme creativiteit, hulpvaardigheid en humor onmisbaar voor onze groep. Arjan Lock ben ik zeer erkentelijk voor de plezierige tijd tijdens conferenties en aansluitende vakanties in Berlijn, Toledo en Vancouver.

Door bovenstaande personen is de sfeer altijd bijzonder goed geweest. Hiertoe hebben verder bijgedragen: Mingcheng Zong, Yves Rezus, Dorte Madsen, Joop Gilijamse, Olaf Larsen, Adriaan Dokter, de overige leden van de afdeling Femtofysica die te veel zijn om ze allen op te noemen, en Teun van Dillen, mijn uitermate gezellige kamergenoot gedurende vier jaar.

Het Amolf onderscheidt zich van andere instituten en van universiteiten door een uitstekende ondersteuning, waarvoor ik de afdelingen E&I, de bibliotheek, de werkplaats en de tekenkamer wil bedanken; met name Idsart Attema en Henk Dekker zijn van onschatbare waarde geweest.

Severin heeft de kaft van dit proefschrift gemaakt, waarvoor dank! Ten slotte bedank ik vrienden en familie voor de morele steun gedurende deze jaren.

Michel Kropman Utrecht, januari 2004